From CLNICAL NEUROSCIENCE
Karolinska Institutet, Stockholm, Sweden

NOVEL MEASURE OF OLFACTORY BULB FUNCTION IN HEALTH AND DISEASE

Behzad Iravani

Stockholm 2021

All previously published papers were reproduced with permission from the publisher.
Published by Karolinska Institutet.
Cover by Behzad Iravani.
Printed by US-AB

ISBN 978-91-8016-234-0

Novel Measure of Olfactory Bulb Function in Health and Disease
THESIS FOR DOCTORAL DEGREE (Ph.D.)

By

Behzad Iravani

Principal Supervisor:
Assoc. Prof. Johan N. Lundström
Karolinska Institutet
Department of Clinical Neuroscience
Division of Psychology

Co-supervisor(s):
Asst. Prof. Artin Arshamian
Karolinska Institutet
Department of Clinical Neuroscience
Division of Psychology

Prof. Per Svenningsson
Karolinska Insititutet
Department of Clinical Neuroscience
Division of Neuro

Prof. Mats J. Olsson
Karolinska Insititutet
Department of Clinical Neuroscience
Division of Psychology

Opponent:
Asst. Prof. Christina Zelano
Northwestern University
Department of Neurology
Division of Epilepsy & Clinical Neurophysiology

Examination Board:
Assoc. Prof. Pawel Herman
KTH Royal Institute of Technology
Department of Electrical Engineering & Computer Science
Division of Computer Science

Prof. Mikael Johansson
Lund University
Department of Psychology
Division of Psychology

Assoc. Prof. Erika Jonsson Laukka
Karolinska Institutet
Department of Neurobiology, Care Sciences and Society
Ageing Research Center (ARC)

To my parents, grandparents, and beloved wife.

POPULAR SCIENCE SUMMARY OF THE THESIS

The sense of smell starts when you inhale odorants that travel up into the nose where they bind to receptors that in turn send the information about the odors to a structure in the brain known as the olfactory bulb (OB). This area is the first brain area that processes odor information and it is critical to the sense of smell. Specifically, the OB responds to odors by generating brain oscillations (i.e., rhythmic electrical activity in the central nervous system) and sends this information to many different parts of the brain for further processing (including areas important for memory, emotion, and motor activity). Understanding how the OB works is of interest not only because it helps the scientific community to better understand fundamental aspects of human olfaction, but also because the OB is involved in many diseases and may have important clinical relevance. For example, the OB is the earliest area in the brain that is negatively affected by Parkinson's disease (PD), the second most common neurodegenerative disease. The OB is well studied in many animals, such as rodents, but it is at the same time among a few regions in the human brain from where it has been very difficult to measure functional signals and thus little is known about its function in humans. Common neuroimaging methods have problems when recording from the OB in humans because of its location. In this thesis, I have solved this problem and present a non-invasive method for measuring the OB's function using a common active electroencephalography system, a method that measures the electrical activity of the brain, but with a new arrangement of electrodes.

Next, I used this method to answer fundamental questions about how the OB works and what its role is in human olfaction. The most salient finding in this thesis is that the OB in humans and animals partially share similar processes, but that some fundamental features are different. Accordingly, I show that odor valence processing in humans, similar to animals, occurs in two separate stages during the first sniff; one fast and one at a later time point. I further show that the early process seems to facilitate a physical whole-body avoidance response when the odor is perceived as unpleasant. However, besides the similarities of human and animal olfaction, there are also some differences, such as the pace of oscillations appearing in the communication between the OB and the brain area that receives information from the OB, the primary olfactory cortex (piriform cortex).

Furthermore, I show that it is possible to dissociate PD patients from healthy age-matched controls by assessing their OB function. These results indicate that this method may potentially be used as an early biomarker for PD diagnosis. However, olfactory dysfunction is not limited to PD and neurodegenerative diseases and it may also potentially be used to study other diseases. Finally, as a reaction to the current pandemic, where the loss of smell has been identified as one of the most salient symptoms of the novel coronavirus that causes COVID-19, I also studied how odor testing might help its diagnosis. In a large-sampled data, I found that a home-made smelling test, using common household items, can predict the estimated prevalence of COVID-19 in a Swedish population. Taken together, my work shows that improving common brain imaging techniques may have a significant impact on basic research as well as clinical practice.

ABSTRACT

Present neuroimaging techniques are capable of recording the neural activity from all over the brain but the olfactory bulb (OB). The OB is the first olfactory processing stage of the central nervous system and the site of insult in several neurological disorders, particularly Parkinson's disease (PD). It has been suggested that the OB has a pivotal role in the olfactory system analogous to primary visual cortex (V1) and thalamus in the visual system. However, due to the existing technical limitations, there has not been any non-invasive technique that can reliably measure the OB function in humans, consequently limiting its functional recording to one intracranial study dating back to the 60s.

Initially in **Study I**, a non-invasive method of measuring the function of human OB is developed, so-called electrobulbogram (EBG). In line with previous animal literature as well as the only intracranial study in human OB, it was demonstrated that gamma oscillations on the EBG electrodes occurred shortly after the odor onset. Subsequently, applying source reconstruction analysis provided evidence that observed oscillations were localized to the OB. Additionally, the OB recording with the EBG method showed a test-retest reliability comparable with visual event related potentials. Notably, the detected gamma oscillations were demonstrated to be insensitive to habituation, the OB's marked characteristic which has previously been demonstrated in rodents. Last, but not least, assessing the EBG response in an individual who did not have the bilateral OB indicated that the lack of OB results in disappearance of gamma oscillations in the EBG electrodes.

Given that **Study I** determined the possibility of reliably measuring the function of the OB using the EBG, in **Study II**, I assessed the functional role of OB's oscillations in the processing of the odor valence. Odor valence has been suggested to be linked to approach–avoidance responses and therefore, processing of odor valence is thought to be one of the core aspects of odor processing in the olfactory system. Consequently, using combined EBG and EEG recording, OB activity was reconstructed on the source level during processing of odors with different valences. Gamma and beta oscillations were found to be related to valence perception in the human OB. Moreover, the early beta oscillations were associated with negative but not positive odors, where these beta oscillations can be linked to preparatory neural responses in the motor cortex. Subsequently, in a separate experiment, negative odors were demonstrated to trigger a whole-body motor avoidance response in the time window overlapping with the valence processes in the OB. These negative odor-elicited motor responses were measured by a force plate as a leaning backward motion. Altogether, the results from **Study II** indicated that the human OB processes odor valence sequentially in the gamma and beta frequency bands, where the early processing of negative odors in the OB might be facilitating rapid approach-avoidance behaviors.

To further evaluate the functional role of the OB in odor processing, in **Study III**, OB's communication with its immediate recipient, namely piriform cortex (PC), was assessed. These two areas are critical nodes of the olfactory system which communicate with each

other through neural oscillations. The activity of the OB and the PC were reconstructed using a combination of EBG, EEG, and source reconstruction techniques. Subsequently, the cross spectrogram of the OB and the PC was assessed as a measure of functional connectivity where temporal evolution from fast to slow oscillations in the OB–PC connectivity was found during the one second odor processing. Furthermore, the spectrally resolved Granger causality analysis suggested that the afferent connection form the OB to the PC occurred in the gamma and beta bands whereas the efferent connection from the PC to the OB was concentrated in the theta and delta bands. Notably, odor identity could be deciphered from the low gamma oscillatory pattern in the OB–PC connectivity as early as 100ms after the odor onset. Hence, findings from this study elucidate on our understanding of the bidirectional information flow in the human olfactory system.

Olfactory dysfunction, due to neurodegeneration in the OB, commonly appears several years earlier than the occurrence of the PD-related characteristic motor symptoms. Consequently, a functional measure of the OB may serve as a potential early biomarker of PD. In **Study IV**, OB function was assessed in PD to answer whether the EBG method can be used to dissociate individuals with a PD diagnosis from healthy age-matched controls. The spectrogram of the EBG signals indicated that there were different values in gamma, beta, and theta for PDs compared with healthy controls. Specifically, six components were found in the EBG response during early and late time points which together dissociate PDs from controls with a 90% sensitivity and a 100% specificity. Furthermore, these components were linked to medication, disease duration and severity, as well as clinical odor identification performance. Overall, these findings support the notion that EBG has a diagnostic value and can be further developed to serve as an early biomarker for PD.

In the last study, **Study V**, the prevalence of COVID-19 was determined using odor intensity ratings as an indication of olfactory dysfunction. Using a large sample data (n = 2440) from a Swedish population, odor intensity ratings of common household items over time were found to be closely associated with prevalence prediction of COVID-19 in the Stockholm region over the same time-period (r = -.83). Impairment in odor intensity rating was further correlated with the number of reported COVID-19 symptoms. Relatedly, individuals who progressed from having no symptoms to having at least one symptom had a marked decline in their odor intensity ratings. The results from this study, given the relatively large sample size, provided a concrete basis for the future studies to further assess the potential association between the deficits in the OB function and olfactory dysfunction in COVID-19.

In conclusion, our proposed method for non-invasive measurement of the OB function was shown to provide a reliable recording with a potential as a diagnostic tool for PD. Combining EBG and EEG allowed for reconstruction of the OB signal at the source level, where specific oscillations were found to be critical for odor valence processing and rapid avoidance response. Moreover, oscillations in different frequency bands were found to be critical for the OB reciprocal communications and transfer of odor identity information to higher order olfactory subsystems. Finally, COVID-19 was found to be associated with a decline in

olfactory acuity which might originate from damage to the patient’s OB. In conclusion, the results from the studies within this thesis provide a new perspective on the functional role of oscillations in the human OB.

LIST OF SCIENTIFIC PAPERS

I. **Iravani B.**, Arshamian A., Ohla K., Willson D. A., and Lundström J. N., Non-invasive recording from the human olfactory bulb. *Nat. Commun.,* 11, 648, (2020).
doi: 10.1038/s41467-020-14520-9

II. **Iravani B.**, Schaefer M., Wilson D. A., Arshamian A., and Lundström J. N. Valence representation in the olfactory bulb entrains avoidance behavior. *Manuscript on bioRxiv*, (2021).
doi: 10.1101/2021.01.20.427468

III. **Iravani B.**, Arshamian A., Lundqvist M., Kay L. M., Wilson D. A., and Lundström J. N., Odor identity can be extracted from the reciprocal connectivity between olfactory bulb and piriform cortex in humans. *NeuroImage,* 237, (2021).
doi:10.1016/j.neuroimage.2021.118130.

IV. **Iravani B.**, Arshamian A., Schaefer M., Svenningsson P., and Lundström J. N., Non-invasive functional measures of the olfactory bulb dissociate Parkinson's patient from control. *Manuscript*.

V. **Iravani B.**, Arshamian A., Ravia A., Mishor E., Snitz K., Shushan S.,Roth Y., Perl O., Honigstein D., Weissgross R., Karagach S., Ernst G., Okamoto M., Mainen Z., Monteleone E., Dinnella C., Spinelli S., MariñoSánchez F., Ferdenzi C., Smeets M., Touhara K., Bensafi M., Hummel T., Sobel N., and Lundström J. N., Relationship between odor intensity estimates and COVID-19 prevalence prediction in a Swedish population. *Chemical Senses*, 45, 6, (2020). P. 449–456
doi: 10.1093/chemse/bjaa034

LIST OF SCIENTIFIC PAPERS NOT INCLUDED IN THE THESIS

I. Arshamian A., **Iravani B.**, Majid A., and Lundström J. N., Respiration modulates olfactory memory consolidation in humans. *Journal of Neuroscience* 38, 48, (2018), P. 10286-10294;
doi: 10.1523/JNEUROSCI.3360-17.2018

II. Hedblom M., Gunnarsson B., **Iravani B.**, Knez I., Schaefer M., Thorsson P. and Lundström J. N., Reduction of physiological stress by urban green space in a multisensory virtual experiment. *Scientific Reports* 9, 10113 (2019).
doi: 10.1038/s41598-019-46099-7

III. Kaboodvand N., **Iravani B.**, and Fransson P., Dynamic synergetic configurations of resting-state networks in ADHD. *NeuroImage* 207, 116347, (2020)
doi: 10.1016/j.neuroimage.2019.116347.

IV. Tremblay C., **Iravani B.**, Lafontaine É. A., Steffener J., Fischmeister F. Ph. S., Lundström J. N., and Frasnelli J., Parkinson's Disease Affects Functional Connectivity within the Olfactory-Trigeminal Network. *Journal of Parkinson's Disease* 10, 4, (2020). doi:10.3233/JPD-202062

V. Snitz K., Honigstein D., Weissgross R., Ravia A., Mishor E., Perl O., Karagach S., Medhanie A., Harel N., Shushan S., Roth Y., **Iravani B.**, Arshamian A., Ernst G., Okamoto M., Poo C., Bonacchi N., Mainen Z., Monteleone E., Dinnella C., Spinelli S., Mariño-Sánchez F., Ferdenzi C., Smeets M., Touhara K., Bensafi M., Hummel T., Lundström J. N., and Sobel N., A Novel Olfactory Self-Test Effectively Screens for COVID-19. *Manuscript on medRxiv*, (2021).
doi: 10.1101/2021.02.18.21251422

VI. **Iravani B.**, Peter M. G., Arshamian A., Olsson M. J., Hummel T., Kitzler H. H., and Lundström J. N., Acquired olfactory loss alters functional connectivity and morphology. *Manuscript on bioRxive*, (2021). doi: 10.1101/2021.01.11.426175

VII. Schaefer M., **Iravani B.**, Arshamian A., and Lundström J. N., No Evidence That Hormonal Contraceptives Affect Chemosensory Perception. *i-Perception* 12, 1, (2021). doi: 10.1177/2041669520983339

VIII. **Iravani B.**, Arshamian A., Fransson P., and Kaboodvand N., Whole-brain modelling of resting state fMRI differentiates ADHD subtypes and facilitates stratified neuro-stimulation therapy. *NeuroImage* 231, (2021).
doi: 10.1016/j.neuroimage.2021.117844

CONTENTS

LIST OF ABBREVIATIONS

ADC	Analogue-to-digital converter
AE	Active electrode
AP	Action potential
BOLD	Blood-oxygen-level-dependency
DICS	Dynamic imaging of coherent sources
DPSS	Discrete prolate spheroidal sequence
EBG	Electrobulbogram
EEG	Electroencephalography
eLORETA	Exact low resolution electromagnetic tomography
fMRI	Functional magnetic resonance imaging
GEEPI	Gradient-echo echo-planar imaging
ICA	Isolated congenital anosmia
MC	Mitral cell
MDD	Major depression disorder
MEG	Magnetoencephalography
MNI	Montreal Neurological Institute
MoCA	Montreal Cognitive Assessment
OB	Olfactory bulb
OFC	Orbitofrontal cortex
OSN	Olfactory sensory neurons
PAC	Phase amplitude coupling
PAM	Posterior-anterior momentum
PC	Piriform cortex
PCG	Postcentral gyrus
PD	Parkinson’s disease
PSP	Post synaptic potential
RSA	Representational similarity analysis
SNR	Signal-to-noise ratio
TC	Tufted cell
t-PAC	Time resolved phase amplitude coupling

1 INTRODUCTION

It is ironic that one of most well-studied mammalian brain areas to a large degree shapes the sense which we know least about in humans. The olfactory bulb (OB)—a well-defined brain area that is the first central processing stage of the olfactory system has interested anatomist for more than 145 years (1,2). The prominent anatomist Pierre Paul Broca thought little of this area, believing that its small size was a prerequisite for free-will in humans (2,3). Today we know that the OB fulfills a role comparable to both V1 and the thalamus in the visual system, to name a few of its functions (4,5). This information is based on more than 79 years (6) of extensive electrophysiological research on mammalian animal models that have been used as human proxies. Yet, and mainly due to lack of non-invasive brain imaging techniques for the human OB, we still know next to nothing about its neuronal and behavior functions in humans.

A large portion of this PhD project has been dedicated to solving this problem by developing a non-invasive method for OB-measurement. I have subsequently used this method to answer fundamental questions about the human OB in health and disease. In the first part of the thesis, I give a brief review of human olfactory function in health and disease. Next, I will state the specific research aims, the methods, my results, discuss the findings, and finally the conclusions I have reached.

2 LITERATURE REVIEW

2.1 HUMAN OLFACTION

To process odors, vertebrates, including humans, bring the odorant molecules into their body via their nostrils or mouth and transmit this information to the brain. This direct link enables humans, as well as other vertebrates, to rapidly identify the smell and respond appropriately (7).

Humans live in the world of smell as much as they live in a world of sight and sound. However, during the 19th century, humans were considered mostly a visual creature and human olfaction was deemed as an extremely rudimentary sense with a negligible role in our survival (8). Compelling evidences now exist that olfaction is critical to our well-being and survival (2). In fact, humans have a relatively high sensitivity towards odors compared to other animals (9), often more sensitive to certain monomolecular compounds than rats or other primates (10). The human olfactory system is adequately sensitive to distinguish the small differences between odor molecules at the level of a single atom of carbon. For example, heptanol is described as violet, sweet, and woody whereas hexanol, with only one extra carbon atom, is described as sweet, orange, and rose-like (7). Finally, humans can distinguish large numbers of smells (8), although there is no consensus on the exact number, ranging from ten thousand to a trillion odorants (11). The discrepancy in the estimation is mainly due to the differences in the starting assumptions—which can be many—that are needed to determine the number of discriminable odors for humans (12).

2.2 ODOR MOLECULE

Typically, odor molecules are volatiles, or semi-volatiles, with low molecular weight found in nature whose source can be either environmental or biological (13). Contrary to visual and auditory stimuli that can be defined by the wavelength and intensity, the basic odor dimension is yet to be determined. The best scientific candidate for categorizing odors is their structure (7,14,15). Odorants include a wide range of substance classes including esters, carbonyls, and alcohols with diverse structures. Indeed, the structure of an odorant molecule is critical for how the odor will smell. For example, the smell of rot or decay can be connected to the presence of sulfurs in the odor. In contrast a sweet and fruity smell can often be attributed to esters. Even the slightest change in the molecular structure can induce a totally different smell, as can be seen between certain enantiomers of the same molecule (9). A recent study indicated that with as few as 21 physicochemical features of odorants, the perceptual similarity of odors can be predicted with high certainty and used to create olfactory metamers, pairs of non-overlapping molecular composition that evoke similar olfactory percept (15).

Odor molecule structure is not the only factor that changes our percept of odor; concentration of the odor is also important (7). For example, in odor mixtures, the intensity of each component plays a key role for the final holistic perception of the odor object. Accordingly, factoring in the influence of molecular weights for the intensity of each component significantly improves the prediction of odor perception based only on the odors' physiochemical features (15). Also, similar to visual objects and sounds that can be identified independent of lighting/angle of view and volume/pitch, humans can identify odorant identities mostly independent of the general concentration (16,17).

2.3 THE OLFACTORY SYSTEM: FROM RECEPTORS TO THE CORTEX

Olfaction is the oldest sense in the animal kingdom, evolved through billions of years, initially in the form of chemotaxis, to enable organisms to discriminate and recognize a large number of low mass molecules in their environment. Detection of these molecules, mostly related to the organic chemical signals were crucial for survival (18,19). Olfaction is preliminary used by animals to localize food, for example in the form of prey tracking, or to avoid danger, such as predators or toxic food. In humans, perhaps due to modernized lifestyle, the role of olfaction is most evident when it is in combination with taste, where it forms the holistic experience called flavor (20).

Nevertheless, the olfactory system has striking homogeneous morphology across mammal species (21). More than a million olfactory sensory neurons (OSN) are placed in the nasal cavity and form what is called the olfactory mucosa. To encode a repertoire of OSNs in the epithelium, more than a thousand genes are involved which enable humans to perceive potentially seemingly unlimited number of odors (9). The OSNs are bipolar neurons whose, at one end, appending olfactory receptors on the cilia, a short hairlike outgrowth from the OSN cell body, are sensitive to chemicals. At the other end, there are unmyelinated axons that bundle together and cross the cribriform plate, forming the olfactory nerve (cranial nerve I).

The odor receptors transmit signals to higher brain regions (9,18,22). OSN can regenerate and proliferate unlike the neurons in other sensory systems (23). They act as primary neurons in the olfactory system and each responds to a variety of odorants (24). Conversely, each odorant can bind to multiple receptors creating an individual and specific activation pattern for a large body of odors (18,22).

In mammals, inspired odorous air is guided through nostrils towards the nasal cavity where the airborne odorants molecules are bond to olfactory receptors and, by extension, regulate our behavior (9,25). For example, olfaction constantly helps us make decisions in our daily life and modifies our interactions with objects in our surroundings (13,26). While, at the first glance it appears that vision and audition are the dominating senses for humans, losing our sense of smell will have detrimental impact on our everyday life. Patients with anosmia encounter life threatening obstacles in their everyday life due to their sensory loss (e.g., not noticing the smell of a fire in the kitchen). Moreover, several occupations, like chefs and bakers, are largely dependent on their sense of smell (27). Furthermore, individuals with anosmia are also in a higher risk of food poisoning as they are unable to detect the warning smell of spoiled food (27). The inability of perceiving smell is also a possible safety hazard because, for example, smoke and natural gas in the environment remain undetected (28). Anosmia can also result in appetite and weight loss; possibly due to the lack of enjoyment of the eating and drinking (29). Thus, olfaction has an important role to play in everyday life.

Compared to other sensory modalities, the olfactory system is spread over a relatively large section of the head, starting from olfactory sensory neurons in the nasal cavity to deep laying regions in the brain (30). Moreover, olfaction is different from other sensory modalities in several fundamental aspects. First, the primary olfactory cortex, in contrast to the topological organization of sensory cortices (e.g., retinotopic maps in the visual cortex), does not have any known spatial or frequency topographic organization outside the OB (31). Second, the olfactory system, in contrast to all other sensory modalities, lacks a mandatory thalamic rely, with odor information traveling to the neocortex independent of trans-thalamic projections (30–32). Finally, and contrary to other sensory modalities, the information received by the olfactory sense projects mostly ipsilateral in the brain throughout the first processing stages, although the trigeminal system, which interacts with olfactory perception, spreads to the contralateral side. Hence, asymmetry in hemispherical activation depends heavily on the equity between the odor and trigeminal properties of the odorant perceived in the nostril (19).

2.3.1 Olfactory bulb: From neurons to electrophysiology

Beyond the OSNs sits the very first central olfactory structure, known as the olfactory bulb (OB). The relative size of the human OB to total brain volume is small compared to other animals. For example, the size OB in mouse is 2% of its brain volume (33) whereas for human, this is smaller by factor of hundreds to 0.01% of the brain volume (21), **Figure 2-1**. Accordingly, due to this large difference of relative size, it has for a long time been believed, although wrongly, that humans have a poor sense of smell compared to other animals. In spite of the

large variation in relative size of the OB across spices, the absolute number of the neurons in OB is always in a range of 10 million neurons with small variation (2).

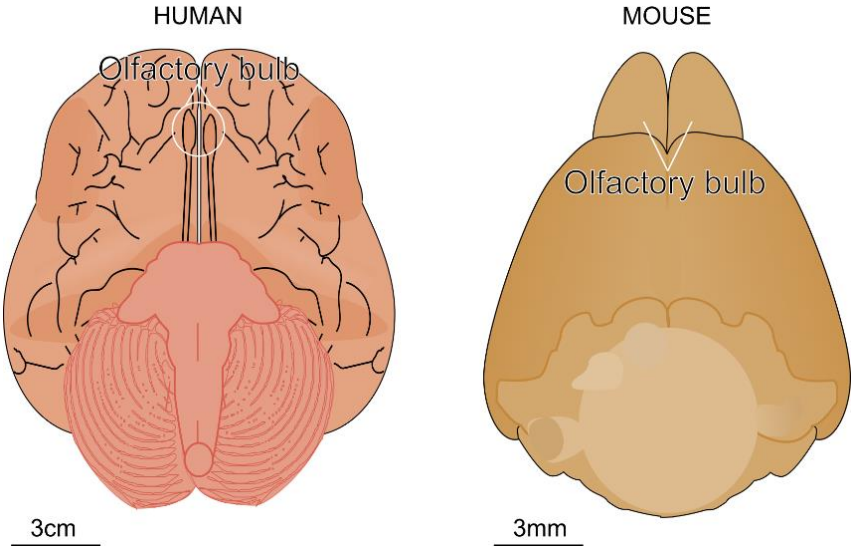

Figure 2-1. *Anatomy of olfactory bulb for human and mouse. The relative size of olfactory bulb in humans is much smaller than in mouse as well as other animals.*

The OB is situated just above the nasal cavity and has both afferent as well as efferent connections with cortex, making it a pivotal hub for the olfactory system (26). Axons of OSN project directly to the secondary neurons of olfactory system laying in OB with fairly specific response to odor classes where OSN axons of same subtypes gather in neuropil encapsulate structures–mirrored in both olfactory bulbs–called glomeruli (34), **Figure 2-2**. The glomerular layer is surrounded by juxtaglomerular cells that include three distinct morphologically cell types: periglomerular cells, external tufted cells, and superficial short-axon cells. Critically, two types of projection neurons–the mitral cells (MC) and the tufted cells (TC) that are interconnected to one another by other neurons in OB (24)–send their axons via olfactory tract to the olfactory cortex (32,35–37), **Figure 2-2**. The OB projections bypass the thalamus and are directly or indirectly received by nuclei in limbic forebrain region (26).

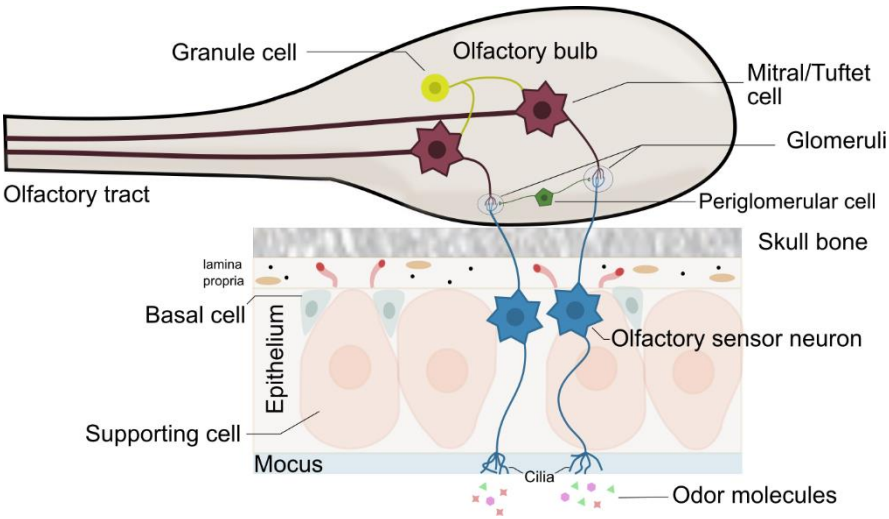

Figure 2-2. *Olfactory bulb is an elongated and cylindrical neural structure, located in the inferior part of the brain. The receptors of olfactory sensor neurons, situated in the epithelium, bond with odor molecules and produce action potentials. The*

same type of olfactory sensor neurons synapse with tufted and mitral cells via glomeruli in the glomerular layer within the olfactory bulb. Further upstream, the mitral and tufted cells, enervate with primary olfactory cortex.

The odor information converts to pattern of spikes from the M/TCs which later is interpreted by higher olfactory regions. Numerous studies have shown that specific combinations of glomeruli are activated in response to a specific odor. This combination of activated glomeruli generates a spatial map of the specific odor reflected in OB that is believed to incorporate odor features. Moreover, animal studies suggested that this spatial map varies as function of time, hence the temporal aspects of these maps contain important olfactory information (32,38,39).

A growing body of evidence in research using non-human animal models suggests close involvement of the OB in the processing of a large list of olfactory tasks. In fact, OB has been suggested to have a functional role within olfactory system akin to both primary visual cortex (V1) (5) and the thalamus in the visual system (4). For example, odor discrimination has been shown to correlate with the extent of activation pattern separation of M/TCs (40). In addition, local field potential recorded from the OB (i.e. changes in power in gamma and beta) in free moving mice has been used as a measurement of odor recognition (41). However, the functional role of OB extends further, including odor segmentation, odor pattern recognition, and many other odor tasks (42).

2.3.1.1 Functional role of the olfactory bulbs in odor perception

The mammalian OB is a layered structure that in a spatially meaningful manner aggregates the action potentials elicited in OSNs (43). Different layers of diverse neurons in the OB serve to adapt signals for further processing in higher order olfactory cortex. Among these layers, the glomerular layer has been known as the fundamental unit of the OB and it is among the brain structures with the highest synaptic density (44). The input from the homogeneous population of OSNs is bundled within glomerular and transmitted to the columnar output neurons of the OB (i.e., MCs/TCs). Moreover, each glomerulus responds uniquely to the odorant inputs (43). The OB in rodents is internally symmetrical; hence, the OSNs project into two mirror segments per bulb (45). Therefore, the total number of the glomeruli in OB is around twice the number of OSN types in the epithelium. However, the spatial organization of human OB has a muddled and less symmetrical arrangement compared with that of in rodents (43,46). For example, glomeruli in the human OB can sometimes be found in deeper spots and layers beyond the habitual glomerular layer. Moreover, the human glomeruli are more heterogeneous and can have different shapes and sizes. The total number of glomeruli in humans does not seem to follow the two-fold rule observed in rodents but it rather corresponds to a ratio of 2-3 glomeruli per OSN type. Odor processing across species at the molecular and synaptic levels resembles one another but it is still not clear how glomeruli in human OB spatiotemporally encode the OSNs' inputs (43,46).

Each OSN excites and inhibits MC through the glomerulus at the same time (47). Theoretical models, such as non-topographical contrast enhancement, suggest that these parallel excitatory and inhibitory routes provide an advantage by modulating the receptive field of the MCs and

maximizing segregation of similar olfactory inputs through contrast enhancement (48). Hence, MCs are only activated when the OSNs with the highest reactivity to a specific odorant are stimulated, whereas the activity of the MCs connected to OSNs with a lesser affinity to the odor appears to decay by the net inhibition (47). Of note, the aforementioned contrast enhancement model, contrary to other proposed models of olfaction, is not dependent on a built-in knowledge of the reactivity level of the glomeruli in response to odors or the physical location of glomeruli within the olfactory bulb (47).

Moreover, the global feed-forward inhibition in the glomerular layer within the OB contributes to the intensity normalization of odors which is imperative to dissociate odor qualities, independent of the changes in the concentration of the input. The network of interconnected glomeruli is believed to follow a "small-world" connectivity pattern. Small-world networks are placed somewhere between regular and random networks. Hence, they tend to cluster as the regular networks but also have shorth path lengths, as found in the random networks (49). The small-word connectivity pattern of the glomerular layer allows for a global estimate of excitation across the OB, given a particular input, which in turn inhibits the MCs and normalizes the activity. Therefore, the OB output reflects relative rather than absolute activity (47). In addition to the spatial distribution of the OB response to the odors, the temporal dynamics of the response also inform the odor coding. These temporal dynamics at the population level emerge as oscillations that are often measured using either invasive (e.g., local field potentials) or non-invasive (e.g., EEG) electrophysiological methods.

However, OB's processing is not limited to the odors alone and its functional role extends to respiration as well. Importantly, even when there is no odor, the mammalian olfactory sensory neurons detect mechanical pressure caused by airflow in the nostrils (50) and send this information to the OB, which in turn generates oscillations that prepare the olfactory system for incoming odors (51,52). Ablation of the OB blocks respiratory-induced oscillations in the rodent brain (53). Moreover, nasal versus oral respiration in humans, where in the later respiratory method OB is bypassed, has implication in odor memory consolidation (54), and shapes oscillations within the limbic network and as well as episodic visual and fear memory (55). That said, the OB's functional role in processing of respiratory input is beyond the scope of this thesis.

2.3.1.2 OB electrophysiological response to odors

In rodents, the incoming signal from odorants to the OB induces gamma oscillations that mostly reflect intra-bulb processes (56). Nonetheless, other frequencies have been observed in OB, including beta and theta, each with a specific function (56). Beta oscillations are believed to be involved in the context of odor associations (57). Relatedly, only gamma, but not beta, oscillations are maintained when the centrifugal input to the OB is blocked (58,59). Oscillations in the gamma and beta bands jointly assist the exchange of odor information between different structures of the olfactory system, such as OB and piriform cortex (PC), the immediate structure after the OB, upstream of olfactory processing. Accordingly, different gamma and beta band can drive connection in a certain direction, but not exclusively, and are

dependent on the odor task. For example, beta oscillations are involved in the bottom-up connection but the directionality of the beta band shifts during odor sampling (60). Finally, theta rhythms in OB, which adopt their name due to their overlap in frequency with hippocampal theta oscillations, are stimulus driven and mostly relate to respiration (51,61). For example, intracranial recordings from humans suggest that the theta oscillations in the PC are synchronized with respiration (55). However, the theta-band activity is not exclusive to respiration but also involved in odor processing (62). Contrary to the PC, little is known about oscillations in the human OB due to the difficulties of non-invasive recording from this brain structure. With that said, in late 1960s, an electrophysiological study of OB function in humans - limited to just one intracranial electrode implanted in 11 individuals - showed that different combination of frequency components is needed to code odor quality. Hughes and colleagues (1970) found gamma oscillations in the OB in response to different categories of odors. This oscillation can be seen as one of the most striking sensory induced rhythms in the brain that had been originally defined by Adrian (6,63) and studied in non-human species. Later, among the earliest electrophysiological studies of the human olfactory system, Sem-Jacobsen and colleagues (1953) implanted an electrode at the vicinity of the OB in a patient and observed burst of high frequency waves when the patient smelled odors (64). Given that there has previously not been a non-invasive method to measure the function of human OB, for a long time, the seminal works of Sem-Jacobsen et al (1953) and Hughes et al (1969) remained the only known publications that directly, as well as indirectly, obtained functional measures from the human OB.

2.3.1.3 Human OB volume

While little is known about the human OB electrophysiology. More is known about how its volume relates to behavior. For example, It has been demonstrated that the volume of the OB is correlated with olfactory functions (65). Accordingly, it has been indicated in several past researches that the depression score/symptom correlates with the olfactory function (66,67). Specifically, decrease in the OB volume was reported in major depression disorder (MDD) and the volume of the OB negatively correlates with depression score (68). Critically, it has also been demonstrated that OB anatomy–both volumetric and cellular– undergoes dramatic changes following Parkinson’s Disease (PD) (see more on the effect of PD on OB function and anatomy below).

2.3.2 Piriform cortex

PC, the largest and arguably critical structure of mammalian olfactory system, is involved in a range of fundamental perceptual and cognitive odor processes, including odor quality discrimination, memory, learning as well as motivation (69,70). Most of OB projections are received by the PC. However, OB also projects to other regions, including the anterior olfactory nucleus, the olfactory tubercle, the enthorhinal cortex, the periamygdaloid cortex, and several areas within the amygdala (30).

The PC encompasses the anatomical junction between the frontal and temporal lobe where the choroidal fissure splits it into two segments, one in frontal lobe, known as anterior part, and the other in temporal lobe, so-called posterior segment (71). It has been demonstrated that the anatomical heterogeneity of PC also mirrors in its function. The functional diversity of anterior and posterior PC has been the subject of several past studies (72–74). A brief overview of PC function is given in the following section.

2.3.2.1 Functional role of the piriform cortex in odor perception

PC is the main source in the olfactory cortex that provides top-down modulation to the OB (75), and possibly rectifies odor maps across the OB. The fine-tuning of sensory input has also been observed in other systems. However, the feedback in the olfactory system is different compared to the other sensory systems where neocortical feedback is received by thalamic nuclei. Accordingly, in the olfactory system, the primary sensory input is directly projected from the OB output neurons to the PC, without being relayed by thalamus (43).

In the bottom-up pathway, PC acts as a divergent-convergent layer which allows the OB's output neurons to enervate to a large number of neurons within PC. Interestingly, propagation of information to the PC does not seem to follow any topographic principle (76). Hence, there is no specific spatial pattern induced by odors in PC. To give an instance, the probability of activation of two adjacent neurons within PC for two similar odors is similar to two different ones. Consequently, for a given odor, scatter neurons across the PC process the odor features that are outlined by the OB and subsequently initialize the formation of odor objects.

Following the notion that PC is anatomically and functionally heterogeneous, it is worth mentioning that the OB projects to both anterior and posterior parts of the PC (46). The anterior portion is thought to code the molecular structure of an odorant as well as the odor valence (74), an odor dimension closely related to molecular structure (14), while the posterior PC is thought to code the quality of the odorant (77). Moreover, it has been demonstrated that the attentional modulation appears in the anterior but not the posterior PC (72), and this modulation may be due to the centrifugal connections between PC to the OB. A predictive odor-specific pattern forms in the posterior PC that might relate to behavioral performance (73).

A large number of functional magnetic resonance imaging studies using blood-oxygen-level-dependency (BOLD) to non-invasively assess the function of PC, particularly anterior and posteriors segments, as well as PC's functional connectivity, have showed that PC is connected to multiple areas in the brain (78). However, acquiring PC's BOLD activity is not always a trivial task considering the signal loss due to susceptibility artifacts at ventro-temporal areas adjacent to PC (79). Moreover, another confound, specifically in olfactory research and regardless of the modality of recording, is the early occurrence of habituation to the odor stimuli (80). In light of this, it has been shown that short odor presentation favors signal amplitude in PC compared to longer one (71). Despite these confounds, PC has been cited as the most consistently active region in response to odors in neuroimaging studies (30).

In addition to functional magnetic resonance imaging (fMRI), studies of the PC have also used intracranial recordings; however, they are far fewer in numbers due to the inherent difficulties and the ethical concerns of such recordings (55,62,81). Contrary to fMRI, intracranial recordings, and their closely related methods, such as electroencephalography (EEG) and magnetoencephalography (MEG), have excellent temporal resolution in the order of milliseconds, which makes them good candidates for studying brain oscillations. For example, it has been shown that odor-related oscillations in the PC are particularly evident in slower frequencies, namely the theta-band (62). Specifically, the theta amplitude can be used to decipher the odor information content within a few hundred of milliseconds after the odor onset (62).

It should be noted that while this thesis has been focused mostly on the OB and to a minor extent on another prominent structure of the olfactory system, that is the PC, the central olfactory system is not limited to these two structures but as mentioned earlier, it stretches out to other areas including the anterior olfactory nucleus, the olfactory tubercle, and as well as to the secondary olfactory cortex.

2.4 PROBLEMS ACQUIRING FUNCTIONAL ACTIVITY FROM THE OLFACTORY BULBS

In humans, the olfactory bulbs are located in the inferior rostral part of the brain where they are placed close to hollow air-filled structures known as paranasal sinuses. The sinuses support the respiratory system with humidify, warming the inhaled air, and produce mucus (82). However, when it comes to neuroimaging techniques, the sinuses play a disruptive part. The juxtaposition of tissue and air creates discrete magnetic permeability of the medium. This inhomogeneity causes problem, especially in fMRI where the gradient-echo echo-planar imaging (GEEPI) is used. GEEPI is based on micro magnetic field changes due the susceptibility effect of the oxygen level of blood. However, it is also sensitive to other type of inhomogeneity and, as mentioned before, there is a large non-uniformity of magnetic permeability of the medium close to sinuses and that causes dropout in readout signal (83). Therefore, obtaining fMRI from OB is inherently difficult with today's methods. Positron emission tomography (PET), contrary to fMRI, is immune towards presence of air in sinuses close to olfactory regions (84); however, the method needs a radioactive isotope paired with a biological molecule to make a radiotracer and it is delivered to blood stream by means of injection. Compared to 1-2% change in fMRI signal, the signal change receives with PET scan is approximately 10% and it is more evident. However, there are some significant drawbacks associated with PET imaging. First, costs are high because the radio tracer needs to be produced on site due to its short half-life. Second, and more relevant to OB imaging, it has a very low temporal resolution compared with other neuroimaging methods (85). Therefore, it is not the optimal choice for rapid, short living phenomenon, like the ones seen for early stages of odor perception. Third, PET also requires that a radioactive substance is injected into the human body (85).

The use of neuroimaging tools, such as MEG and EEG, have played a pivotal part of brain research during the last decades. These techniques allow researchers to study a wide range of

perceptual and cognitive functions in health and disease (i.e., pathophysiologic states) in vivo. Whereas fMRI measures the relative slow BOLD response, both MEG and EEG measure direct neural activation with high temporal resolution (86,87). Specifically, MEG and EEG each measures different aspects of the same ionic current source, with MEG recording the neural magnetic activation, while EEG records the neural electrical activation (88–90). The post synaptic potentials of a synchronous activation of population of neurons form electrical and magnetic fields that are sensible to EEG and MEG at the scalp level (91). However, these fields get attenuated and distorted as they travel through different tissues on their way to the scalp, a distortion that is graver for electrical fields (EEG) as compared to magnetic fields (MEG) (90).

Electrophysiological cortical responses can be divided into evoked and induced responses based on the phase of the response in respect to the stimulus. Evoked responses are phase locked to a stimulus whereas the induce responses are not (92,93). To date, neither MEG nor EEG have not been used to assess OB's function in humans. Studying olfaction using methods with high temporal sensitivity is naturally difficult given that chemicals reach OSN with different speeds based on their molecular weight and volatility as well as the arrival of odorants is also dependent on the respiration pattern. For example, small variations in respiration seem to change the latency of the signal in the OB or, in other word, the phase of responses from trial to trial and confound evoked responses in OB. However, an induced response in OB is less affected by potential variations in respiration. Another possible approach to presenting odors is to use passive odor presentation where the odorants are blown into the nostrils regardless of the respiration cycle. However, this approach has a lower ecological validity. Hence, to capture the OB response and to maintain the ecological validity of the experiments throughout this PhD project, we focused only on the induced response of the OB.

As mentioned above, MEG and EEG are two methods with the highest temporal resolution. However, MEG is only sensitive to tangential sources whereas EEG can detect both tangential and radial sources (94). There is no knowledge of how dipole orients in OB. However, if we consider the anatomical orientation of OB and the olfactory tracts there is a high possibility that the majority of dipoles form along the radial direction, a direction which MEG cannot detect. The other problem with MEG is a poor sensor coverage on frontal regions close to OB (95). However, recent cutting-edge research has proposed magnetic field sensors that can operate at room temperature, and thus remove the urgency of having a MEG helmet (96). Without a helmet, it would be possible to have sensors close to the OB on the forehead. However, at the moment this technique is only at the experimental stage and very expense to conduct.

This leaves EEG as the potential best technique to image and record signals from the OB. Electrical activity on the scalp level can be measured with small size electrodes. Contrary to fMRI, this electrical field is not distorted by air cavities and EEG electrodes can easily be placed above any desired area. Furthermore, the high temporal resolution in milliseconds makes it sensitive to rapid and short-lived signals. However, to date, there are no known attempts to use EEG/MEG to record from human OB.

2.5 APPROACH AVOIDANCE IS A CORE OLFACTORY BEHAVIOR RESPONSE

Aversion and attraction are behavioral responses critical for the survival of any organism. In the olfactory context, what greatly shapes these behavioral responses is odor valence. Accordingly, odors with positive valence, such as food odor, are attractive whereas odors with negative valence are aversive and warn of a potential danger. Hence, it is believed that the first principal dimension of perceptual space is valence (26). Humans spontaneously use odors valence to either discriminate odorants (97) or combine them into groups (98). Interestingly, both studies on non-human animals (99) as well as human infants (100) suggest that part of odor valence processing is innate. Particularly, newborns express disgust face encountering butyric acid – an odor rated unpleasant by adults – compared with pleasant vanillin odor (100). Nevertheless, change in hedonic response can occur after mere exposure, more familiar odors are for example more likable; however, this association is odor dependent meaning that not all familiar odors are rated pleasant (13). More precisely, experimental studies suggest that mere exposure to odors shifts the hedonic value of odor to neutral level rather than towards the positive end of the valence scale (13,101).

Beyond mere exposure that can change the hedonic value of an odor, pairing with another chemical sense, namely taste, can also change the valence level (13). Odors, together with tastes, form a special bond that is known as flavor, a holistic experience that occurs in our mouth during food consumption. According to the associative learning theory, repeated exposure of odor-taste is believed to change the hedonic value of an odor. In light of this, several past studies found that pairing odors with sucrose shifts the odors towards the positive end of the valence scale (102,103). However, in a recent study with a larger sample size, no evidence was found for associative learning between odor and tastes, thereby suggesting more research in this area is needed to draw conclusive evidence (104).

Moreover, stimulus evaluation is modulated by the interplay between intensity and valence of the sensory input (105). For example negative stimuli (picture of a snake or spider) are typically rated as more intense and arousing compared to positive ones (picture of a puppy) (106,107). Also, stimulus with a specific negative valence (e.g. high pitch noise) becomes more negative as the volume intensifies (louder noise is more unpleasant than the one with lower volume) (107). However, the intensity and valence of olfactory stimuli are more independent from one another compared to that of vision or audition (107,108). For example, odors can have low and high concentration but virtually maintain their valence level. Accordingly, there may be weak negative or positive odors as well as strong negative or positive odors. However, it is worth noting that the relative independence of intensity and valence might only be valid for a certain range in the perceptual space that is not falling into the extreme ends of the scales. In light of this, it can be assumed that the intensity and valence of odor stimuli are relatively independent which makes odor the best candidate to disentangle arousal, if approximated as the intensity of odor, and valence (108).

2.5.1 Olfactory nervous system response to odor valence

There is psychophysiological evidence that odors with different hedonic values are processed differently (109). Valence-based change in the processing of odors can be observed at both the peripheral and central level.

On the peripheral level, odor valence ratings have been found to be associated with autonomic nervous responses. For example, electrodermal activity, or as it is better known as, skin conductance response, is associated with arousal index of odors (110). Arousal and valence of odors have an overall U-shape relationship (111). Consequently, the odor arousal can be interpreted as magnitude of odor valence, regardless odor being positive or negative (110), emphasizing that odors at both ends of the valence scale have higher processing value.

On the central level, it has been demonstrated that odors with more negative valence are processed with higher speed (112). Specifically, hedonic value of odors is found to modulate the amplitude of startle reflex such that unpleasant odors increase, and pleasant odors decrease, the amplitude response of the startle reflex (113). There are compelling evidences that pleasant and unpleasant odors elicit activity in dissociable neural substrates; a finding that is reported both in functional neuroimaging studies (74,114,115) and electrophysiological recordings (116–118). For example, a past meta-analysis, including fMRI and PET studies, demonstrated that the core olfactory valence processing network includes bilateral parahippocampal gyrus/amygdala, the left middle frontal gyrus, the right middle frontal gyrus/lateral orbitofrontal cortex (OFC), and other regions (115).

It is yet unclear if the process of odor valence begins earlier in the chain of process, for example in the human OB. However, in rodents, negative odors have been indicated to modulate the activity of MCs in OB (119). Moreover, OB has been demonstrated to have a special function in processing of stimuli that are innately associated with threats (99). Thus, it could be speculated that the human OB also processes odor valence to some degree.

2.6 PARKINSON'S DISEASE AND OLFACTORY IMPAIRMENT

Five percent of the population suffers from total olfactory impairment (anosmia). Total olfactory impairments can be divided into congenital or acquired anosmia. The most common reason for acquired anosmia/hyposmia is age related changes and it affects both sexes; however, more men than women are affected in all age groups, even before puberty (120,121). Twenty-five percent of individuals above 50 years suffer from olfactory dysfunction and it appears to have inverse correlation with life expectancy, where people with more severe olfactory impairment have lower life expectancy (120,121).

Trauma, viral infection, and other nasal causes can be the reasons of acquired anosmia in addition to smell dysfunction associated with neurological disorders, such as Parkinson Disease (PD) or Alzheimer Disease (120).

More than 90% of PD patients during the early stage of the disease show significant olfactory impairment (122,123). A growing body of evidences shows that olfactory dysfunction in PD

exists from the earliest stages of the disease regardless of olfactory task (i.e., odor detection, identification, discrimination, or odor memory) (123). However, it has been shown that olfactory dysfunction does not correlate with the duration or severity of PD (124). Additionally, there is no evidence that the common medication that is used to alleviate motor symptoms of PD, namely *Levodopa*, has any positive effect on olfactory disturbance (125).

2.6.1 Parkinson's disease and the olfactory bulb

The presence of an early olfactory dysfunction in PD patients has prompted researchers to study the olfactory system, and specially the OB, in relation to PD. However, the lack of existing non-invasive recording methods has hindered researchers to contemplate an inexpensive olfactory test with a direct measurement of the underlying impaired neural function to differentiate PD patients from healthy individuals early on in their disease. Especially, a test that is not affected by the patient's general cognitive ability. This is problematic as the OB, and related impairment of olfactory functions, might be one of the earliest areas and functions to be negatively affected across a variety of brain disorders, such as multiple sclerosis, Huntington's disease, Alzheimer's disease, and importantly, PD (126). Besides the characteristic motor symptoms, PD is associated with non-motor symptoms that occur years earlier. Loss of the sense of smell, either partially or completely (hyposmia or anosmia), is one of PD's non-motor symptoms that occurs in 95% of the patients and, critically, precedes the motor symptoms by many years (127,128). It has been hypothesized that the cause of such olfactory loss in PD is related to the early pathology that occurs in the OB (123).

Most of past behavioral studies substantiate a lack of association between the duration or clinical severity (quantified by Unified PD rating scale; UPDRS) of the disease and olfactory disturbance (123,129,130). However, studies have found that specific electrophysiological measures correlate with PD severity, namely the latency of the late evoked related potential (P3), yet nothing has been directly linked to OB. (131). The fact that electrophysiological measures from the scalp correlate with severity of PD is a promising finding. Nevertheless, these measures do not target the OB and might not be sensitive to the small deterioration in olfaction that might be indicative of an early detection of PD. This is important as there is a large body of evidence suggesting that the olfactory system is negatively affected in PD. First, the accumulation of *Lewy bodies* and *Lewy neurites* in dopaminergic pathways, while these pathways are associated with the olfactory processing (e.g., amygdala, cingulate gyrus, and other regions). Second, the post-mortem studies of PD patients demonstrated an increase of dopaminergic neurons in the OB. Moreover, the glomerular volume decreases to the half in PD compared to that of a normal brain. Third, the distribution of the cells along the dorsal-ventral dimension of the OB alters in PD (132). Relatedly, there are higher metal deposits in the OB of PD patients' brain compared to healthy individuals (133). Taken all together, these findings support the involvement of the central olfactory system in pathophysiology of PD (134,135).

PD is most often associated with neuron loss, therefore increase in the neural population within the OB seems to be counterintuitive because usually impairment is linked to decrease in

number of neurons. However, these neurons are inhibitory and overpopulation of them is believed to be the reason for hyposmia in PD patients. Nevertheless, no association has been found between the boost in number of dopaminergic neurons and PD's medication (e.g. levodopa) which shows that the increment is part of the disease pathology (135).

PD is connected tightly with α-Synuclein (i.e., a protein in the brain) pathology in the basal ganglia structure known as substantia nigra. Same type of pathology has been reported in the OB and can differentiate PD patients from healthy individuals with high degree of confidence (123,136,137). The microtubule-associated protein, so-called tau, is the other pathology linked mostly to Alzheimer Disease but also has been found to colonize in the anterior olfactory nucleus in PD (138). In addition, there is evidence from research in transgenic mice that overexpressed human tau in the OB may also lead to olfactory dysfunction (139).

Several attempts have been made to use odor related electrophysiological measures as an objective test of olfactory performance in post-traumatic dysfunctions (140), neurodegenerative disorders (123,131,141,142), or to assess recovery of olfactory functions (143,144). In all of these studies, latency of odor evoked related potentials is found to correlate with olfactory performance. Moreover, a MEG study showed that odor related change of a connectivity measure (i.e., synchronization likelihood) can differentiate PD patients from control. However, it failed to show any change in power across frequency bands (145). Moreover, in all these studies, the source of the underlying signal has probably been secondary cortex regions and not the OB. In summary, it is predicted that more than 9 million individuals will be affected by PD all over the globe in 2030, yet the cause of this neurodegenerative disease remains unclear and there is no direct way to screen for early PD. Thus, enabling a way to measure the OB would be a major breakthrough in the neuroimaging and early diagnosis of PD.

2.7 COVID-19, EMERGING CAUSE OF OLFACTORY IMPAIRMENT

Upper respiratory infection has been known to be the most common reason for persistence olfactory impairment (hyposmia or anosmia) (146). It is well-known that a reduced OB volume is common in post-viral olfactory loss (147). Different strains of pathogens can cause upper respiratory infection that leads to post-viral anosmia, including the novel coronavirus (SARS-CoV-2) that appeared in 2019 and created a worldwide pandemic (148). A meta-analysis on ten recent studies indicated that 52.73% of COVID-19 patients develop anosmia. Importantly, the prevalence of anosmia is significantly more in the mild cases compared with moderate-to-critical forms (149). Hence, anosmia is considered as an early and common symptom of COVID-19 (149). Although, 95% of patients regain their olfactory function after 6 months (149), given the magnitude of infected individuals around the globe, a considerable increase in the number of individuals with anosmia is expected in the coming years. It is too early to conclude the cause of the anosmia in COVID-19; however, some evidences are pointing to impairments in the micro-structures of the central nervous system (150,151) as well as peripheral causes (151). A recent postmortem study indicated the highest concentration of SARS-CoV-2 genetic materials in olfactory mucosa in epithelium, that is in the vicinity of neurons in the OB, as well as in some cases directly in the OB (152). Given the reported neurological symptoms

of COVID-19, especially anosmia, it is probable that SARS-CoV-2 uses the mucosa-neuronal interface to enter the brain (152) and causes a potential damage to OB. This is in line with the previous finding where it has been demonstrated that SARS-CoV, a closely related virus to the novel corona, can invade OB from the nasal cavity in mouse model (153). In view of this finding, OB edema in COVID-19 patients has also been reported in several recent researches (154–156). The infection per se is capable of damaging neurons in the OB but also the impairment can occur due to immune response or combination of both (155). Moreover, there are some tentative indications that the OB undergoes atrophy and its volume decreases during a COVID-19 infection (157,158). As a first step to study the relationship between COVID -19 and the sense of smell it is important to establish a relationship between early symptoms of smell loss and COVID -19 in the population.

3 RESEARCH AIMS

In this PhD thesis, we aimed to increase our understanding of the function of the human OB, the first and one of the most prominent structures of the central olfactory system. The OB has been well studied in the rodents. In sharp contrast, studies on the functional processing of the human OB are rare which, at the time of writing this thesis, have been limited to one intracranial study with small sample size back in the late 60s (159). The main reason that hinders researchers to study OB in humans is that there is no non-invasive method to measure functional signals from the OB. Moreover, due to ethical concerns, intracranial studies on OB are extremely rare. Therefore, in **Study I**, a non-invasive EEG-based recording method was developed to study the function of the human OB. The proposed method was subsequently used in **Study II-IV** to answer the research questions asked in these studies. Moreover, in response to an ongoing pandemic where olfactory dysfunction served as a prominent symptom, **Study V** was conducted where the potential link between olfactory dysfunction and COVID-19 was assessed to provide a basis for further research on the possible pathology of SARS-CoV-2 on OB.

3.1 NON-INVASIVE RECORDING FROM THE HUMAN OB

3.1.1 Study I

The primary aim of **Study I** was to develop a valid and reliable method, allowing for recording of functional signals from the OB in response to odors at the sensor level. To achieve this aim, we only focused on the induced response in the OB rather than the evoked response. Next, we used a localizing framework to confirm that the observed activity on the sensor level was indeed produced by the OB. We subsequently assessed the test-retest reliability of the measure in a separate dataset over three sessions. Moreover, we replicated the most robust finding of the OBs function in the animal literature and eventually evaluated a human lesion model.

3.2 BASIC KNOWLEDGE OF OB FUNCTION IN ODOR PROCESSING

After we developed a reliable method to measure OB responses to odors, in two separate studies, we next used this measure to study fundamental functions of OB in the processing of odors:

3.2.1 Study II

First, in **Study II**, we aimed to assess how odor valence is processed in the OB. To this end, we used the developed method to extract the OB time-series and assessed the relationship of the OB function and odor valence ratings using state-of-the-art methods of second order isomorphisms. The subsequent aim was to evaluate whether avoidance response to odors was related to OB functional processing. This aim was answered in two steps. First, we established the temporal and functional relationship between valence-driven OB activity and motor cortex activity. Second, based on the neural data, we assessed the temporal structure of full-body approach-avoidance movement and how it matched the neural results. We did this using a force plate while odors with different valences were presented to participants. Critically, the temporal

aspect of negative valence coding in the motor cortex matched the timing of full-body avoidance movement to unpleasant odors.

3.2.2 Study III

The aim of **Study III** was to characterize the functional and effective connectivity between the OB and PC, the main recipient of OB projections, across time and frequencies with the help of our developed method. This assessment allowed to establish the role of this connectivity in odor coding. Accordingly, we showed a bottom and top-down information exchange between OB and PC. Importantly, the critical time and frequency intervals for odor information exchange between OB and PC were identified using a machine learning method demonstrating that there was enough information to decipher odor identity from the OB-PC oscillatory circuit.

3.3 OLFACTORY MEASURES AS A CLINICAL DIAGNOSTIC TOOL

Olfactory dysfunction has been cited as a common symptom in several diseases, including neurodegenerative diseases (e.g., PD). One of the possible applications of our developed method for the functional assessment of the OB is diagnostic purposes. Olfactory impairment is one of the early symptoms of PD which stems from the fact that OB is one of the first sites of insult in PD (123,160).

3.3.1 Study IV

The aim **Study IV** was to assess whether the EBG method can be used to differentiate PD patients from heathy age-matched control participants. The sensitivity and specificity of the EBG-based method were compared against a clinical odor identification test. We demonstrated that the measure could differentiate PD patients and moreover that we could establish a relationship between the EBG measure and individual clinical PD parameters, such as disease duration, severity, and medication.

3.3.2 Study V

As mentioned above, odor dysfunction is not exclusively a symptom of neurodegenerative disease. Notably, soon after the outbreak of a novel respiratory viral infection (SARS-CoV-2) in 2019, anecdotal evidence emerged suggesting that olfactory dysfunction was a major symptom of COVID-19. In the course of time, olfactory dysfunction was established as a salient and possibly early symptom of COVID-19 (161,162). **Study V** of this thesis was dedicated to this novel virus and its impact on olfactory performance. At the time of writing this thesis, it was not yet conclusively determined how SARS-CoV-2 affects the olfactory system and whether the damage to the olfactory system is peripheral or central. The main aim of **Study V** was to assess whether odor intensity estimates could be used as an estimate of COVID-19 prevalence in the population. Moreover, this study establishes a model for future work to assess the pathology of olfactory impairment in COVID-19 using at home testing in large populations.

4 MATERIAL AND METHODS

4.1 PARTICIPANTS

Three cohorts of participants were studied in this PhD project, including two groups of healthy individuals with normal olfactory function, namely normosmics, from two different age distributions, explicitly young and older healthy adults. Moreover, a group of PD patients was the third cohort of interest in this PhD project. In addition to the above-mentioned cohorts, one individual with isolated congenital anosmia (ICA) was also tested as a control experiment in **Study I**.

Young healthy individuals were recruited through Karolinska Institutet's recruitment system (kibehavioraltesting.sona-systems.com) and formed the largest cohort in this project. We collected EEG recordings from 69 young healthy individuals through three data collection phases. The first phase of young healthy data collection included recordings from 29 individuals (age = 27.07 ± 5.30, 18 women) included in the first experiment of **Study I** and **Study III.** In the second phase, 19 healthy young individuals (age = 28.88 ± 4.52, 7 women) were recorded through 3 seemingly identical sessions, of whom data from 18 individuals were used in the second experiment of **Study I** (one individual was removed due to poor scalp electrode signal) and the data from all 19 individuals were used in **Study II**. Multisession recording from all individuals enabled us to acquire enough clean and a set of large recursive data points per individual, thereby making it suitable for test-retest reliability analysis in **Study I** and representational similarity analysis (RSA) in **Study II**. In the third phase of the young healthy cohort's data collection, 21 individuals (age = 29.55 ± 5.59, 11 women) were tested and used in the third experiment of **Study I**.

In the fourth experiment of **Study I**, a 27-year-old male who was diagnosed with ICA, but otherwise healthy, by an ENT physician within the Swedish healthcare system was recruited and studied. His inability to identify, discriminate, and detect different odors was confirmed by us using clinical olfactory testing. Additionally, T1-weighted and T2-weighted MR images of the individuals were used to find morphological indicators that characterize congenital anosmia, including lack of bilateral OB and having an average olfactory sulcus depth below 1.12 mm.

For the second experiment in **Study III,** a pilot experiment was initially carried out to pinpoint the time interval relevant for the full body approach-avoidance response. The pilot experiment entailed recording of full body posture of 21 healthy young individuals (age = 28.71 ± 5.84, 11 women) in response to odors with positive and negative valence using a force plate to explore the different time points post stimulus. Subsequently, in the main experiment, 47 healthy young individuals (age = 25.94 ± 4.2, 29 women) were assessed to test the specific and preregistered hypothesis generated by the pilot experiment.

In **Study IV**, a total of 40 individuals from two cohorts, namely PD patients and healthy older adults, were enrolled in the experiment. Two individuals from the healthy control group were

unfortunately forced to be excluded due to poor EEG signal quality. Hence, the final sample included 20 PD patients (age = 46-75, 4 women) and 18 age matched healthy normosmics (age = 41-74, 4 women); so-called Control group.

Finally, in **Study V,** data from 2930 unique individuals were collected through a web-based platform https://smelltracker.org/. In the analysis, we removed 33 individuals who were below 18 years old, 374 individuals who did not rate any odors, and 83 individuals who rated all odors' intensities above 95 on a 0-100 scale. Hence, the final sample included 2440 individuals (age = 47.4 ±14.11, 1680 women).

All designated healthy participants included in **Studies I-IV** declared themselves as generally healthy, non-smokers, with no history of head trauma leading to unconsciousness or neural disorder, except PD patients. However, not all participants included in **Study V** were healthy. A total of 1668 individuals indicated that they had at least one of the common COVID-19 symptoms including Fever, Cough, Shortness of breath or difficulty breathing, Tiredness, Aches, Runny nose, Sore throat, Loss of the sense of smell, and/or Loss of taste at the time of testing. A total of 772 individuals indicated they had no symptoms and identified themselves as healthy subjects during the recording sessions. Moreover, all participants in **Studies I-IV** signed informed consent prior to their participation in the experiments and participants in **Study V** agreed to Terms of Use prior to creating their accounts on the website and entering their responses.

4.2 COVID-19 POPULATION PREVELANCE

The data on the prevalence of COVID-19 from March to April 2020 was obtained from the Public Health Agency of Sweden (Folkhälsomyndigheten). The prevalence model of COVID-19 in the Stockholm population over time that they provided, was estimated based on randomly sampled individuals (n = 738) in combination with available data from the health care system as well as the estimated contagion factor of the SARS-CoV-2 virus.

The assumption of the model included 98.7% unreported cases with infectivity rate of 55% compared to the reported cases. Model details, raw data, scripts, and figures for Folkhälsomyndigheten's model (version 2) used as a predictor in **Study V** can be found on an open data repository: https://github.com/FohmAnalys/SEIR-model-Stockholm.

4.3 OLFACTORY TESTING

Self-assessment of olfactory ability does not accurately correspond with objective olfactory measures. Consequently, it is imperative to quantitatively test the functional ability of participants to rule out the accidental assignment of individuals with anosmia or hyposmia as individuals with a normal sense of smell. Given the prevalence of olfactory dysfunction in older adults (121), an objective olfactory assessment matters even more in cohorts of older adults.

The most common method for olfactory evaluation is the olfactory identification test using alternative force choices. The functional olfactory ability of all the individuals participating in

the studies of this thesis was assessed prior to the main experiments using a subset of well-known olfactory performance tests, the Sniffin' Sticks (163). Sniffin' Sticks consist of flat tip pens containing odor instead of ink. In the odor identification test, participants are presented with a Sniffin' Stick at the time along with corresponding cue cards with names of four objects with familiar odor. Participants were asked to determine which one of the four objects on the cue card corresponds with the odor of presented Sniffin' Stick. A subset of only five odors from the 16-item odor identification test were used in **Studies I-III**. Given the young age-range of the tested cohort, and the scarcity of anosmia in this age range, the probability of erroneously assigning individuals with anosmia as healthy controls is less than 0.05%. To reduce testing time and avoid fatigue during the main EEG recording session, a shorter version of the olfactory test was carried out in **Studies I-III**. However, in **Study IV,** to increase the accuracy of the olfactory test in the older adult cohort, among whom the olfactory dysfunction is more common, a 16-item test was used.

In **Study V**, self-odor assessment with household items was conducted during which each participant picked a total of five odors from 5 different categories and total of 70 various odors to rate. In each category, there was a fixed list of common household odors. The first 2 categories contained odors with minimum trigeminal component, whereas the remaining 3 categories had items with a mixture of odor and trigeminal perception. Participants were instructed to prioritize odors from the top of the list but they could choose the first item that was available to them going down the list in order. With no time pressure, participants could smell the odors as many times as needed before rating the intensity and pleasantness of each odors on a visual analogue scale ranging from very weak/very unpleasant to very strong/very pleasant. Subsequently, ratings were mapped to a numerical scale with the minimum of 0 and the maximum of 100.

4.4 ODOR STIMULI AND DELIVERY

Depending on study, different odors were chosen as stimuli. Despite different molecular structures and naturally miscellaneous valence, stimuli were selected to have three common features: 1) iso-intense perception; 2) limited trigeminal sensation; 3) ecological relevance. These features are necessary to acquire a clean and impartial recording.

In **Studies I- IV**, odors were delivered using a computer-controlled olfactometer with a known raise time – the time needed to reach 90% of maximum concentration after the trigger – of 200ms (164). To minimize the potential undesirable tactile stimulation caused by blowing odor stimuli into the nostrils, the odor stimuli with a flow rate of 3 l/min were inserted into an ongoing constant 0.3 l/min air flow. Hence, the total flow rate was 3.3 l/min meaning that flow rate for each nostril was 1.65 l/min; this value is much lower than the threshold commonly found to cause nasal irritation (164). In **Study V**, the odors were freshly prepared and manually delivered by the participants themselves.

4.5 DEMOGRAPHIC AND COVID-19 SYMPTOM DATA COLLECTION

Participants in **Study V** created an account and logged into the Swedish version of the multilingual website smelltracker.org and provided demographic and COVID-19 related

information. The recorded data included age, sex (Woman/Man/Other), and whether they had been tested for COVID-19 (No, Yes-Pending, Yes-Positive, and Yes-Negative). Next, participants were asked to report any COVID-19 related symptoms they were experiencing at the time of testing. Available symptoms were: “Fever, Cough, Shortness of breath or difficulty breathing, Tiredness, Aches, Runny nose, Sore throat, Loss of the sense of smell, Loss of taste, and No symptoms”. As mentioned above, each participant had a unique account by which they could log in again and repeat the testing on different days.

4.6 EEG

The first non-invasive electrical recording, later known as EEG, goes back to 1920s and 1930s, when a German psychiatrist, Hans Berger, demonstrated the presence of 10 Hz oscillations, in his recordings between frontal and occipital electrodes. This was the first discovered brain rhythm, namely the alpha rhythm, which initially encountered skepticism. For example, this finding was criticized for being confounded by muscle/cardiac artifacts. Also, some critics challenged the rationale of attenuation of rhythmic brain activity when eyes were open. Most importantly, it was often believed that the discovered alpha rhythms were too slow to have any neural origins (165). The skepticism towards Berger’s finding continued until 1941 when the British physiologists, Edgar Adrian and Bryan Matthews, replicated Berger’s observations and EEG was broadly accepted as a non-invasive method for measuring neural electrical fields (165).

Neurons at rest maintain a stable membrane potential ranging from -40 to -80mV. This potential difference between the inside and outside of a neuron is achieved by consuming energy and transporting ions. Once the stimulus with a sufficiently large magnitude is applied to the neurons and the axon hillock depolarizes to the firing level, an action potential (AP) occurs. APs are pulses with an amplitude of about 100mV that propagate along the axon of a neuron with a constant speed and strength. However, the AP duration is very short (about 1-2 ms) compared to the duration of post synaptic potential (PSP) that lasts for a 10-50 times longer duration. Consequently, the major contributors of EEG potential are the PSPs rather than APs (166). PSPs occur as the neurotransmitters bind to the receptors in the synaptic cleft, the permeability of the ion channels changes, and consequently, the postsynaptic membrane potential diverges from its resting state level. Dependent on the excitatory or inhibitory nature of the neurotransmitter, depolarization/hyperpolarization of membrane develops and this result in PSPs that last from 10-100ms with amplitude of 10mV (166).

To have PSPs form a macro-current or dipole that is detectable on the surface of the scalp, neurons need to have a special geometry and alignment in their population. Fortunately, the pyramidal neurons are elongated with apical dendrites, which is the desirable geometry to form the dipole (**Figure 4-1 A**). Moreover, in a large part of the brain, these neurons are aligned which results in an open field and formation of a macro-current. However, there are regions in the brain, such as the hippocampus, that has a curved structure and therefore mostly generates a closed field which is hard to measure at distance (**Figure 4-1 B**) (166).

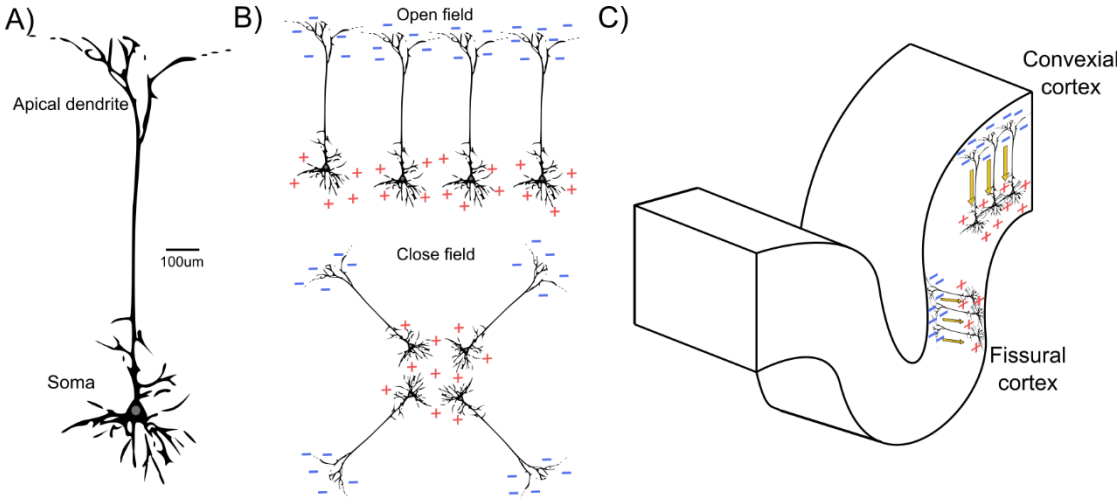

***Figure 4-1. A**) Pyramidal neurons are consisted of elongated apical dendrite, soma, and axon. **B**) Neuron alignment results in producing open fields and macro-currents that are detectable remotely on the scalp whereas radial arrangement results in a close field and hard to measure remotely. **C**) Piece of cortical fold and the pyramidal neurons are illustrated. Pyramidal neurons produce perpendicular macro-currents that in the converxial areas create a radial whereas in the fissural areas create tangential dipoles, respectively.*

The pyramidal neurons in the convexial cortex produce a radial current dipole, while neurons in the fissural cortex create a tangential current dipole (**Figure 4-1 C**). EEG measurements are sensitive to both radial and tangential dipoles, whereas MEG is only sensitive to the tangential ones, meaning that MEG mostly measures the activity in the wall of fissures. For example, measuring the auditory-evoked responses from the brainstem using EEG is much easier than that with MEG (166). Although, this is not generally a principal confounding factor for the MEG given that two-thirds of the cerebral cortex is located within the fissures. However, MEG has some more drawbacks compared with the EEG, including its high price, not being portable, and impossibility of simultaneous recording (or combining it) with fMRI, and incompatibility with transcranial magnetic stimulation. More specifically, to this date, MEG scanners have poor coverage on the forehead, where the OB is located. This problem seems difficult to solve in the common commercial MEG scanners because the sensors are fixed on the MEG helmet. However, a new generation of MEG sensors are being developed that work at room temperature and are moveable (96). This new generation of MEG sensors may solve the poor coverage on the forehead, yet this does not mean that the OB can be easily measured, even using the new generation MEG. Indeed, it is very probable that the dipoles orient themselves along the olfactory nerve and create a radial macro-current to which MEG is fundamentally insensitive to it; although, note that there is still no definitive insight on the orientation of dipoles in the OB. However, as mentioned earlier EEG is sensitive to both radial and tangential dipoles and it seems to be more proper for measuring the function of OB.

4.6.1 EEG instrumentation

4.6.1.1 Electrodes

EEG electrodes convert the ionic physiological voltage to the electrical signals (167). They come with different varieties, including various shapes or materials. Metallic disks, also known as passive electrodes, are the most commonly used electrodes which provide a low resistance

path between the scalp and the EEG amplifier, once coupled with the conductive gel medium. It is worth mentioning that there exist another type of passive electrodes which can work without any gel medium, namely dry electrodes, as opposed to the wet electrodes, at the expense of higher electrode-tissue impedance. The impedance of dry electrodes is much larger than that of wet electrodes, in the range of several hundreds of kΩ up to a few tens of MΩ. The high impedance of dry electrodes increases the vulnerability to the artifacts. Dry electrodes, themselves, can be categorized into resistive (contacting) and capacitive (non-contacting) (167).

The EEG electrodes are usually made from silver (Ag) or silver chloride (AgCl). Although other materials like gold and platinum are also sometimes used in the electrodes to acquire high quality signals above 0.1 Hz. However, gold/platinum electrodes, in addition to being costly, are polarizable and not suitable for recording DC (< 0.1 Hz) signals.

Each EEG signal is the voltage difference between two given electrodes. Commonly, EEG systems record from a large number of electrodes, yet recording from a few or even a pair of electrodes forming one single EEG signal (168), is also practically performed (169,170). EEG systems with a large number of electrodes are produced in the form of washable caps or meshes which makes it possible to put the electrodes placement on the scalp in less than 20 minutes.

4.6.1.2 EEG amplifiers

The amplitude of the potentials measured on the human scalp is extremely small, in the range of 10 µV to 100 µV (171). This amplitude is too low for the electronic equipment to digitize (analogue-to-digital converter (ADC)), filter and store the signals. Consequently, prior to any manipulation of the signal an amplification step is required by which the minuscule brain activity is intensified to the level that is suitable for the rest of the electronic equipment. The EEG signal is normally amplified at two stages, namely preamplification and power amplification (166).

The measured EEG signal is subjected to different nuisance sources including the power line interference (which occurs at 50/60 Hz), poor interface at the junction of the electrode and the skin, and other undesired sources. Considering these disturbances, the preamplification stage is of high importance because it is the first stage handling the signal and to some extent deals with the noise. Often, amplification is performed beyond the electrodes, that is, after the signal is picked up by the electrodes. However, this preamplification can sometimes be integrated with the electrodes which consequently forms the so-called active electrodes (AEs). The amplifier integrated in the AEs can either be a simple buffer, an amplifier with a gain, or it may even include an ADC (172).

AEs have some advantages compared with the passive electrodes. Firstly, the proximity of the amplification stage to the recording site decreases interferences picked up by the electrodes (167,173). Secondly, the AEs are free from the impedance variation of skin-electrode interface that is produced by subject movements (174); consequently, AEs are less prone to motion artifacts (174). Thirdly, AEs are not dependent on heavy shielding of cables to maintain signal

quality. However, AEs require more wiring compared to the conventional passive electrodes, which makes them more ponderous to work with (167).

In all studies assessing neural signals, **Studies I-IV**, we used an EEG system with AE (ActiveTwo, BioSemi, Amsterdam, The Netherland) and acquired signals from either 32 or 64 scalp recordings depending on the experiments. In addition to the scalp electrodes, we placed four extra electrodes on the forehead, so-called electrobulbogram (EBG). The EEG/EBG data were sampled at 512 Hz.

4.6.1.3 Electrode placement

EEG electrodes are usually arranged according to the 10-20 system in which electrodes are positioned relative to the designated anatomical landmarks on the head (175). The electrodes are labeled with an uppercase letter together with a number, where the letter indicates the scalp segment, and the number marks the position of electrode within the segment. Electrodes with odd numbers are placed on the left hemisphere and those with even numbers are placed on the right hemisphere. Moreover, electrodes which should be placed on the midline (sagittal line) between left and right hemispheres are labeled with an uppercase letter followed by a lowercase 'z' (instead of a number). For example, an electrode labeled as 'F1' is placed on the left frontal segment, an electrode label as 'F2' is placed on the right frontal segment, and the one labeled as 'Fz' refers to the electrode on the sagittal line of frontal lobe.

However, these conventional placements will not capture electrical potentials form the OB. Thus, as a first step, we simulated the lead-field of two hypothetical radial dipoles, operating in the gamma band, placed in left and right OB (x: ±6, y: 30, z: -32) in Montreal neurological institute (MNI) space. The simulation of the lead-field refers to solving the forward problem, thereby estimating the electrical field for the hypothetical OB dipoles. Accordingly, the simulation suggested that most of the OB potentials were concentrated on the forehead (**Figure 4-2 A**). Hence, we extended the standard 10-20 system with four additional active EBG electrodes on the forehead. The EBG electrodes were placed bilaterally and slightly above the eyes, following the outline of the individual's eyebrow (**Figure 4-2 B**).

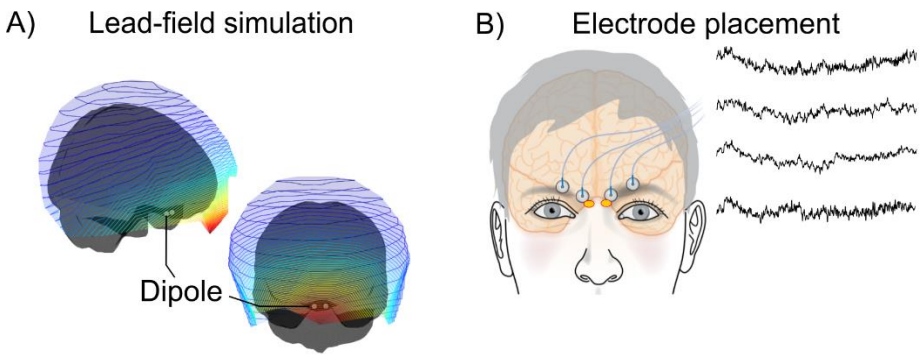

***Figure 4-2. A**) Simulated lead-field of hypothetical radial dipole place in OB, operating in gamma band. **B**) Four EBG electrodes were placed on the forehead following the outline of eyebrows.*

4.6.1.4 Electrode offset

Having a low electrode offset is important for acquiring high-quality EEG data. High offset either saturates or significantly reduces the dynamic range of AEs (167). Based on international electrotechnical commission standards (176), EEG recording systems should be able to handle ±300mv electrode offset. In all experiments of this thesis, the offset was kept below ±40mv. Accordingly, prior to the recording, all electrode offsets were manually checked and those above the threshold were adjusted until all offsets reached below ±40mv.

4.6.2 Brain rhythms

The brain produces different rhythms that are associated with perception, memory, and cognition (177). These rhythms are generally critical to efficiently control timing of the neural firing by which the information transformation can be temporally coordinated and consequently linking the single neuronal activity to behavior (177). During the early years of EEG recording (1929-1938), all major brain rhythms were discovered and to date, they have been numerously assessed *in vitro*/*in vivo*, in both EEG and MEG studies (166,178). However, the classical categorization of brain rhythms was too simplistic. Today, it is understood that a specific brain rhythm can have multiple functions depending on the brain region which produces that rhythm (179). Correspondingly, each brain region can also produce different rhythms (180,181).

4.6.2.1 Alpha and mu rhythms

With the invention of EEG, Berger also discovered that the electrical activity of the brain shows a rhythmic behavior, mostly around 10 Hz, the so-called alpha band (8-13 Hz). Later, Lord Adrian and his colleague Matthews observed that the brain rhythm that had been described by Berger is strongest when the cortex has minimal working load, thereby they proposed the *idling* hypothesis for the first time (182). The rationale behind the idling hypothesis is that during low demand periods the brain stays in a ready state that provides a quick path for attainment of full capacity when it is needed. Contrary to Berger, who believed the whole cortex produces alpha rhythm, Adrian and Matthews showed that mostly the occipital part of the cortex is responsible for the alpha-like oscillations while eyes are closed (166). In addition to eye opening, the alpha rhythm has been shown to be modulated by painful stimuli, loud noises, and mental effort (166,183). However, the alpha rhythm does not seem to be directly involved in the olfactory system.

Mu brain rhythm, sometimes also called Rolandic rhythm due to its proximity to the Rolandic fissure, can be considered as an alpha-like variant that appears over the sensory-motor cortex (183). The occipital alpha and the mu rhythm together are the two well-known brain rhythms. The mu rhythm was first described by Henri Gastaut back in 1952, when he noticed an arced shaped wave that its reactivity was related to the executed motor action; hence called it mu for ‘motor’ (166,184). The main component of the mu rhythm varies from 9 to13 Hz and it is often found symmetrically on the left and right sides of the scalp, but independent of each other, indicating that they have separate underlying sources (183). Moreover, the arced shape of mu rhythm insinuates that this wave, in addition to the main 10 Hz component, should also include

higher components around 20 Hz. However, it has been shown that the higher frequency components are not the exact harmonics and have different time-courses (185). Moreover, source localization of mu sources in MEG data confirms that the source of the 20 Hz component is located more anterior than that of 10 Hz; hence, receiving more input from the precentral cortex (186). Accordingly, the 20 Hz rebound of mu source has a somatotopic arrangement, while the 10 Hz source cluster is concentrated to the hand region (187).

4.6.2.2 Beta rhythm

In addition to the alpha rhythm, Berger also observed faster oscillations in the range of 14 to 30 H that are now known as beta rhythm and which can be roughly divided into rhythmic and less rhythmic oscillations (166). Although the physiological mechanisms underlying the beta rhythm are not fully understood, beta rhythm is found to be critical for multiple diverse functions, including, inhibition of movement, preservation of the status quo, indicating the sufficient level of evidence for decision making and coordinating between different neocortex regions, depending on the peak frequency and their generation site (178).

Moreover, the beta oscillations are prominently present in the olfactory system, yet had been initially glossed over until after performing experiments in awake animals (56). Accordingly, olfactory beta oscillations have been linked to the repeated presentation of highly volatile odors, learning to associate odor discrimination with rewards, modulation of the OB signals by higher order regions, and motor behavior in an olfactory reaching task. Critically, olfactory areas have coherent activity in the beta band, although their activity is not limited to only beta (56).

The emergence of beta rhythm is dependent on the integrity of the feedforward/feedback loops between the OB and its direct recipients, and any disturbance in the information exchange in these loops result in the reduction of beta rhythms. Hence, this implies that the beta activity in the OB mirrors events in the deep layers. However, the function of beta oscillation in the olfactory system is not clearly understood (56).

4.6.2.3 Gamma rhythm

The gamma rhythm covers a large range of frequencies from 30 Hz to 600 Hz. However ultrafast oscillations (200-600 Hz) do not reach the scalp and they are not visible on the surface recording; either due to the distortion caused by skull or the lack of forming a macro-current in the sources (188). Therefore, in MEG/EEG studies, gamma oscillations are commonly assessed in the range of 30 Hz to 100/200 Hz, and there is a body of evidences suggesting an increased gamma synchronization in various perceptual and cognitive tasks (166).

Odor-evoked gamma oscillations have earned the title of the most studied oscillatory events in the mammalian brain (56). These odor-related oscillations had been defined as early as the 1940s (6); nevertheless, these oscillations are still the topic of ongoing researches. In contrast to most other oscillations, gamma synchronizations exist even during anaesthesia; however, in

a cruder form compared to the awakened state during which the gamma synchronizations are modulated by the animal's past experience and behavioral states (189).

Mammalian and non-mammalian vertebrates' micro-circuits in the OB resemble one and other, suggesting that the underlying mechanism of producing the odor-evoked fast oscillations is common among different species (56). Correspondingly, invertebrates with similar micro-circuit architectures to that of the mammalian OB, produce similar odor-evoked fast oscillations (190). The OB in humans, as well as in non-human mammals, produces gamma rhythms in response to the odors (56,159). However, as mentioned in **Section 2.3.1**, due to the dearth of non-invasive recordings, the human OB synchronization is understudied and the only related research is an intracranial study with a low sample size, from the late 1960s (159).

The origin of gamma–like oscillation in the OB is the reciprocal dendrodendritic synapses of MC/TC and granule cells (56). Relatedly, subthreshold gamma oscillations have been indicated to disappear in the intercellular data if the inhibitory input to the MCs is blocked (191). Moreover, theoretical modelling studies provided further evidence regarding the key role of the dendritic synapses in the generation of the gamma rhythms (192,193).

Both studies in honeybees and rodents suggest that gamma oscillation in the OB facilitates fine odor discrimination. For example, ablation of honeybee's antenna lobe, a neuropil in the insects nervous system that corresponds to the OB in mammals, removed fast oscillations and consequently rendered the insect unable to discriminate related odors (194). Moreover, both genetical manipulation and behavioral studies in rodents confirmed the role of gamma oscillations in fine odor discrimination.

4.6.2.4 Theta rhythm

Theta rhythm was described for the first time in 1936 (195). In the animal literature, theta rhythm has been largely linked to the hippocampus with functions in encoding and retrieval of spatial information from episodic memory as well as maintenance of working memory (196,197). Gamma power is often synchronized with the theta cycle, meaning that for certain part of the theta cycle, gamma activity is the strongest. This cross-frequency synchrony, also called phase-amplitude coupling (PAC) (please see **section 4.6.8**) has been suggested to effectively facilitates information transfer in a "packaging" manner (198).

Theta rhythm in the olfactory system was described in the1950s (199). During the early years of its discovery, there were several attempts to determine whether theta rhythm has neuronal origin and is not merely driven by the respiratory movements (56). In the light of neural origin of theta rhythm, it has been found that 50% of MCs/TCs in the rats, as well as some other animals, are phase locked to respiration (56). Odor stimuli is delivered to the OB in a wave like fashion in the sense that it appears during inspiration and fades during expiration. Hence, it is sensible to imagine synchronization between the olfactory processing and respiration (56).

At a different level of studies, including computational modelling, both glomerular circuits and the olfactory nerve have been suggested as the underlying circuitry for producing the theta

rhythm (56). Nevertheless, theta rhythm does not seem to be confined to the sensory input, but other centrifugal connections including brainstem and mid-brain respiratory circuits (56,200).

Although theta rhythms in the OB and hippocampus are closely related in terms of their frequency, the two rhythms seem to be independent as they are not phase–coherent and are independent. However, there are circumstances where the OB and hippocampal theta are linked. For example, when the contingency of odors is reversed, the phase of OB and hippocampus theta rhythms are coherent during the early phase of learning, but the coherence gradually drops (201). Additionally, during learning of difficult odor identification tasks, the two theta rhythms become coherent. Critically, level of coherence between the two regions linearly correlates with learning level (202).

4.6.3 Origin of signal

It is not clear how modular systems of the brain integrate their processed information into coherent representations in perception, memory, and action (203). Indeed, dynamic neural activities distributed over the brain give rise to a unified percept in the central nervous system (204); however, the underlying mechanism is not yet understood (*c.f.,* the ***binding problem***). For example, it is not clear how thousands of neurons, each responding to certain features of a visual stimulus, converge to reach a whole representation of the visual object.

Accumulating evidence suggests that complex information processing in the brain is achieved by synchronization of neural populations, and, indeed, accurate timing of neuronal discharges is critical for information integration. Multi-electrode recordings in animals show decisive proofs of synchronized discharges in the visual cortex with a millisecond precision in response to visual stimuli. This synchronization is stimulus-induced and context dependent in the gamma band (205).

EEG provides the opportunity to non-invasively investigate this cortico-cortical synchrony in the human brain. However, the signal recorded on the scalp cannot directly be attributed to the underlying cortical region. The relationship of the cortical source and the detected signal at the sensor-level is known as the ***forward problem*** (206). However, in practice, the sensor data is known, and the cortical activity is unknown. Therefore, activity of the cortical sources needs to be calculated from a set of observations (i.e., recorded EEG scalp channels), through a process known as ***inverse problem.*** Solving the inverse problem is not as easy as the forward problem, as it does not have a unique solution.

Sensor level potentials do not provide conclusive information about the location of the underlying sources. To localize these sources, we have to solve the inverse problem. There are different approaches with different assumptions proposed in the literature to estimate source location with a greater precision. The source localization methods can be categorized into two major groups, namely overdetermined model and underdetermined models (207)

Overdetermined models assume that the underlying sources are small number dipoles that can be estimated from scalp potentials. On the other hand, an underdetermined model assumes that

the exact number of sources cannot be determined a priori, therefore, there are many distributed sources in the brain. Often, this is known as a distributed model. In distributed models, every point in the brain can potentially be the source of scalp potential. Solution of the inverse problem is here the unique configuration of the source activity that can explain by the scalp potentials. However, an infinite number of such configurations exist. This high uncertainty urges the application of constraints to identify the most likely solution (207).

One of the approaches to solve the inverse problem for the distributed model is Beamformer that originated from radar and sonar signal processing (208). Beamformer has been used in analysis of electrophysiological brain imaging (mainly MEG) signals (206). In the Beamformer framework, the objective is to minimize the interference of other regions' activity and can be divided into two steps: 1) linear estimation of the sources and 2) normalization of the estimation by the noise power (209).

4.6.4 Pre-processing

4.6.4.1 Filtering

Filtering of electrophysiological data is usually performed twice; one time during the recording, known as anti-aliasing filter, and second time during the preprocessing to increase signal-to-noise ratio (SNR). The preprocessing filtering is not mandatory and can be avoided. However the anti-aliasing filtering must always be applied to avoid serious distortion in the signal after the digitization of the analogue data (166).

Filters are very useful to remove some of the interferences. For example, it is possible to use a notch filter to remove the power line noise (50/60 Hz). However, it should be noted that the notch filter introduces discontinuity in the power spectrum of EEG/EBG data and should be used only if there is no other alternative. Within this thesis, we often used discrete Fourier transform filters (DFT filtering or spectrum interpolation) instead of notch filters. DFT filtering has the advantage of removing the occurrence of filter ringing artifacts as well as minimizing the potential corruption of frequency bins away from 50/60 Hz. However, this method might not be optimal for long trials or continuous data as it neglects the possible variation in the amplitude of power line noise (210).

Another interference that can be easily removed by filters is the slow drift that occurs due to sweating or change in the conductivity of gel medium. A high pass filter with cut off frequency of ~0.1-0.2 Hz is often appropriate to remove this slow drift. Particularly in the studies within this thesis, considering that the ultra-slow oscillation was not of interest, a high cut off frequency of 1 Hz was used to remove the slow drifts.

4.6.4.2 Artifact detection and rejection

Different biological and nonbiological nuisance sources can contaminate the EEG/EBG or MEG data. The best approach to resolve the artifacts' interference is to avoid them in the first place. Preventing artifacts is always preferred to removing epochs or correcting them in post

processing. However, artifacts occur and cannot be totally circumvented, therefore, in practice, trials with artifacts are detected and often removed. However, some of the remaining artifacts can be corrected/compensated with various methods of which, independent component analysis (ICA) is one of the most popular methods when correcting for artifacts.

The main strategy in the thesis was to avoid artifacts in the first place. In all EEG/EBG recording sessions, to minimize the number of trials containing artifacts, participants were asked to sit as still as possible as well as avoid blinking and swallowing during the stimulus presentation. The experiments were designed in a way to have enough long inter trial intervals to provide time for participants to relax for several seconds before each trial, helping them control blinking and swallowing, but also to avoid habituation to odor stimuli (increased the desired signal). A head rest was used to minimize muscle artifacts and an EEG system with AE was used to increase SNR and to diminish power line noise through using a driven right leg circuit/closed loop system to increase common mode rejection. Moreover, all the cables for mouse and screen which presented the experiment's instruction and scales for rating, were shielded with copper foil to minimize potential electrical interference. Finally, participants sat far enough (~80-100cm) from the screen to further decrease the electrical noise.

The remaining trials were identified in the preprocessing step and trials with artifacts were removed for further analysis. Particularly, two types of artifact including muscle and blink were identified using an automatic algorithm. The general pipeline of artifact detection algorithms started with band-pass filtering, Hilbert transformation to extract instantons amplitude followed by z-transformation, and thresholding. The parameter for filtering and the threshold value is dependent on the type of the artifact that is desired to detect. A Butterworths filter was used with the 8th order and cut off frequency was set to 110~140 Hz for muscle artifact. For blink artifact, a similar type of filter was used but with 4th order and cut off frequency 1~15 Hz. The threshold value for detecting muscle artifacts was set to 6 and for the blink artifacts was set to a lower value of 4.

4.6.5 Time frequency analysis

Time frequency analysis enables us to calculate the spectral amplitude of EEG signal as a function of time, so-called time frequency map, aka. spectrogram. However, in this type of analysis there is a conundrum; when time resolution increases, the uncertainty in the frequencies also increases, thereby the frequency resolution decreases and vice versa. Therefore, there is an inherent trade-off between the time and frequency resolution.

There are different methods to compute the time frequency map/spectrogram of EEG signal, including Fourier transform, Hilbert transform, wavelet-based method, as well as a time-domain analytic approach, namely empirical mode decomposition (211). Most of these methods are mathematically equivalent, but the wavelet approach is currently the most popular method for computing spectrograms (166). Wavelets, contrary to the sine and cosine waves in Fourier analysis, are relatively localized both in time and frequency (212). There are some conditions that a signal has to fulfil to be recognized as a wavelet: (1) the mean amplitude of wavelet is

zero, (2) the energy of the wavelet has to be finite over its time course, (3) the energy of wavelet must decay at least as fast as its frequency. Accordingly, any function which has the above mentioned conditions, or in other words fulfils the admissibility condition, can be used as the mother wavelet (213). The admissibility condition can be defined mathematically as follows:

$$\int \frac{|\Psi(\omega)|^2}{|\omega|} d\omega < +\infty \qquad \text{Equation (1)}$$

Where $\Psi(\omega)$ is the Fourier transform of $\psi(t)$. Hence, to satisfy the inequality in Equation (1), the Fourier transform of $\psi(t)$ for small ω must decline to zero, indicating the wavelet must have a band-pass-like spectrum. There are several choices for mother wavelet function but in EEG analysis, the mother wavelet function with basis of sine and cosine is preferred. However, often different tapering methods are used including single [e.g., gaussian (Morlet wavelet), Hanning] or multi tapering [e.g., discrete prolate spheroidal sequence (DPSS)] to construct the wavelet. The multi tapering method provides better control over the frequency smoothing and it is preferred for assessing oscillatory gamma activity (214).

In **Studies I-IV**, a multi taper method has been used to increase the sensitivity and control over the frequency smoothing. Depending on the time and frequency resolution of the analysis, between 2 to 7 windows from the DPSS were selected to generate wavelets and subsequently estimate auto or cross spectrograms.

4.6.6 Source reconstruction methods

An EEG source in the brain can be modeled as a local dipole which can be defined using 6 parameters, three describe the dipole location in the brain and three others outline the strength of the dipole in each coordinate axis. In case of modeling the EEG with a single dipole, parameter can be determined by means of nonlinear least-square search where the pattern of EEG is compared to the pattern that is produced by an ideal dipole for every point in the brain (166). However, often the single dipole model is not adequate to explain the data, therefore, multi-dipole models or distributed models are used where several dipoles with fixed positions, but slow and varying strengths, are considered as the underlying source of EEG data. A general solution for such a setup requires solving the inverse problem that is known as ill-posed problem. Currently, different methods have been introduced in the field to solve the neurophysiological inverse problem. Here, minimum norm estimate (MNE), Beamformer, and exact low-resolution electromagnetic tomography (eLORETA) are the most used methods for finding a solution to the inverse problem. In this thesis, due to the location of the OB, we used volumetric methods, namely dynamic imaging of coherent sources (DICS), a type of Beamformer, in **Study I** and eLORETA in **Studies II-III** for source space analyses.

Beamformer and its variants (e.g. DICS) are advantageous in modeling of oscillatory behavior and assessing evoked related synchronization/desynchronization (215). Hence, in **Study I**, DICS method was used to localize the source of gamma evoked related synchronization. DICS is a linear transformation and coherence based method to solve the inverse problem (206). Therefore, to apply the DICS on EEG signals, one needs to measure the coherence among EEG

electrodes. Coherence is the measure of synchrony of two signals in the different frequencies; hence, spectral density for each EEG electrode is estimated. To do so, the signal has to move from time domain to frequency domain by a transformation known as Fourier transformation.

In the late 1960s, Peter Welch pointed out the capability of Fourier transform in power spectral estimation and offered an algorithm to approximate power spectral of a signal or in case of two signals cross spectral density. His method is known as Welch method and involves fewer computations compared with other methods (216).

The electrical activity of the cortical sources travels through tissues and reaches the scalp and is observed as a time series of vibrations in the electrical field (217). These changes in electrical fields can be sensed with enough electrodes on the scalp. To unravel the relationship between the channels, different approaches can be used. As mentioned earlier, one possible good candidate for finding the association between EEG channels is to examine coherence (i.e. the paired-wise cross spectral density of these time series using Welch method) that is defined as follows (218):

$$C_{xy}(f) = \frac{|G_{xy}(f)|^2}{G_{xx}(f)G_{yy}(f)} \qquad \text{Equation. (2)}$$

Where C_{xy} is the coherence between channel x and channel y as function of frequency bounded to [0 1], 1 represents a perfect linear relationship between the pair given the frequency of (*f*), G_{xy} is the cross spectral density of channel x and channel y, G_{xx} is the auto-spectral density of channel x and G_{yy} is the auto-spectral density of channel y. G_{xx} , G_{yy} and G_{xy} can be estimated using the Welch method and they are usually stored in a square matrix with the number of rows and columns equal to the number of recorded electrodes (in this case two).

$$\begin{bmatrix} G_{xx} & G_{xy} \\ G_{xy} & G_{yy} \end{bmatrix} \text{ Equation. (3)}$$

Thus, Diagonal elements of the matrix represent the power spectrum of each electrode whereas cross spectral density of all possible combinations can be found in non-diagonal elements.

Having the coherence values among electrodes enables us to construct the linear transformation that maps the scalp potential to cortical activities**.** This transformation is implemented as the weighted sum of recorded signals from different scalp electrodes while it is linearly constrained to pass activity from the specified areas of the brain and block it from other regions. This method does not require any prior assumption**.** This linear transformation turns into a constrained optimization problem and it can be solved with Lagrange function. By solving the associated Lagrange function, solution (A) can be written for every point (r) in the brain given a frequency *f* as follows:

$$A(r,f) = \left(L^T(r)C_r(f)^{-1}L(r)\right)^{-1}L^T(r)C_r(f)^{-1} \qquad \text{Equation. (4)}$$

L is the matrix contains solution for forward problem at point of r, the superscript (T) shows transposed matrix, which is basically the flipped version of the original matrix over its diagonal. C_r is equal to cross spectra density plus a regularization parameter. The regularization parameter balances the sensitivity of the algorithm to the noise level and the accuracy of localization. This value has to be determined based on the SNR of the recorded signal.

In order to calculate matrix L in Equation 3 one needs to model the head volume conductor and the brain activity. One of the common head volume conductor models that has been used in EEG source localization is multi-shell spherical model. Each sphere is assigned to different tissues with various conductivity properties. The spherical models are computational efficient; however, they lack the anatomical detail of the human head. On the other hand, this shortage seems to only affect temporal and occipital regional sources when compared with more realistic models such as boundary element model or finite element model. The other dissimilarity between spherical models and more realistic ones is that the latter relies on numerical solutions whereas earlier uses analytical solutions (219).

The behavior of the electrical field of each source in the brain can be considered as a quasi-static approximation equal to the volume current density at a columnar level. A volume conductor is needed to link the source's behavior to the potentials measured at sensor level on the scalp. The head volume conductor model explains how the current propagates through different tissues and reaches the scalp.

Source power of each point (r) at each frequency in the brain can be derived with a solution matrix A (r, f) as follows:

$$P(r,f) = A(r,f)C(f)\,A^{*T}(r,f) \qquad \text{Equation. (5)}$$

Where superscript * denotes the conjugate form of the original matrix. Therefore, real parts of A and A^* are equal while the imaginary parts have different signs but same magnitudes. P (r, f) is the matrix, however, one scalar (number) is normally desired which can reflect the quantity of power in the certain frequency in that particular point in the brain. This number is usually noted in the literature with p and it can be estimated as first singular value of P (r, f) under the condition when the first singular value is much bigger than second singular value of the matrix, otherwise one can use the summation of diagonal elements of matrix P (i.e. trace of P) and use it as estimation of p. Similarly, noise power estimated for each point where cross spectral density is changed with noise cross spectral density (206). The evoked activation of point r is derived as noise normalized power. Therefore, for every given point in the brain at a certain frequency the cortical activity can be assigned.

As mentioned earlier, eLORETA is another method to solve the inverse problem and localize the EEG sources. eLORETA is currently the most robust method for EEG source localization (220). However, when eLORETA was compared to DISC and other methods, in terms of localization accuracy, there was no clear winner. eLORETA seems to have slightly more focal width source compared to DICS, but on the other hand, DICS has more accuracy for single- or

two-point dipoles even in low SNR (220). eLORETA can be used both in time and frequency domain. In time domain, the covariance across the EEG/EBG electrodes, instead of coherence, can be used to estimate the power of sources.

In **Study I**, coherence in the gamma band during the time window of 100-250 ms was used in the DICS with 10% regularization parameter to reconstruct and localize the underlying source. Moreover, the same parameters were used in eLORETA to validate the results found with DICS. In **Studies II-III** the time domain of eLORETA with covariance during the whole stimulus time (1s) was used to reconstruct the time course activity of sources.

4.6.7 Representational similarity analysis

In RSA, instead of assessing the conventional first-order isomorphism between the stimulus and brain representation, the RSA method assesses how dissimilarity matrices are matched to one another, so-called second order isomorphism, within the individual (221). This comparison is based on the principle that each stimulus induces an activity pattern and by comparing each of these patterns with one another, we obtain a representation dissimilarity matrix that can characterize the representation of the stimulus using standardized and normalized values (i.e., correlation coefficients). In their seminal work, Kriegeskorte and colleagues (2008) demonstrate that RSA is not only useful to bridge different level of experimentation, but also a very powerful tool for connecting external stimuli to brain representation. For example, linking ratings of valence perception with brain-activity values (221). The RSA method has now been used in more than 1,000 publications.

In **Study II**, RSA allowed us to directly compare the link between valence perception and neural responses in the OB on the individual level by comparing how the 6 odors were represented in both neural and perceptual spaces: first on the individual level and then assessing potential consistencies between individuals using permutation testing. It is here important to note, however, that contrary to conventional correlation or linear association (first order morphisms) the absolute values (e.g., absolute gamma/beta power or absolute valence rating) are not directly compared to each other but rather the relation between stimuli on both levels are compared. This way, the relationship within brain-activity data is compared with the relationship within the behavioral data, regardless of the absolute values of both. This enables assessment of links between parameters beyond mere linear associations.

4.6.8 Phase-amplitude coupling

Neural oscillation can be defined by three properties: amplitude, frequency, and phase. Theoretically two rhythms derived from neuronal population can be coupled by each pair of oscillation's characteristic features. However, it is more likely that the coupling occurs between parameters that have a similar time scale such as phase-amplitude coupling (PAC) (222). PAC is a subclass of cross frequency-coupling phenomena, in which neural oscillations with different frequencies are coupled to one another. When the amplitude of fast oscillation is modulated by the phase of slower oscillation PAC emerges. PAC has been determined as a neural mechanism detectable in most mammals and critical for information processing in a multitude of

brain regions (223–228). The physiological assumption that fosters PAC is that the slow oscillations represent the cycle of net excitability of neural ensembles during which the probability of neural firing increases and give rise to intermittent fast oscillations (229,230).

PAC is the most well studied type of cross frequency-coupling (229). Particularly, theta-gamma PAC, which can occur both intra-/inter- regional (231), has been extensively assessed in the literature (222). Several studies have been indicated that PAC has a function role in attentional selection (232), signal detection (233), and executive functions (234). Recently, the functional relevance of PAC in olfaction has also been demonstrated, whereby PAC shapes the early sensory processing in OB. Moreover, it has been shown that the level of PAC fluctuates as a function of olfactory learning (235).

PAC has been quantified using different models of which many were originally applied to invasive recordings (166). A few of the more common methods of quantifying PAC include phase locking value (PLV), modulation index (MI), and mean vector length. However, these conventional methods have poor time resolution (236). Therefore, in this thesis, and particularly in **Study II**, we used time-resolved phase-amplitude coupling (t-PAC; (236)), a method that also incorporates the temporal dynamic of the signal. Therefore, the higher time resolution of t-PAC mitigates the necessity of long epochs for reliable estimation of PAC which is a constraining factor given the non-stationary characteristic of electrophysiological recording during behavioral task (236).

It is worth mentioning that most cross frequency-coupling in the literature, including PAC, have been observed in invasive recordings obtained in both animals and humans. Hence, it is reasonable to perform this type of analysis in the source space rather than sensor space when conducted on MEG and EEG data (166).

4.7 FUNCTIONAL AND EFFECTIVE CONNECTIVITY

The term connectivity refers to the assessment of the relationship between two brain regions without taking into account any assumptions about the underlying biology (237). Different metrics can be recruited for quantifying the functional connectivity between a pair of regions/networks, including linear (e.g., temporal correlation, spectral coherence) (238), and non-linear measures (e.g., phase synchronizations) (239,240). Connectivity measures are often bivariate meaning that only two regions/electrodes at a time are considered to estimate the level of connection. Although this assumption is not close to how the brain functions, it is currently the most prevalent method for assessing the functional organization of the brain's neural network. Yet, there exist some efforts to advance functional connectivity analysis by considering the importance of intermediate regions for information exchange (c.f., 241).

Connectivity analysis for EEG data is mainly divided into two categories. In the first category, known as functional connectivity which dates back to the 80s (238), the mere statistical dependency of two populations is measured either based on the association of their phase or amplitude/power. In the second type of connectivity, that is often known as effective connectivity, the predictive relationship between two variables is quantified. For example, Granger causality

estimates how much of one variable's variance can be predicted based on the past samples of another variable (242).

In **Study III**, in a bivariate setup, both functional and effective connectivity between the two olfactory regions, namely the OB and PC, were assessed. The level of OB-PC functional connectivity was estimated based on their cross-spectrogram, where each bin reflects the level of linear information transformation between OB and PC. Moreover, using the extension of Granger causality, namely the spectrally resolved Granger causality (243), the causal association between those two regions was estimated in both directions.

4.8 SUPPORT VECTOR MACHINE

Support vector machine (SVM) is a prevalent type of supervised machine learning algorithm that can either be used to classify, known as SVM classifier, or to predict a value, recognized as SVM regression. In this section, we concentrate only on one of the specific types of SVM classifier, namely linear SVM classifier that will hereafter be referred to as SVM. SVM, by design, finds the decision boundary with the largest margin; hence, often it is also known as large margin classifiers.

The basis of every supervised classifier is to minimize the expected discrepancy between the predicted and true labels quantified as a so-called loss function. The loss function $J(\theta)$ for SVM can be defined as follows:

$$J(\theta) = \frac{1}{N}\sum_{n=1}^{N} \max\left(1 - y^{(n)}\left(\theta^T x^{(n)} + \theta_0\right), 0\right) + \lambda|\theta|^2 \qquad \text{Equation. (6)}$$

Where the $y^{(n)}$, represents the label of every input $x^{(n)}$. θ denotes the vector parameter and θ_0 is a scalar which together, defines the decision boundary. The $\lambda|\theta|^2$ is so-called the penalized term and λ weights between the margin size and whether or not the data lies on the correct side of the margin (244).

In the case of higher dimensional data, the decision boundary forms a hyperplane in the feature space. For example, in EEG the features are often defined in time, frequency, and location which constitutes a multidimensional feature space for a given condition. To attribute classification accuracy to a particular time, frequency, or location to gain an insight into the underlying mechanism, a technique known as searchlight is often used in which the classifier is trained and tested on the small volume of future space defined by a hypersphere with known radius. The radius is selected by the examiner depending on prior assumptions. Next, the whole feature space is explored, and the accuracy map is constructed. Occurrences in the accuracy map that significantly surpass the chance level indicate existence of a link between the neural mechanism within that specific location, latency, and frequency with behavioral outcome.

In **Study III**, a SVM classifier paired with the searchlight method was trained and tested on the cross spectrogram, as the quantifying measure of functional connectivity, of the connection between the olfactory bulb and the piriform cortex (OB-PC). A circle with a radius of 5 samples were considered to define the neighbors for each bin in the cross spectrogram, given the two

axes in the cross-spectrogram map (i.e., frequency and time), 121 samples are considered to construct the feature space for each bin. Subsequently, the whole cross spectrogram is explored. Features were unity normalized and SVM was trained and tested using a one-leave-out scheme. Finally, the accuracy map is created as the average of accuracy maps across the folds.

4.9 STATISTICAL TESTS

EEG/MEG data has spatiotemporal structure consisting of channels and time points. When assessing the effect of interest, several thousand of (channel × time) pairs usually have to be compared which, by itself, brings an inherent statistical conundrum, the so-called multiple comparison problem (MCP). In EEG/MEG data, due to the large number of statistical tests needed, it is not feasible to control for family-wise error rate (245). One solution for this problem is to use a non-parametric statistic.

Initially, non-parametric statistics was suggested for assessing the EEG/MEG waveforms for a specific channel (246). Later, it has been also used to test the topographical maps of EEG/MEG data for a specific time point and finally for the whole spatiotemporal data (247). Particularly, non-parametric tests have been successfully used to assess EEG/MEG data in frequency domain (248,249).

Non-parametric test, contrary to parametric test, is very general since the validity of the test is not dependent of the probability distribution of the underlying data, nor on the type of statistical test. Hence, whether the probability distribution of data is non-normal, or the statistical inference is t-/F-statistics, has no effect on the validity of the non-parametric test. Accordingly, solving the MCP in the non-parametric statistic is straightforward because it allows for any test that one considers appropriate. Moreover, non-parametric statistics enables us to incorporate our prior knowledge into the test. For example, clustering electrode pairs that are adjacent to one another to adjust for potential signal bleeding (245).

A combination of parametric and non-parametric statistical tests was used to pursue the research questions sought to answer in **Studies I-V** within this thesis. Particularly for the EBG power change in **Studies I-IV** and t-PAC level in **Study II**, non-parametric permutation tests were used to assess statistical significance. Moreover, to assess the correlation between behavioral and neural data in RSA space, a Monte Carlo permutation test with all possible combinations (720 randomizations) was performed to estimate exact p-values.

In **Study V**, data on odor intensity estimates were first averaged across every three days to increase the reliability and match the data with the COVID-19 prevalence prediction model. Potential missing values of odor intensities were replaced with median of the specific odor category and then averaged across odors. The global, unimodal, and bimodal odors intensities were assessed by averaging all categories, Categories 1-2 and Categories 3-5, respectively. Specifically, for individuals reporting more than one session only the first session was included in this analysis. Next, Spearman correlations were used to assess the relationship between odor intensity and COVID-19 prediction model as well as odor intensity and number of COVID-19 symptoms. Eventually, individuals who reported more than one session were identified and the

intensity ratings of those who progressed from no symptom to symptom in the following session were analyzed using a paired two-tailed Student's t-test.

4.10 ETHICAL CONSIDERATION

First and foremost, the experiments in this thesis were designed in such a way to avoid possible harm to the participants. The details of the experiments and the procedure were informed to participants on the recruitment day, separated by a couple of days from the day of testing to give participants enough time to think whether they are willing to participate or not. On the day of testing, participants were also instructed to ask about any unclear issues about the experiment and its procedures.

On the testing day, participants sign an informed consent which had been provided to them in advance when recruited. They were again reminded that participation is strictly voluntary and that they could choose to abort the experiment at any time, without any adverse consequences. All recording techniques and stimuli methods were free of known causes of harm.

4.10.1 Privacy and confidentiality

To assure a high level of privacy and confidentiality for the research participants included in this thesis, several steps were taken. In terms of participants' privacy, it was ensured that our recruitment methods did not violate participants' privacy by not searching for qualified participants through existing databases and contacting them without their consent. Recruitment of participants for **Studies I-III** and **V** was carried out by passive advertisement, including posting flyers, announcements on the Karolinska Institute testing recruiting system (https://ki-behavioraltesting.sona-systems.com/) and local newspapers. This method of recruitment assures that only those individuals who, by their own free will, sought out to participate in research were recruited. Moreover, collecting non-essential sensitive information was avoided. For **Study IV**, patients were invited to experiment upon their regular clinical visit by their attending physician. The healthy control participants of this study were recruited by similar means that were mentioned above. Data collected include personal demographic information, medical history of Parkinson patients and the individual with ICA, as well as electrophysiological recording.

To assure confidentiality of the collected data, the data was first anonymized and then saved on the Karolinska institutet data server to which only authorized researchers have access. The code sheets that link each data to the actual individuals exist only in physical form and were archived in a locked cabinet which only limited authorized staffs have access to. Moreover, individual data which could potentially be linked to an individual were never presented in publications to ensure the anonymity of participants. Finally, in the informed consent, participants were explicitly notified that their data would be kept safe and remain confidential within the research group.

4.10.2 Olfactory testing

Olfactory testing (either 16-item identification or a shorter version with only five items, depending on the studies) was performed as a screening test in **Studies I-IV**. Although incidental

finding of anosmia is rare, especially in the younger cohort used in most studies, it is still possible. If indication of olfactory dysfunction would appear, the researcher explains reasons for fluctuation in olfactory ability, such as nasal congestion due to allergies or common cold. Next, the researcher would inform the participant that if the problems persist, the individual should seek medical attention via their primary care physician. Similarly, in **Study V**, no explicit information or medical advice was given to the individuals regarding the COVID-19 diagnosis based on their olfactory performance.

4.10.3 Testing Parkinson patients

In **Study IV,** the function of the OB in PD patients was tested using the EBG method. The current version of the test is not validated to function either as a clinical indication of PD or olfactory dysfunction. Participants were informed prior to entry about the research goals and the fact that their participation would not provide any advantages to their own personal well-being or provide a potential prognosis of their disease progression. Moreover, to avoid the fact that potential financial incentives could potentially force participation, no compensation for participation was awarded. All patients, knowing this information, volunteered to participate in this study.

5 RESULTS

5.1 STUDY I: ODOR INDUCED OB RESPONSE

In the present study, the objective was to assess whether it is possible to measure OB's gamma synchronizations from electrodes placed on the forehead. As mentioned in the method section (**section 4.6.1.3**), prior to experimentally assessing this possibility, a simulation was carried out to assess the possible distribution of surface potentials, given hypothetical radial dipoles operating in the gamma frequency which are placed in the left and right OB. This simulation suggested that the detectable potential concentrates on the forehead (**Figure 4-2 A**). Hence, 4 active electrodes (EBG) were placed on the forehead (**Figure 4-2 B**) and the average time-frequency response was assessed for three different odors (Odor), contrasting against clean air (Air). A gamma synchronization was found early after odor onset, at around 100ms (**Figure 5-1 A**), that did not appear in corresponding Air trials (**Figure 5-1 B**).

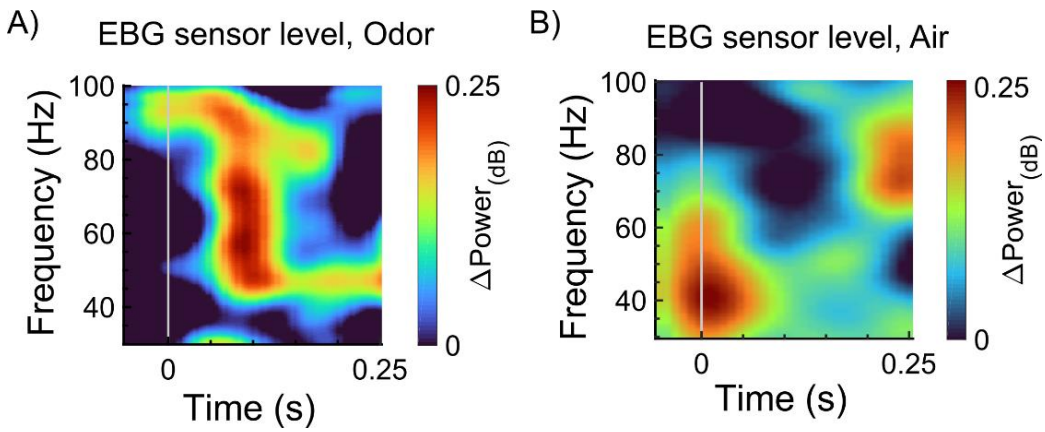

Figure 5-1. EBG time-frequency response. A) *Heatmap shows the group level average and areas where Odor produced synchronization compared with Air. An increase in the gamma power was observed shortly (~100ms) after the odor onset.* ***B)*** *Similarly, heatmap shows the time-frequency average response for Air on the group level. No synchronization in the gamma band around 100ms was observed. The warmer colors show synchronizations, and the cooler colors show desynchronization.*

A non-parametric Monte Carlo permutation test with 1000 randomizations demonstrated that significant differences emerged between Odor and Air. Next, the power for significant time/frequency bins was averaged and a post-hoc t-test was carried out on the averaged values across Odor and Air to directly determine the direction of effect. A significant effect, $t(28) = 3.62$, $p < .01$, CI = [0.23, 0.91], was detected and provided further support that Odor, but not Air, mediated the demonstrated effect.

5.1.1 Determining and localizing early odor response

Subsequently, source localization of the EBG gamma synchronization was performed using DICS method where OB was found to be the underlying source. The power in the OB source for the time-frequency window corresponding to gamma synchronization, found on the EBG sensor, was 8% stronger than the background noise. No other potential source elsewhere in the brain showed this clear level of activation (**Figure 5-2**).

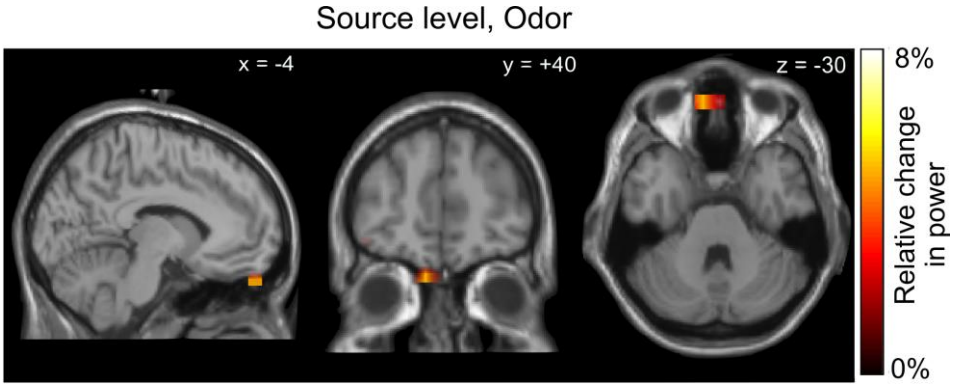

Figure 5-2. Source localization. *The source of the gamma synchronization around 100ms was localized to the OB. Power in the OB was 8% stronger for the Odor compared to Air.*

The source localization was repeated with the eLORETA method to rule out that this finding was an artifact due to the choice of source localization method. The localization map of eLORETA corresponded with DICS method, albeit with a slightly more dispersed source. However, one might expect blurrier localization map of eLORETA compared to DICS for single source with low SNR (220).

5.1.2 Test-retest reliability of OB measure

The EBG method could detect gamma synchronization that was localized to the OB. However, to be a successful measurement method, a high precision and reliability are needed. Hence, the test-retest reliability of the OB measure was assessed by comparing the EBG in the same individuals across repeated testing sessions separated by several days. The reliability of the EBG measure was evaluated using both intra-class correlation [ICC(2, k)] and pairwise Pearson correlation. There was high agreement (r_i = 0.47) between EBG measurement of sessions determined by ICC(2, k) and a subsequent F-statistic indicated that this agreement was statistically significant, $F(2, 26.65) = 3.99$, $p < .03$. Furthermore, the pairwise correlations provided further support for high test-retest reliability, as indicated by large values of similarity ranging between $r = .76$ to $r = .81$.

Beyond reliability, precision is of importance for any measurement. Although test-retest correlation is widely used to assess reliability, the magnitude of similarity is to some extent dependent on within participants variability. Hence, to assess the precision of the EBG method, effect size was assessed across the 3 sessions, rendering a medium effect size (Cohen's d = 0.44). Moreover, the standard error of mean was estimated to be as low as (±0.067) relative to mean EBG power of 0.75 across three sessions, thereby indicating that the EBG method has a high precision. Finally, the dispersion rate, determined by meta-regression across the 3 sessions, was found to be 0.04; a value that is smaller than the experimental degrees of freedom (i.e., 2) and demonstrates that the EBG measure has a low dispersion rate.

5.1.3 Validity of the EBG measure

The OB was determined to be the origin of the EBG signal. Moreover, the measurement was found to be reliable and precise. However, the source localization is merely an approximation

of the underlying source given the acquired data per se is unable to validate the EBG measurement. Moreover, direct validation of EBG requires accessing invasive recording directly from the human OB, a procedure that due to ethical concerns is not possible to achieve unless there is a clear medical need to obtain these signals. Hence, the validation needs to be indirect. Two different experiments were performed to indirectly validate the EBG method. In the first experiment, direct replication of one of the most robust findings in the animal literature in relation to the OB, namely insensitivity to habituation, was carried out. As the second validation method, assessment of EBG signal in a human OB lesion model was performed.

5.1.3.1 Habituation insensitivity

In sharp contrast to other areas in the olfactory cortex, such as the PC, the signal from the OB demonstrates insensitivity to habituation (250,251). In rodent models, exposure to repeated or prolonged odor stimuli rapidly reduces signal from the PC (71,251) whereas no, or only a minor, habituation effect is seen in the OB. The rapid odor habituation at the cortical sources is clearly visible in scalp ERPs when rapid odor presentation is performed. In contrast, the OB does not demonstrate a decrease in signal magnitude even after repeated odor exposures. Therefore, insensitivity of EBG signal to repeated exposure of odors would support the notion that the signal originates from the OB.

In **Study I**, rapid odor stimuli with long duration were presented to participants to assess potential effects of habituation on the EBG over time. This result was compared to that of scalp electrode over parietal cortex (Pz) where the difference (delta) in amplitudes between the N1 and P2/3 ERP components has been shown to correlate with perceived odor intensity (118). After each trial, participants rated the perceived intensity of the odor on an analogue scale. As expected, a rapid decline in perceived odor intensity was detected after only a few trials, thereby demonstrating that the paradigm successfully induced odor habituation.

The gamma power of the four EBG electrodes was assessed during the time/frequency window that was attributed to the OB. As predicted, no reduction in power as function of trials ($slope = 0.008$, $t(437) = 1.58$, $p > .11$, $CI = [-0.002, 0.02]$) was observed (**Figure 5-3 A**). Moreover, to increase statistical power and biasing our testing towards finding effects of habituation on the OB signal, trials were segmented into two halves, early and late trials (**Figure 5-3 A**). Using a 1000-permutation test, the two halves were contrasted against one another. No change in the power was observed. In contrast, the Pz scalp electrode showed significant decline over time in peak-to-peak amplitude of N1-P2/P3 component as a function of trials in response to repeated odor presentations ($t(971) = -3.15$, $p < .002$, $CI = [-0.010, -0.002]$) (**Figure 5-3 B**), determined by linear mixed effect model.

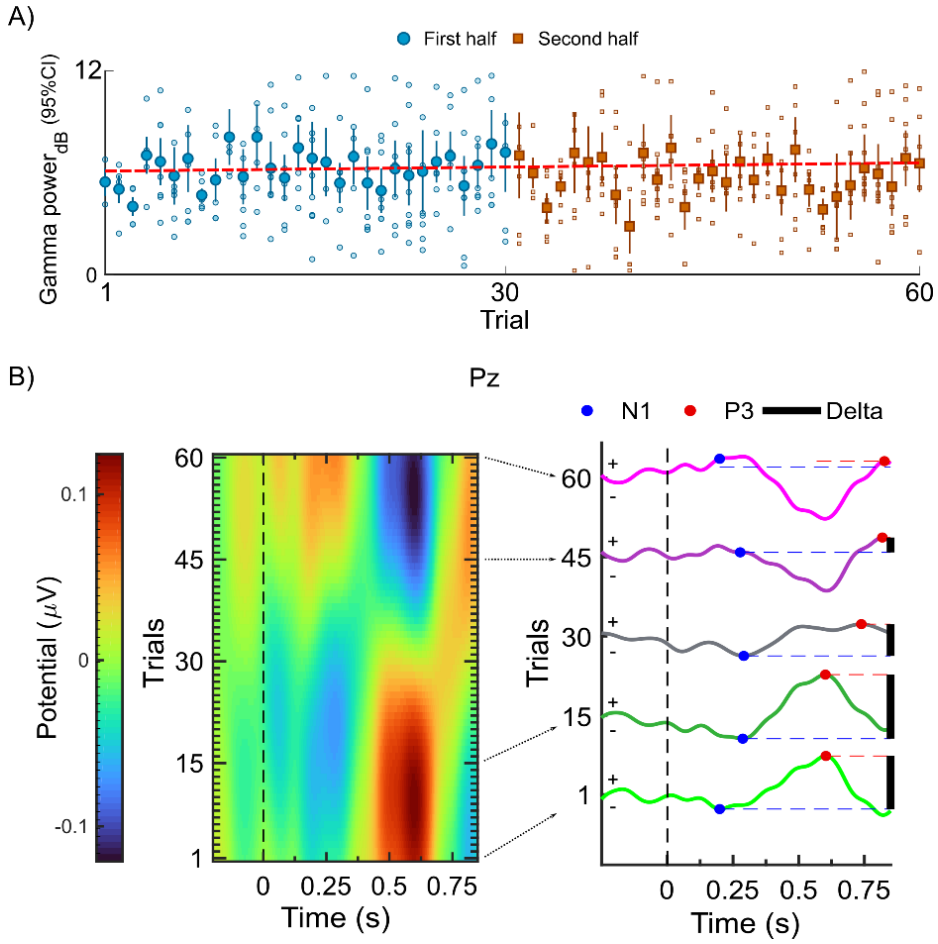

Figure 5-3. The OB is insensitive to habituation. A*) The gamma power of the EBG electrode did not change as a function of trials. The blue circles and rust-colored squares denote the first and second segments of the data where the closed and open makers show the mean and individual data points respectively. The error bar shows the 95% confidence interval and the dashed red line shows the slope for the mean power.* ***B****) The heatmap shows the magnitude of ERP over the parietal cortex (Pz). The x and y axes show time and trial number where the warmer colors show larger and cooler colors show smaller magnitude (left panel). The ERPs for selected trials 1, 15, 30, 45 and 60 are shown and the N1 and P2/3 are marked with blue and red filled circles. The peak-to-peak magnitude of N1-P2/3 is shown with the vertical black line on the right side (right panel).*

5.1.3.2 Human lesion model

At this point, we had determined that the EBG method can reliably detect a gamma synchronization that was localized to OB and possessed characteristics similar to that of non-human animals. To test this even further, a human OB lesion model, an individual born without OB, was used to assess whether absence of OBs will render the gamma synchronization found in the EBG channel to disappear. The omission of gamma synchronization in the lesion model would rule out any residual mediator of gamma synchronization, such as a systematic imbalance in attentional load, task-demands, sniff-related motor activity, microsaccades, or other unknown sources.

A 27-year-old individual with isolated congenital anosmia (ICA), born without a sense of smell and bilateral absence of OBs but otherwise healthy, was tested. Neither he nor his parents had any recollection of him ever being able to smell odors. Moreover, a magnetic resonance imaging with an image sequence sensitive to OB was acquired from him and indicated a complete bilateral absence of OB. Moreover, the depth of his olfactory sulcus was a mere 1.22 mm, a value more than 3SD smaller than average normosmics. A recent study demonstrated that

olfactory sulcus with the depth of less than 8mm is more prevalent in individuals with isolated congenital anosmia compared to healthy controls (252).

No gamma synchronization beyond background noise was detected in this individual's EBG measure. Comparing the normalized power with distribution from normosics indicated that the gamma power in the time/frequency window attributed to the OB is 2.5SD less than the average gamma power of normosimics. All in all, this further indicates that the EBG electrode is sensitive to OB response.

5.2 STUDY II: ODOR VALENCE RELATES TO EARLY GAMMA AND LATE BETA IN THE OB

In **Study I**, a non-invasive reliable method for assessing OB was developed. Consequently, in **Studies II-IV**, the EBG method, in combination with scalp EEG, were used to assess basic and clinical aspects of OB in health and disease. Specifically, in Experiment 1 of **Study II**, 4 EBG and 64 scalp EEG electrodes, in combination with eLORTEA source reconstruction method, were used to reconstruct OB time-series in response to 1s presentation of 6 different odor stimuli with different level of valence ranging from very pleasant to very unpleasant. After removing trials with muscle and blink artifacts, on average 167.52 ± 25.81 trials per individual were included in the analysis. There was no significant difference in the number of clean trials across odors, $F(5,108) = .39$, $p > .86$, demonstrating that after removing trials with artifact, the experimental design still remained balanced.

Initially, the cross-frequency coupling between OB activity in gamma and beta was assessed using t-PAC. The time-frequency window around 250ms after odor onset (~53-65 Hz) was identified where there was significantly higher coupling between gamma and beta compared to background noise. All significant testing were performed using Monte Carlo permutation test. Subsequently, assessing co-modulogram between beta and detected range of gamma indicated that the coupling occurred in the beta band within 16 to 18 Hz, $t = 2.57$, $p < .009$, $CI = [0.002, 0.012]$.

After identifying the coupled frequency ranges in gamma and beta band within the OB, the association between each of these frequency ranges and valence rating was assessed. However, the odor perception is to a large extent dependent on the individuals' judgment, meaning that a large inter-subject variation is expected whenever the odors aspects are rated. To resolve this large inter-subject variation, representational similarity analysis (RSA) was used to assess the relationship between the neural data and behavioral responses. RSA is a multivariate approach in which the representational geometry of data is assessed on the individual level (221). Moreover, RSA allows direct comparison despite of difference in scaling and other confounding characteristics of measuring methods. Particularly within this experiment, the association between OB neural activity and valence rating for each time point during 1s of odor presentation was assessed. Thereby, the representational dissimilarity matrices (RDMs) for OB neural activity and odor valence rating were quantified as Euclidean distances on the individual level. Next, RDMs were created for the both neural and behavioral data (253) and the similarity

between them was measured using Pearson correlation, resulting in time resolved correlation values between OB neural activity and odor valence. Subsequently, significance of each time point (n = 13) was tested by non-parametric Monte Carlo permutation test. Around 250-350ms, a significant association (r = .60, p < .010, CI = [.56, 1]) between OB neural activity and odor valence was found in the gamma band (**Figure 5-4 A**).

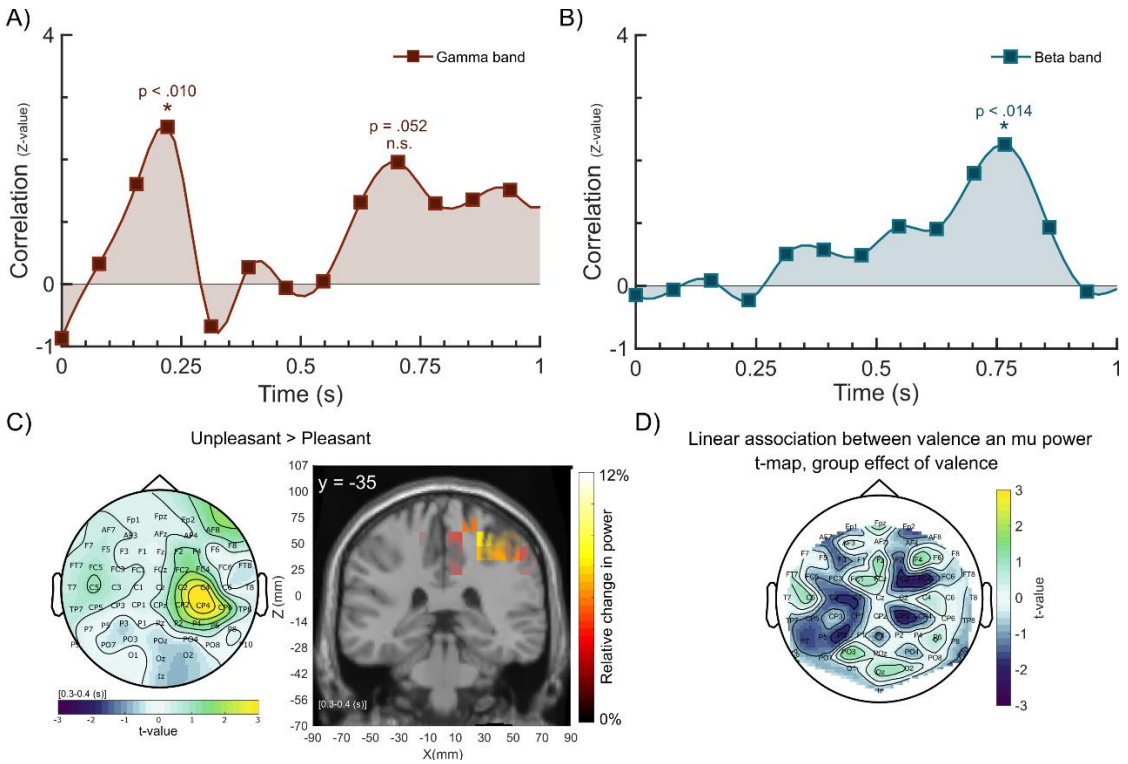

Figure 5-4. Odor valence, OB and motor cortex. A*) The graph shows the t-value for the correlation time course between the gamma power and the odor valence in the RSA space. A significant peak (t > 1.96, that is equal to p < .05) was found around 200ms.* ***B****) Similarly, for the beta band there was a significant peak around 700-800ms.* ***C****) The topographical map shows the distribution of the mu power over all the scalp electrodes where a larger mu power was found for the unpleasant odors compared with the pleasant odors over the right motor cortex (left panel). This mu synchronization was localized to the right motor cortex, where 12% increase in the mu power was found for the unpleasant compared to the pleasant odors (right panel).* ***D****) The t-map derived from the beta values of the generalized linear model indicated a significant inverse relationship between the odor valence and the mu power over the motor cortex for unpleasant odors.*

Similarly, for the frequency range identified by the t-PAC analyses for beta band, the correlation between OB neural activity and valence rating was assessed in RSA space and significance was tested using Monte Carlo permutation test. There was a significant, r = .65, p < .014, CI = [.59, 1], association between beta activity and valence in a time-interval around ~800ms after odor onset (**Figure 5-4 B**).

To this end, two significant peaks were identified in gamma and beta band that had significant correlation with valence. Next, the representation of odor valence was assessed within these two peaks. Particularly, RDMs were scaled down and each odor was placed in 2D space with respect to one another according to the corresponding RDM in that frequency band. Graph theory was used to statistically test which frequency band has embedded more odor valence information. Initially, the RDMs were transformed to similarity matrices and the modularity was estimated based on the Newman algorithm (254). The projected odors in the 2D plane were hierarchically clustered from 1 to 6 and the ideal number of clusters was estimated to 3

as the elbow of the modularity index (Q) graph. Next, given 3 clusters suggested as the best solution, we estimated the modularity index for each of gamma and beta peaks. Values were normalized to a corresponding null model from 5000 random re-wirings (255). A larger Q-value was found for beta compared to gamma peak indicating that odors form more coherent pleasant unpleasant clusters for the beta band. A subsequent Monte Carlo permutation test indicated that modularity index for beta was significantly larger than for gamma, $Z = 2.95$, $p < .003$, $CI = [0.009, 0.018]$.

In the modularity analysis, odor valence was assessed as a single continuous dimensional measure and therefore restricting assessment of whether either one of the contrasting valence dimensions (pleasant or unpleasant) contributes more to the OB processing. Previously, it has been argued that the odor valence is not a single continuum scale but rather two separate axes, one for pleasant and one for unpleasant odors (97). To directly test whether the OB processes pleasant and unpleasant odors differently, only the two most pleasant and two most unpleasant odors were further assessed with the two neutral odors excluded, all based on the individual's ratings. A higher beta activity was found for unpleasant odors during the early segment of odor presentation (around 50 to 200ms, $t = 3.01$, $p < .004$, *probability CI-range* = .004) whereas pleasant odors induced a greater beta synchronization during the late segment of odor stimulus (around 690 to 780ms, $t = 3.49$, $p < .002$, *probability CI-range* = .003), all determined by 5000 Monte Carlo permutation tests.

Subsequently, it was hypothesized that the larger beta synchronization during early time points facilitate early avoidance response. Indeed, mu synchronization over the motor cortex during the early time points (300-400ms) was larger for unpleasant compared to pleasant odor. Evaluating the whole-scalp mu rhythm indicated that power over electrodes C2 ($t = 2.17$, $p < .014$, *probability CI-range* = .003), C4 ($t = 3.00$, $p < .003$, *probability CI-range* = .001), CP2 ($t = 2.01$, $p < .022$, *probability CI-range* = .004), CP4 ($t = 3.27$, $p < .001$, *probability CI-range* = .001), and CP6 ($t = 2.23$, $p < .012$, *probability CI-range* = .003) was larger for unpleasant odor compared to pleasant odor (**Figure 5-4 C**). Using eLORETA source localization algorithm, we determined that this synchronization was localized in cluster around the right motor cortex (x: 27, y: -35, z: 60) where the power was 12% stronger for unpleasant compared to pleasant odors (**Figure 5-4 C**).

Furthermore, a generalized linear model was fitted on the trial level for negative valence odors to assess the linear relationship between odor valence and the power of mu synchronization on scalp. Subsequent t-test on the group level indicated a linear association between the mu power of electrode CP2 ($t(17) = -2.20$, $p < .042$, $CI = [-1.46, -0.03]$), FC4 ($t(17) = -2.25$, $p < .037$, $CI = [-.96\ -.03]$) and valence for negative odors. Accordingly, the more negative the perceived odor valence was, the more mu power was detected over the motor cortex (**Figure 5-4 D**).

5.2.1 Unpleasant odor elicits a fast avoidance response

Larger mu power for unpleasant compared to pleasant odor over the right motor cortex, paired with the linear modulation of the mu power magnitude with odor valence for unpleasant odors,

suggested that there was a link between the valence processing of unpleasant odor in OB and an early avoidance response. Hence, to directly test if odor valence cues approach-avoidance responses, the stance of individuals was measured continuously using force-plate and either pleasant or unpleasant odors were delivered in random times, unbeknown to the participants. The approach-avoidance response was quantified as posterior-anterior momentum (PAM). A force plate measures participants whole-body micro-sway in the form of posterior-anterior angular motion which later was normalized to individual's height and band-pass filtered to produce PAM.

In an initial pilot experiment, PAM values in response to pleasant or unpleasant odor presentation were assessed for t = [250ms, 500ms, 750ms and 1000ms] corresponding to the aforementioned OB-valence results as gamma oscillations, gamma oscillations plus motor response, beta oscillations and beta oscillations plus motor response. Using a linear mixed effect models with participants as random intercept and random slope for conditions, the association between PAM and odors was assessed where a significant main effect for condition was found only at t = 500ms after odor onset, $t(61) = 2.13$, $p < .037$, $CI = [.01, 0.04]$, with no other significant effects at other time-points. Post-hoc t-test determined that leaning backward in response to unpleasant odors was significant, $t(61) = 2.06$, $p < .04$, $CI = [-0.28, -0.04]$, whereas no potential effect found for forward motion in response to pleasant odors, $t(61) = 0.64$, $p > .74$, $CI = [-0.19, 0.39]$.

Consequently, the main experiment with identical design as the pilot experiment, but testing a larger sample, was carried out to assess PAM for the time point t = 500ms, as identified in the pilot experiment. The sample size was estimated based on the effect size of 0.3 (derived from the pilot experiment), required power 0.95, alpha error probability .05, and a correlation among measures of 0.4. The result of the pilot experiment was replicated and there was a significant difference, $t(174) = 3.24$, $p < .001$, $CI = [0.06, 0.23]$, for PAM values between unpleasant and pleasant odor at 500ms post odor onset. Furthermore, given that the pilot experiment provides prior from an independent dataset, the effect was also assessed within a Bayesian framework where, in line with the frequentist analysis, substantial support for the effect of odor valence on PAM was found ($BF_{10} = 3.31$). Again similar to the pilot experiment, a subsequent t-test indicated that the effect was mediated by unpleasant and backward motion, $t(174) = 2.47$, $p < .007$, $CI = [-\infty, -0.016]$, rather than pleasant odors and forward motion $t(174) = 1.22$, $p > .11$, $CI = [-0.04, +\infty]$.

It has been demonstrated that respiratory flow is linked to perceived odor valence (256). However, no relationship was found between the respiration flow and PAM at the time point of interest (500ms), $rho = -0.02$, $p > .75$. The lack of association between respiration and PAM was also further supported by Bayesian analysis.

5.3 STUDY III: RECIPROCIAL CONNECTIVITY BETWEEN OB AND PC OPERATES IN DIFFERENT BANDS

In **Study I,** the validity of the method for extracting OB signals was examined through multiple experiments. Similarly, in **Study III**, prior to assessing the functional association between OB and PC, the quality of the extracted PC activity was probed. The method's sensitivity for different sources, including the PC, was quantified as the odor SNR and operationalized as the mean amplitude of odor trials versus clean air trials. Odor SNR for different sources was computed and sources were sorted by their depth from the cortical surface. The odor SNR was found to be clearly above the upper bound of 95% confidence interval at the depth corresponding to the PC (80-100mm) for both the left PC, $t(28) = 8.53$, $p < 3e\text{-}9$, CI = [0.21 0.34], and the right PC, $t(28) = 7.44$, $p < 4e\text{-}8$, CI = [0.18 0.30].

To fully characterize the functional connectivity between OB and PC, two separate, yet related analyses were performed. The functional and effective connectivity between OB and PC were assessed using cross-spectral density and spectrally resolved Granger causality. With help of cross-spectral density, information that is linearly exchanged between OB and PC during odor presentation can be quantified. Initially, the source time-series of OB and PC were reconstructed using eLORETA and digitized stereotactic positions of each electrode. The time-series were then transformed to the time-frequency domain, implemented by a tapering convolution method. Next, auto- and cross-spectral densities were estimated and compared between the odor and clean air conditions. As predicted, initial gamma synchronization was found in OB which later evolved to beta synchronization. However, assessment of the PC's auto spectral density indicated that synchronization occurred in the lower bands (delta/theta) within the PC. The cross-spectral density demonstrated that OB-PC functional connectivity begins around 100ms after onset in the gamma band, $t(28) = 2.131$, $p < .042$, $CI = [0.003\ 0.151]$, and transfers to the beta band around 740-840ms, $t(28) = 2.466$, $p < .020$, $CI = [0.018\ 0.194]$, and later to theta/delta band around 670-1000ms, $t(28) = 2.620$, $p < .014$, $CI = [0.031\ 0.257]$ (**Figure 5-5 A**).

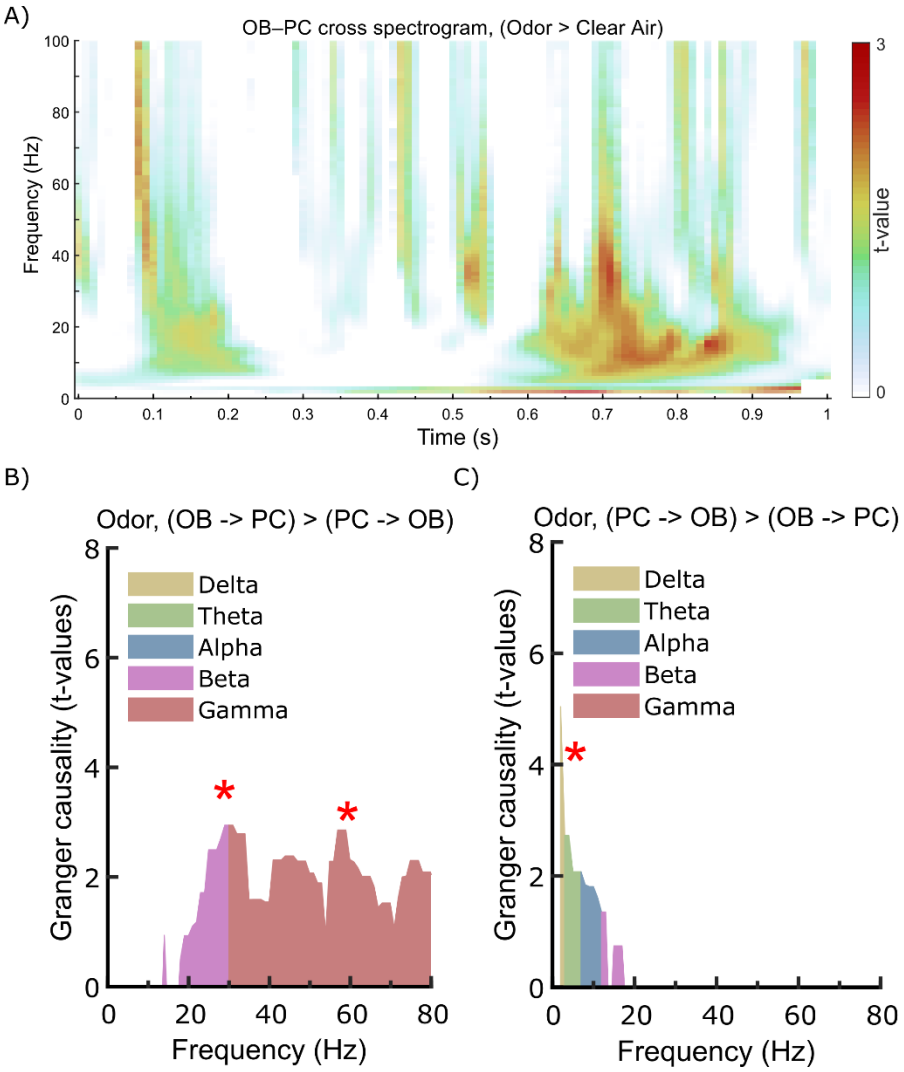

Figure 5-5. The functional and effective connection between the OB and the PC. A*) The cross-spectrogram shows the frequency/time points where there is more function relationship between the OB and the PC for the odor compared to the air trials.* ***B****) There is an effective connection in the gamma and beta bands from the OB to the PC compared to the reverse direction, from the PC to the OB, during 1s odor processing.* ***C****) The effective connection in the delta and theta band was significantly larger for the PC to the OB compared with the OB to the PC during odor processing. Significant peaks are denoted with red asterisks.*

In addition to functional connectivity, effective connectivity from OB to PC, and vice versa, was assessed using spectrally resolved Granger causality (257), a method that allows for characterizing the connectivity between the olfactory nodes in a directed manner and in frequency domain. The reconstructed OB and PC time-series were transformed to the frequency domain using a multi-tapered fast Fourier algorithm. Effective connectivity between OB and PC was subsequently assessed as a function of frequency in both bottom-up and top-down directions, using multivariate spectrally resolved Granger causality. Significant peaks in the gamma band (~58 Hz), $t(28)=2.865$, $p < .008$, $CI = [0.148\ 0.888]$, and the beta band (~30 Hz), $t(28) = 2.953$, $p < .006$, $CI = [0.208\ 1.150]$, were detected during odor processing for the bottom-up connection from OB to PC (**Figure 5-5 B**). Conversely, for the top-down connection (i.e., from PC to OB), significant peaks were found in lower the delta band, $t(28) = 5.074$, $p < .0001$, $CI = [1.076\ 2.533]$, and theta band (~6 Hz), $t(28)=2.078$, $p < .047$, $CI = [0.011\ 1.605]$, during odor processing (**Figure 5-5 C**).

5.3.1 Odor identity is reflected in OB and PC connection

The time-frequency representation of OB-PC connection, estimated as the cross-spectral density, was assessed using SVM to identify clusters in time and frequency where the three odors could be classified above chance level (0.33). Detecting a significant cluster would provide further support to the notion that the OB-PC connection includes odor-specific information whereas lack of significant cluster would indicate that the occurred synchronizations in OB-PC connection are due to non-specific odor processing. Moreover, classification using SVM also indicates when, and in what frequency, the odor information is exchanged between OB and PC. To train the SVM, a neighbouring cluster was defined as 5 and 5 samples for time and frequency axes. For each bin in the time-frequency map, from the defined neighbouring cluster, 121 features were extracted, and unity normalized. Next, within a searchlight framework, the whole 1s was assessed. A cluster was found around 100ms at 35-45 Hz where odors could be classified above chance level with a mean peak accuracy of .42. Subsequently, this peak was determined to be statistically significant, $t(27) = 3.29$, $p < .002$, using 5000 Monte Carlo permutations test (**Figure 5-6 A**). However, the above chance performance was not only limited to this early cluster but extended to an area 300ms post-odor onset in the 50-70 Hz frequency range, another cluster around 30Hz, and oscillating clusters in the theta band over the whole 1s.

Finally, to control for the specificity of the significant clusters to OB-PC connection, the same analysis was performed between OB and a control region, namely postcentral gyrus (PCG). The PCG was picked as a negative control area because PCG is part of the greater olfactory system and has been demonstrated to process intranasal trigeminal stimulus, yet has a low functional connectivity with PC based on a large online Neurosynth database (www.neurosynth.org). No above chance classification accuracy was found around 100ms and in the 35-45 Hz frequency for OB-PCG connection, suggesting that the odor classification within this time window is specific to OB-PC connectivity (**Figure 5-6 B**).

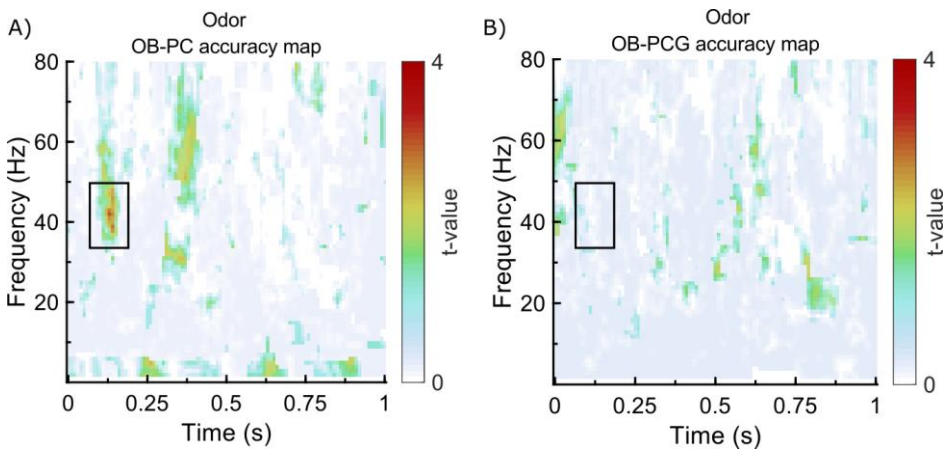

Figure 5-6. SVM accuracy map. A*) The time-frequency accuracy map for OB-PC connectivity. A cluster around 100ms was detected with classification accuracy above chance level and mean peak accuracy of .42.* ***B****) The time-frequency map for the connection between OB and postcentral gyrus (PCG) acted as a negative control area. No above chance accuracy was found for this control connection within the time/frequency window of interest shown by the black box.*

5.4 STUDY IV: THE EBG MEASURE DISSOCIATES PD PATEINTS AND RELATES TO PD PARAMETERS AND OLFACTORY ID

Given the fact that the OB is the first site of insult in PD, an OB measure would be a method that could potentially be used as an early biomarker for PD. However, measuring the OB function in humans is a non-trivial task. In **Study I**, a non-invasive method (EBG) for measuring the function of OB was developed where the test-retest reliability indicated that EBG is a reliable measurement. Hence, in **Study IV**, the EBG method was used to explore the possibility of finding a biomarker that dissociates PD patients from age-matched controls. The EBG time-frequency response to different odors was estimated using a multi-taper convolution method and compared between PD patients and Controls (**Figure 5-7 A**). Subsequently, a non-parametric statistical test, namely 1000-permutation Monte Carlo test, was used to isolate the clusters that are significantly different between the two cohorts. Clusters in the gamma band, around 460ms after odor onset, $t(37) = 3.28$, $p < .001$, the beta band around 620ms, $t(37) = 2.7$, $p < .006$, and finally in the theta band around 680ms, $t(37) = 3.87$, $p < .001$, were found with increase in power in Control compare to PD (**Figure 5-7 A**). Conversely, clusters with decrease in power were found in the gamma band around 660ms, $t(37) = 3.13$, $p < .002$, as well as 980ms, $t(37) = 2.23$, $p < .012$, and alpha/beta bands around odor onset, $t(37) = 3.50$, $p < .02$, when Control was compared with PD (**Figure 5-7 A**).

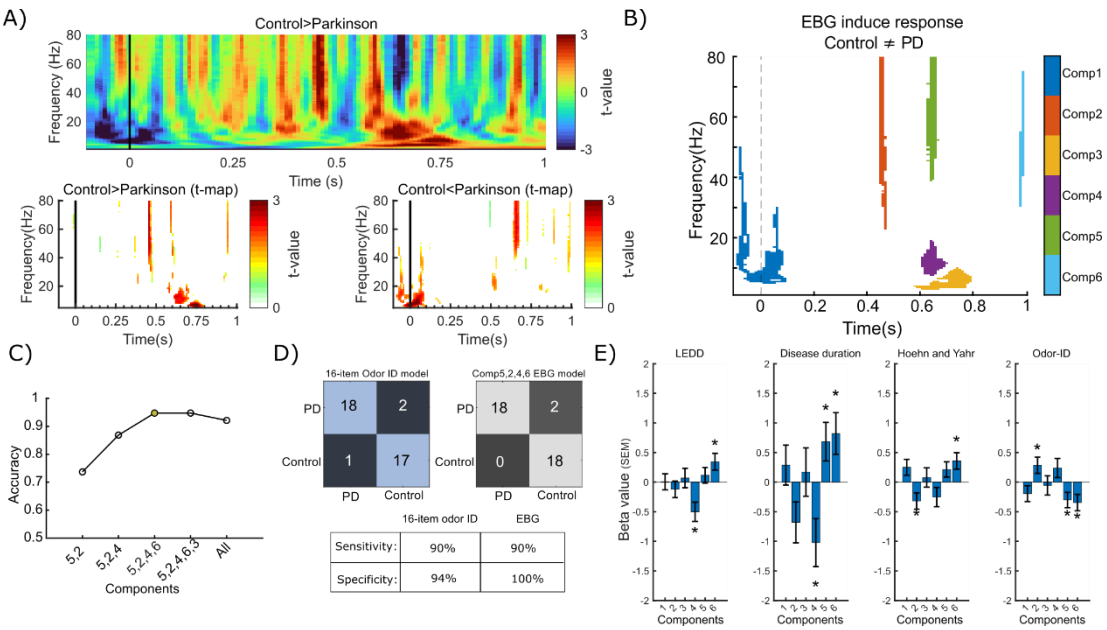

*Figure 5-7. EBG spectrogram dissociates PD from Control. **A**) the heatmap shows the contrast between Control and PD of the EBG spectrogram. Warmer colors show the clusters where Control had larger power whereas the cooler colors show areas where PD had larger power (upper panel). T-map shows the significant clusters (p < .05) where spectrogram power was more for Control compared with PD (lower left panel). Similarly, t-map shows the significant clusters (p < .05) where spectrogram power was more for PD compared with Control (lower right panel). The warmer colors in t-maps show higher t-value. **B**) Total of 6 clusters are identified and named with respect to their time of appearance. Each component is shown with a specific color and the corresponding labels for the colors can be found in the color-bar on the right side of the panel. **C**) The accuracy for each step as the Components were adding to the model in a stepwise manner. The peak accuracy is marked with a closed yellow circle. **D**) The cross-table illustrates the number of true/false positives/negatives for each model as well as the level of sensitivity and specificity. **E**) The bar graphs show the beta values of each component in a linear mixed effect model to predict LEDD, disease duration, Hoehn and Yahr disease severity and odor ID performance. The significant components are marked with asterisks and the error bars denote the standard error of means. LEDD: Levodopa equivalent daily dose.*

Clusters ($p < .05$, cluster size >100) were subsequently labeled in order of occurrence as Component 1, Component 2, etc. A total of 6 components were found and labeled during 1s post odor onset (**Figure 5-7 B**) of which Component 2, 3, and 4 had higher power but Component 1, 5, and 6 demonstrated lower power in Control when compared to PD. Next, the generalizability of the components was assessed using intraclass correlation – ICC(2,k) – where a medium agreement ranging [.46 - .78] was found for the EBG components; hence, demonstrating that these results are likely reproducible in independent sample with similar individual characteristics.

Next, through logistic regression, EBG components were used to assign individuals to their groups belonging (i.e., PD or Control) and in-sample error, sensitivity, and specificity of each component were compared to that of a 16-item odor ID model. None of the EBG components outperformed the 16-item odor ID, neither in in-sample error, determined by Akaki information criteria (AIC), nor in sensitivity or specificity. We then introduced the components to the logistic regression in a step-wise manner and the accuracy was computed for each of these steps. Maximum accuracy (94%) was found for the model including Component 5, 2, 4, and 6, the so-called EBG model (**Figure 5-7 C**). Moreover, when sensitivity and specificity of the EBG model and 16-item odor ID were compared, higher specificity (100%) was found in the EBG model as opposed to 94% in the 16-item odor ID, but equal sensitivity (90%) was found (**Figure 5-7 D**). Despite the higher specificity in the EBG models, the in-sample error (AIC = 279.11) was nominally higher than that of the 16-item odor ID model (AIC = 276.27).

The errors occurring in the 16-item odor ID model were either a Control participant who was on the border line of hyposmia (false positive) or PD patients who did not display hyposmia (false negatives). On the other hand, the EBG model correctly assigned all of these individuals to their corresponding groups. However, two other individuals within the PD group were wrongly classified as a Control participant (false negative). Assessing the demographic and PD parameters of these two patients did not indicate any commonalities that led to the misclassification.

Finally, the association between the EBG components and PD parameters were assessed by linear mixed effects. The relationship between the power level of each component and LEDD, disease duration, H&Y disease severity, and odor 16-item ID performance was determined. For LEDD, Component 4, $t(31) = -3.07$, $p < .004$, $CI = [-0.83, -0.17]$, and Component 6, $t(31) = 2.43$, $p < .021$, $CI = [0.055, 0.63]$, were found to have significant positive associations. Additionally, Component 4, $t(31) = -2.52$, $p < .017$, $CI = [-1.85, -0.19]$, Component 5, $t(31) = 2.10$, $p < .018$, $CI = [0.018, 1.35]$, and Component 6, $t(31) = 2.34$, $p < .026$, $CI = [0.10, 1.54]$, were significantly associated with disease duration. Component 2, $t(31) = -2.35$, $p < .027$, $CI = [-0.60 , -0.039]$, and Component 6, $t(31) = 2.56$, $p < .015$, $CI =[0.073, 0.64]$, could significantly predict H&Y disease severity. Finally, there was a significant association between the power levels of Component 2, $t(31) = 2.07$, $p < .046$, $CI = [0.005, 0.56]$, Component 5, $t(31) = -2.33$, $p < .027$, $CI = [-0.56, -0.037]$, as well as Component 6, $t(31) = -2.48$, $p < .018$, $CI = [-0.63, -0.062]$, and Odor ID performance (**Figure 5-7 E**). It is worth mentioning that there was

no relationship between age and any of the components (all *p*-values above .18); however, there was a significant negative association between Montreal Cognitive Assessment (MoCA) score and Component 3, r (16) = -0.60, $p < .009$, as well as Component 4, $r(16) = -0.49$, $p < .04$, in PDs.

5.5 STUDY V: ODOR INTENSITY RELATES TO COVID-19 PREVELANCE PREDICTION IN SWEDEN

Data from a web-based and self-assessed olfactory test was used for the first time to determine the relationship between rated perceived odor intensity and the prediction prevalence of COVID-19 in a population, in our case the population in Stockholm, Sweden. The development of olfactory ability in the test group, manifested as mean intensity perception per day, was assessed and compared to the prediction of COVID-19 prevalence. As the predicted prevalence increases over time, the mean odor intensity ratings decrease, as evident in **Figure 5-8 A**. Further analysis indicated that both unimodal (odors with low trigeminal components, **Figure 5-8 B**) and bimodal (odors with high trigeminal components, **Figure 5-8 C**) had similar psychometric functions. Assessing the association between the mean odor intensity and the prediction prevalence using ranked Spearman correlation indicates a high correlation $\rho = -0.83$, $p < .001$ for all odors, $\rho = -0.79$, $p < .003$ for the unimodal odor category, and $\rho = -0.83$, $p < .001$ for the bimodal odor category.

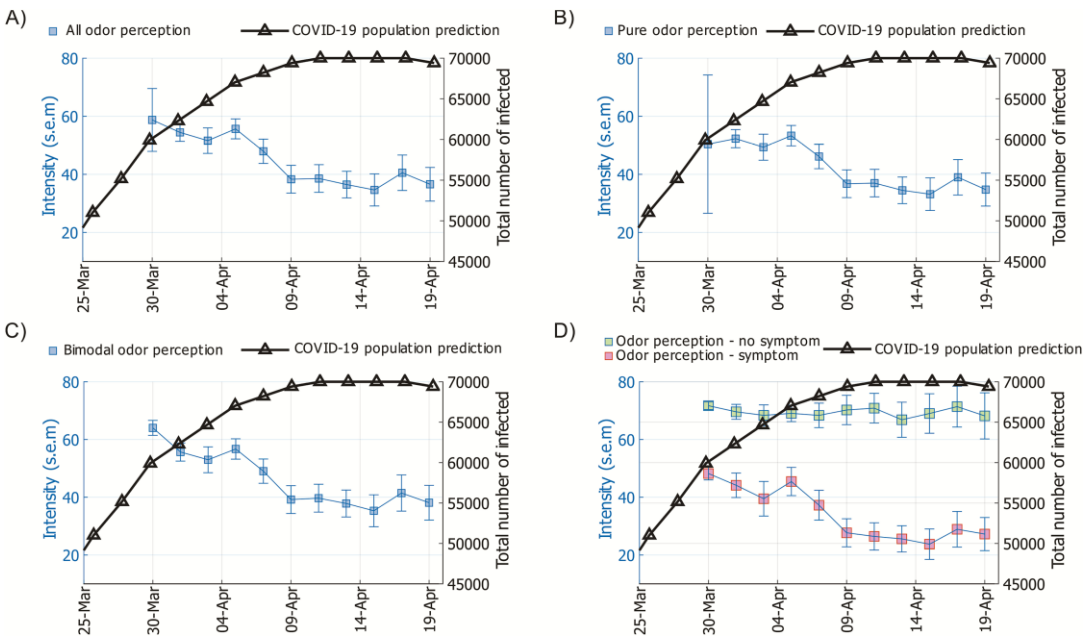

Figure 5-8. Odor intensity and COVID-19 prevalence. *A) The blue graph together with blue axis show the development of the mean odor intensity ratings per day across 5 categories with respect to the prevalence prediction of COVID-19 in Stockholm region that was denoted by the black graph and axis.* ***B****) Similarly, the mean odor intensity for unimodal odors (category 1-2) and the prevalence prediction of COVID-19 are shown.* ***C****) The graph shows the mean odor intensity for bimodal odors (category 3-5) and the prevalence prediction of COVID-19.* ***D****) The mean odor intensity across five odors was divided -depicted for individuals without (green squares and blue axis) and with (purple squares and blue axis) COVID-19 symptoms- and plotted with respect to the prevalence prediction of COVID-19 in Stockholm region (black graph and black axis). The error bars show the standard error of the mean (s.e.m).*

The data sample in this study also included healthy individuals who did not have any COVID-19 symptoms. Therefore, to assess the potential influence of COVID-19 symptom on odor intensity, the individuals were separated between groups with either no symptom or symptom

and rated mean odor intensity was compared with respect to prediction of COVID-19 prevalence. A clear difference between no symptom and symptom group was observed (**Figure 5-8 D**). The more symptoms an individual reported, the weaker the odors were perceived. Accordingly, Spearman correlation indicated a negative relationship, $\rho = -0.29$, $p < .001$, between the number of reported COVID-19 symptoms and rated odor intensity (**Figure 5-9 A**). However, the decrease in perceived odor intensity could have other possible reasons, such as seasonal allergy or gastroenteritis viruses. Therefore, the association of the mean odor intensity with pollen levels in the Stockholm region and the incidence of reported confirmed cases of the common gastroenteritis-causing virus, Caliciviridae, was also assessed. No correlations were found for either of those measures and rated odor intensity.

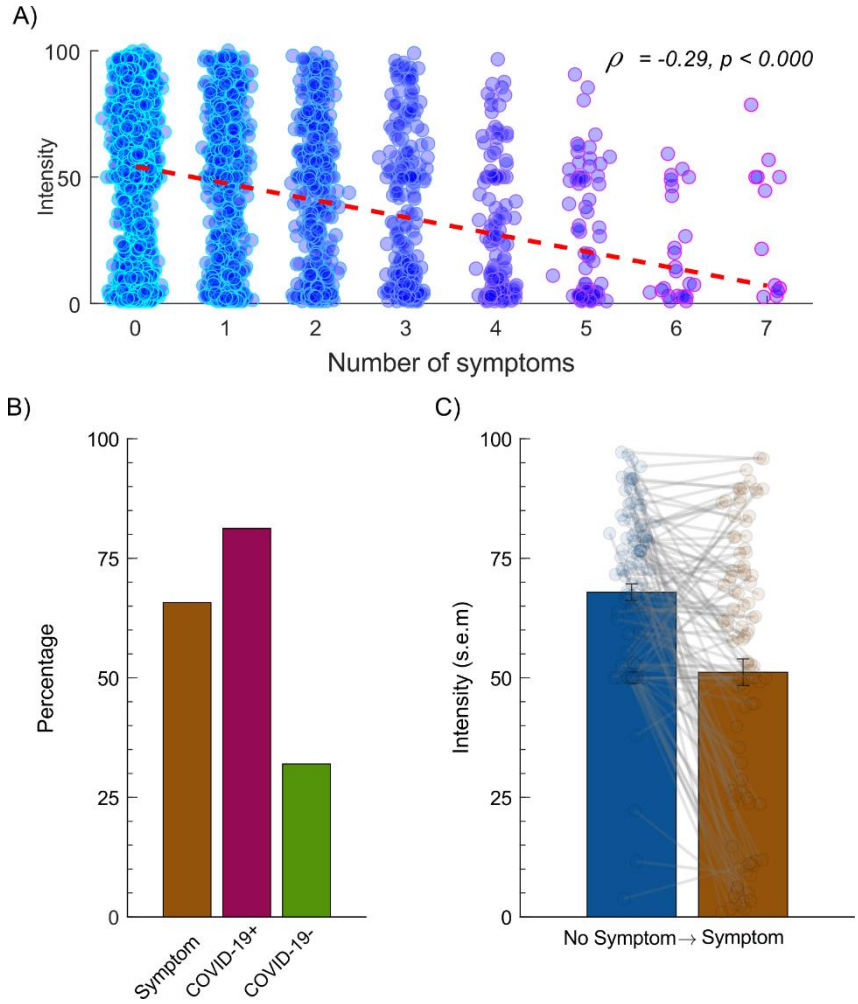

Figure 5-9. Mean odor intensity and COVID-19 symptoms. A*) The mean odor intensity negatively correlated with the number of symptoms. Each filled circle denotes an individual data point. The dashed line shows the man slope of decline.* ***B****) The bars show the percentage of individuals within each group who were identified as olfactory dysfunction* ***C****) The transgression from declaring no symptom to symptom indicated a significant drop in odor intensity rating. The bars show the mean odor intensity in the session individuals reported no symptoms and subsequent sessions where they declared having at least a symptom. Scatter plot shows the individual rating and lines connecting the value of the same individual. Error bars show the standard error of mean (s.e.m).*

Mean odor intensity was found to be lower in individuals with COVID-19 symptoms compared to those who did not have any symptoms. Subsequently, the prevalence of olfactory dysfunction was assessed in the subsamples. Olfactory dysfunction was, similar to previous research (258), defined as intensity ratings below the 10th percentile of the no symptom group's odor

intensity rating. Notably, this threshold is a conservative assessment since the no symptom group might include asymptotic COVID-19 patients or individuals with olfactory dysfunction prior to COVID-19 pandemic. Given this threshold and intensity ratings, 66% of individuals in the symptom group (n = 2469) were categorized with olfactory dysfunction (**Figure 5-9 B**). The proportion of the individuals falling under the olfactory dysfunction grew to 81% when only assessing those who were clinically diagnosed with COVID-19 (n = 16, COVID-19+) and decreased to 32% for individuals with negative result for COVID-19 test (n = 25, COVID-19-)(**Figure 5-9 B**).

Furthermore, the repeated testing regime provided us with the opportunity to assess odor intensity rating in transition from “No symptoms” to “Symptom”. A total 107 individuals were identified who made this transition, meaning that these individuals' responses shifted from having no COVID-19 symptom to have at least one COVID-19 symptom in the next session at some point during testing. The odor intensity rating on the group level significantly decreased, $t(103) = 6.15$, $p < 0.001$, equals to 29% reduction, from “No symptoms” session to “Symptom” session. The average time elapsed between two sessions was 1.82 ± 2.64 days.

Finally, the test-retest reliability of the test regime was assessed within individuals who performed two sessions and reported “No Symptoms” in both sessions (n = 130). The relationship between two sessions of the odor intensity was assessed using a Spearman correlation test where we found a high test-retest value of 0.66, $\rho(128) = .66$, $p < .0001$.

6 DISCUSSION

The overarching aim of this thesis is to expand the knowledge on the role of oscillations in odor processing within the OB as well as in its communication to the primary olfactory cortex. However, given the lack of a non-invasive method allowing recordings from the human OB, the initial objective was to develop a reliable non-invasive, yet easily accessible measuring technique. In **Study I**, through multiple experiments, a non-invasive method of measuring OB function, the EBG measure, was developed and its validity and reliability determined. Measuring the function of the OB is of importance for our understanding of how the olfactory system works in humans as well as enables the development of novel biomarkers, particularly for various neurodegenerative diseases, many of which where the OB is of interest. In **Studies II-III**, the EBG method was then used to evaluate OB function, especially processing of odor valence, as well as assessing the OB's connection to higher order olfactory regions, namely the PC, to extend our understanding on human OB function and its communication with PC. In **Study IV**, the EBG was used to assess the feasibility of whether measures of how the OB responds to odors could correctly classify PD patients and healthy age-matched controls. Finally, in **Study V**, the association between odor intensity perception and prevalence of COVID-19 in a Swedish population was assessed to provide a foundation for future work using EBG method to assess what impact, viral infection, particularly the SARS-CoV-2 virus, might have on the function of the OB.

6.1 WHY EEG-BASED METHOD

Functional measures of OB processing are indispensable data if the assessments of human olfaction should be used as future diagnostic tools. Olfactory dysfunction is common in seemingly non-related diseases, including depression (259), neurodegenerative disorders (123,160), and more recently, respiratory viral infections (e.g., SARS-CoV-2)(123,260). However, the non-invasive functional assessment of OB is not a trivial task. Non-invasive methods including functional near infrared spectroscopy or PET lacks temporal resolution for reliable measuring OB. Conversely, MEG has high temporal resolution but the helmet in which the MEG sensors are embedded does not cover the forehead well enough. Moreover, MEG is only sensitive to tangential sources, although there is no clear information of how dipoles form in OB, there is a high chance that dipoles are created radially along the olfactory nerve, hence, hidden to the MEG method. Among non-invasive methods for functionally assessing brain responses, fMRI is the most common method, and it can acquire functional data from almost everywhere in the human brain, except a few regions; among these the OB. The human OB is situated close to paranasal sinuses, cavities filled with air within the skull, creating inhomogeneity in magnetic permeability and consequently creating large susceptibility artifacts that prevent acquisition of BOLD-fMRI signals. However, contrary to fMRI, EEG is not affected by the presence of air cavities and in contrast to MEG, the montage of EEG sensors is flexible meaning that the placement of electrodes can be easily changed. Also, EEG is sensitive to both tangential and radial sources. Finally, EEG does not have a low temporal resolution such as functional near infrared spectroscopy, PET or fMRI. Therefore, EEG was selected as the technology for developing a

non-invasive method for functional assessment of OB. Moreover, from a clinical and accessibility perspective, EEG is by far the cheapest and among the most available brain imaging tools in clinical settings.

6.2 THE OB UTILIZES GAMMA SYNCHRONIZATION FOR ODOR PROCESSING

Intracranial data obtained directly from the human OB demonstrated the presence of a gamma synchronization in response to odors (159). Moreover, past findings in the non-human literature indicated that the gamma synchronization mostly originates from intra-bulb processing with only minimal influence from centrifugal projections. Accordingly, when the centrifugal projections to OB are blocked, only gamma synchronization remains intact in the OB in response to odors (59,261). Moreover, gamma oscillations in the anterior piriform cortex, one of the main recipients of signal from the OB, are disturbed when gamma oscillations are reduced in the OB (57). However, beta oscillations in anterior piriform cortex are not affected by manipulating gamma in the OB, therefore, providing further evidence that gamma oscillations reflect intra-bulbar processing. However, it is likely that the OB also functions in other bands, including beta and theta. Especially beta oscillations are more apparent when processing odor context or associations (57). Given that the odor induced gamma oscillations in the OB is one of the most robust electrophysiological phenomena and have been found across every mammalian species studied so far (56), it is likely these oscillations are the best candidate to target with the EBG method to acquire high fidelity OB signal; therefore, oscillations in the gamma band were the focus in **Study I**.

Using four active electrodes on the forehead and two reference electrodes, through multiple experiments, the EBG method was demonstrated to reliably detect OB processing via a clear gamma synchronization around 100ms post odor onset. There is strong evidence to believe that the OB is the source of the detected signal. The timing of the gamma synchronization suggests that the OB is the underlying source given that it is too fast for the PC, or other more cortical structures, to process the odor. Furthermore, the source reconstruction indicates the OB as the most probable underlying source for the acquired gamma oscillations around 100ms post odor onset. Specially, the marked gamma oscillation was replicated in OB's source reconstructed time-series in **Studies II-III**, suggesting that the signal picked up by the EBG electrodes can be directly linked to the OB.

Like any method, the EBG method is only useful if the measurement is robust and reliable. In **Study I**, the ICC result indicated high agreement of the EBG measurement across individuals and sessions which was further supported by the high test-retest correlations across sessions. Specifically, the test-retest correlations were between .76 and .86, a range that is comparable to event related olfactory and non-olfactory EEG measures. For example, the test-retest of olfactory-derived scalp ERPs typically produce values as low as .05 (262) to as high as .81(263), dependent on the experiment. Likewise, past ERP studies in visual and auditory produced similar values in the range of .48 – .80 (264). Moreover, in **Study IV**, the gamma synchronization was found again in EBG sensor space; this time in an independent sample of older healthy

adults, suggesting that the EBG method is not restricted by age. Although past non-invasive and invasive electrophysiological recordings from humans provided strong evidence that *1/f* noise increases by age (265), the replication of gamma synchronization using EBG method in older adults indicated that the method is robust enough to detect OB signal also in the presence of elevated *1/f* noise in older adults.

Insensitivity to habituation is another unique feature of the OB (250,251). Oppositely, PC has demonstrated rapid decrease in signal amplitude in response to repeated and prolonged odor exposure (71,251). The results presented in **Study I** demonstrated no change in the EBG gamma power as a function of trials for the time-frequency window attributed to the OB. However, the peak-to-peak potential over the parietal lobe, the hallmark ERP signal for odor responses, decreased across trials, thereby demonstrating occurrence of habituation in higher order olfactory regions. Moreover, when participants rated the perceived intensity of odors for each trial, their ratings rapidly decreased across trials. Hence, in clear contrast to the decrease in the odor ERP response and odor intensity rating, the lack of habituation for the EBG gamma power further supports the notion that the underlying source is the OB rather than other cerebral areas, such as the OFC. Notwithstanding, OB's insensitivity to the habituation is mainly based on data obtained in anesthetized mice and later studies suggest that odor-induced neural activity in anesthetized animal might not always generalize to awake state (266).

Furthermore, the lack of EBG results from an individual with ICA suggests that removing the OB will eliminate the gamma synchronization in question. Although non-significant result should not be interpreted as accepting the null hypothesis, the gamma synchronization during the time-window of interest in the individual with ICA was more than 2.5 standard deviations smaller than the average obtained from individuals with a normal sense of smell. Thus, in addition to the source localization result and the reliability of the EBG signal with characteristic OB responses, the lack of EBG results in an otherwise healthy individual that lacks OBs demonstrates that non-specific odor parameters, such as systematic saccade eye movement, attention shift, frowning, or other muscle movement due to potential irritation from odor stimuli, is unlikely to be the source of the demonstrated gamma synchronization in the EBG electrodes.

6.3 THE OB PROCESSES ODOR VALENCE

Odor valence is one of the core dimensions of odor perception. Valence shapes our approach-avoidance responses, the critical behavior that survival of any organism is dependent on. Approach-avoidance responses are the driving force for finding foods and avoiding dangers such as predators and poisons. The OB is located at the very frontline of the central olfactory system, directly connected to the olfactory receptor neurons, and as such, an ideal stage for facilitating fast processing of odor valence (119). However, the role of the human OB in valence processing is not clear. EBG provided the opportunity to non-invasively assess the processing of valence in the OB. Specifically, results from **Study II** demonstrated that the human OB is linked to valence at two specific time intervals. Perceived odor valence was related to an early gamma synchronization followed by a late beta oscillation in the OB. This sequential

processing of valence in OB agrees with the two-stage model of odor processing in the OB suggested by Frederic and colleagues (57). Their proposed model specifically postulates that initial processing in gamma allows for fast discrimination of odors and the second slower process in beta allows incorporating information from centrifugal inputs for more accurate decision. In line with this model, results in **Study II** indicated that early gamma processing of valence likely cued and facilitated fast avoidance responses to unpleasant odors. Odor induced gamma synchronization has in past studies been attributed to local processing within OB (58,267) that is, to some extent, dependent on the individual's past experience (189). This provides further reason to believe that the gamma synchronization aids avoidance response. Moreover, anatomically, OB is privileged for processing of olfactory stimuli associated with threat given its early location in the olfactory processing stream, receiving direct inputs from the OSN, as well as displaying monosynaptic connection to the amygdala, a cerebral area responsible for the processing of saliency and threat (268).

Assessing the relationship of the OB's neural data in gamma and beta bands with valence ratings in RSA space demonstrated that the late beta peak, around 700-800ms after odor onset, is more associated with the final valence percept than what the gamma peak demonstrated. This finding further aligns with Frederic and colleagues' two-stage model (57) of odor processing in which separate afferent and efferent processes are considered in the OB. Beta oscillations are often known to correspond with top-down processes in contrast to gamma oscillations that are more frequently connected to bottom-up connection (56,269,270). This view of strict separation between gamma and beta is, however, not straightforward given that a past study suggests that beta can be detected in the OB during initial odor sampling (271). Moreover, when effective connectivity between OB and PC was assessed in **Study III**, efferent connection from OB to PC was determined to operate in the gamma/beta band whereas the afferent connection from PC to OB was demonstrated to operate in the theta/delta band. It is possible that the beta oscillation found at late time points in the OB is nested within slow delta/theta oscillations of the efferent connection from PC to OB. I argue, however, that the most parsimonious explanation for the late beta oscillations is that these represent valence-dependent efferent projections to the OB from higher order olfactory cortices, including the OFC, amygdala, and the PC. These projections are needed to update and integrate information where the odor object identity (42) and past experiences (272), two aspects among several that strongly influence the final odor valence precept, shape the interpretation of the odor (26,273) and prepare the OB to process the second sniff of the same odor.

Mu desynchronization has previously been demonstrated to correspond with preparatory motor responses to salient stimuli (274,275). Accordingly, in **Study II**, we found that mu desynchronization increases for unpleasant compared to pleasant odors over the motor cortex. Moreover, this valence-dependent motor response occurs around 150ms after the increase in gamma and early beta activity within the OB and consequently allows for the time needed for transmission of valence-related signals between the OB and motor cortex. Importantly, in preregistered experiments, including a pilot and main experiment, odors with a negative valence were further demonstrated to trigger a full body avoidance response expressed as a backward motion; i.e.,

leaning away from the odor. However, no effect was found for positive odors. It is possible that a similar effect occurs for neutral and pleasant odors but that the response to these odors occurs at later time points than the analyses window determined by our pilot experiment. In light of this, previous studies on rodent detected an increase of power in the gamma and beta bands within the PC, primary motor cortex, and the magnocellular red nucleus just before executing a motor response for the Go trials in a Go/No-Go paradigm. Of note, the power increase only occurred during the final sniff – either second or third sniff (276). Hence, the lack of effect for pleasant odors in **Study II** during the first sniff could be simply explained by the fact that latter sniffs are more relevant for the pleasant odors.

Although result from **Study II** indicates that human OB processes subjective odor valence, it does not demonstrate that OB is the first stage of valence processing. Several studies, both in human and non-human animals, suggest that odor valence is linked to the physicochemical properties of the odorants in question (14,277–279). Moreover, the odors' physicochemical properties can to some extent predict the olfactory receptor neuron activation. Hence, coding of the odor valence seems to begin within the olfactory epithelium rather than OB (278). However, whether the physicochemical-dependent valence coding on the receptor level reaches OB or not, is still an open question. Accordingly, it is worth noting that the results in **Study II** were based on the subjective valence rating and the included odors were not a priori valence ranked. Hence, the detected synchronizations during certain frequency bands and time periods in the OB demonstrated a uniform representation of subjective perceived valence across participants and not a pre-defined odor classification. This suggests that odor identity per se has only partial contribution in the OB process during the early gamma and late beta oscillations.

6.4 ODOR IDENTITY AND RECIPROCAL CONNECTION BETWEEN OB AND PC

In **Study III**, assessment of the temporal and frequency information in functional connectivity between the human OB and PC during odor perception demonstrated that the frequency range of the connection is dependent on its direction and latency from the odor onset. Furthermore, what odor the participant smelled could be decoded from the OB-PC connection within 100ms after odor onset. Accordingly, the odor identity, defined here as the odor per se rather than the object associated with that specific odor, is embedded in the OB-PC connection and can be partly retrieved by assessing the pattern of the OB-PC connection in frequency and time.

Using the EBG method developed in **Study I**, besides the scalp EEG and source reconstruction method, the activation time-series for OB and PC were reconstructed. It is worth noting that the spatial specificity of the EEG reconstructed sources is less than, for example, surgically implanted intracranial electrodes. Nevertheless, the EEG source reconstruction method was recently shown to be effectively sensitive to radially deep dipoles (280). Moreover, as mentioned in **section 6.2**, the EBG method was demonstrated to be capable of extracting a reliable OB signal in multiple experiments. However, validating the PC dipole is more difficult. To address this issue, the sensitivity analysis was performed by which a high odor SNR was determined for bilateral PC compared to surrounding regions. Furthermore, the spectrogram of

PC contained some of the key features of past intracranial recording (62). Hence, it was concluded that the source reconstruction method, with help of the EBG, was successful in extracting a valid PC signal.

Subsequent assessment of the OB and PC connectivity using spectrally resolved Granger causality indicated a causal communication in multiple bands during odor perception. For the clean air trials, no connection was found, except a weak gamma afferent connection. Consequently, the lack of extensive communication during the clean trials emphasizes the importance of odors for eliciting the causal link between the OB and PC. More importantly, the afferent connection was found to operate mainly in the gamma and beta bands, whereas the efferent connection was operated in the theta/delta bands. This is in line with previous researches in which different frequencies were attributed to afferent and efferent connections in both the olfactory (281) and the visual systems (282).

Past rodent and intracranial studies in human have demonstrated that odor identity can be decoded from PC activity (62,283). Notably, Jiang and colleagues recently demonstrated that oscillatory signal in PC transmits odor information within a few hundred milliseconds (62). In **Study III**, we demonstrated that the odor can be deciphered from the OB-PC connection within 100ms after odor onset using a machine learning method. A significant cluster with the peak mean accuracy of 42% was identified in the 35-45Hz frequency. Although this analysis lacks directionality, it is likely that this cluster in gamma band is related to the transmission of odor information from the OB to the PC given that our earlier analysis of Granger causality connectivity indicated that the afferent connection is dependent on the gamma/beta frequency. Moreover, the failure of decoding odor identity from the connection between the OB and the control region, the postcentral gyrus, within the same time points and frequencies as the significant cluster found for OB-PC connection, further supports the specificity of this finding. However, assessing each odor separately demonstrated that performance of the classifier varies across odors. This can possibly be attributed to differences in the frequency and latency of odor representations in the OB-PC connectivity. Given the difference in perceived valence between the included odors, valence might have been the underlying parameter that mediated the ability to dissociate odors in the machine learning decoding paradigm. That said, the confusion matrix demonstrated that odors with opposite valence were often confused by the decoding machine; hence, there was no support for valence being the determining parameter in machine learning classification results.

6.5 EBG CAN DISSOCIATE PD FROM CONTROL

In **Studies I-III**, it was demonstrated that the EBG method can reliably assess functional processing within the human OB. Given that olfactory dysfunction in PD precedes the characterizing motor symptoms by several years, EBG has considerable diagnostic potential for PD. Hence, in **Study IV**, the possibility of dissociating PDs from age-matched healthy controls using EBG was assessed. Using EBG, clusters were found in the time-frequency map that had significantly different levels of power in multi-bands and intervals post odor onset between PD

and healthy controls. Subsequently, these components allowed us to dissociate PD from controls with high accuracy in a logistic regression model.

Our results indicated that the power of each cluster in the gamma, beta, and theta bands were different during odor processing between PD and Control. Impairment in the gamma band, given that gamma is linked to intra-bulb processes (58,59), might be caused by the well supported PD-dependent neuronal loss in the OB (284). Moreover, the impairment in the top-down projection is likely responsible for the difference observed in the beta and theta band (57), which is further supported by considering their late latency of these clusters. Hence, this result suggests that the reciprocal connections (i.e., afferent and efferent) between the OB and higher olfactory cortices involved in the processing of various odor aspects, including valence, are impaired in PDs. In line with this, odor valence perception is abnormal in PD patients compared to controls (285). Moreover, this is also in line with the notion that most of the identified EBG components occurred relatively late in the temporal chain of neural processes. Relatedly, the late components of the event related potentials have been demonstrated to have a lower amplitude in PDs compared with Controls (286).

The logistic model including EBG components achieved higher specificity, but similar sensitivity, compared with the 16-item odor ID model. However, the 2 falsely classified individuals in the EBG and 16-item odor ID models were different patients. The misclassification that occurred in the odor ID model is easy to understand. These were PD patients who did not develop hyposmia, therefore occurring as false negatives, and one Control participant who was on the borderline of hyposmia, therefore occurring as a false positive. Notably, the PD patients who were erroneously classified as a Control by the odor ID model were correctly classified as a PD patient in the EBG model. This suggests that the EBG model is not as dependent on olfactory dysfunction as the odor ID model and reflects information beyond mere olfactory impairment.

One of the EBG early components (Component 2) that was associated with PD disease severity (but not cognitive measures) occurred in the gamma band, a frequency range that is known to be related to intra-bulb processes. Hence, this association suggests that within-OB processing is potentially most associated with behavioral measures in PD but also that it is independent from cognitive deficits. Moreover, the independence of this component from cognitive measure further indicates that sensory processing might be more involved with the gamma band within early time intervals. Moreover, in line with the view of olfactory loss as a common symptom of PD (123,160), the temporally late Components 5 and 6 were associated with olfactory odor ID; a test that is partially dependent on cognitive function (287), such as the processing of labels and cues. Additionally, Component 6 had an inverse association with H&Y disease severity and therefore, the olfactory performance of the PD patients with high EBG response was closer to Controls and they had lower H&Y disease severity. However, these results should be interpreted with caution because when a conservative 1000-randomization bootstrap test was used to assess the results for statistical significance, the association between H&Y disease severity and odor ID with EBG components only marginally survived.

Olfactory related electroencephalography measure has previously been used to dissociate PD patients from Controls (141,286,288). However, in **Study IV**, the function of the human OB in PD was here assessed for the first time. This is of importance for PD diagnosis because the OB is the most vulnerable and earlies site of insult in PD. Accordingly, EBG has several benefits as a potential diagnostic tool. Firstly, it is independent of cognitive ability, thereby might be a more suitable test than odor ID tests which are affected by dementia and other cognitive impairment associated with PD (289,290). Secondly, it is non-invasive and accessible clinical test that potentially dissociates PD from healthy controls by targeting part of the cortex that is directly involved in PD. However, it is worth mentioning that EBG is currently not a turn-key ready clinical method. The method needs to be tested in an at-risk population and in various PD subgroups before it can be implemented as a clinical test.

6.6 ODOR INTENSITY RELATES TO COVID-19 PREVELANCE PREDICTION

Results from **Study V** demonstrated that simple perceptual rating of odor intensities can have a great potential for effectively and inexpensively track COVID-19 prevalence. Odor intensity ratings were demonstrated to closely follow COVID-19 prevalence prediction over time. Moreover, the magnitude of the decrease in mean odor intensity was associated with the number of reported COVID-19 symptoms. This association was further highlighted by the decrease in odor intensity ratings for individuals who progressed from having no COVID-19 symptom to reporting having a COVID-19 symptom in the next session.

During a pandemic as widespread as the ongoing one, an accessible, inexpensive, and easy to use test for quick diagnosis is vital. The results of this study suggest that olfactory self-testing using common house-hold items can provide a simple and inexpensive solution for individuals to achieve a quick assessment of olfactory dysfunction that might indicate the onset of COVID-19 infections, but also for the governments and health organizations to track the spread of the disease in a society. In this study, odors were categorized to high and low trigeminal groups to assess whether the level of trigeminal stimulation was a factor of interest. However, all the categories demonstrated a similar pattern and followed the predicted COVID-19 prevalence prediction. Hence, this indicated that the odor intensity test can be conveniently carried out without the confines of the trigeminal aspects of the odors. This is of importance given that most household items activate the trigeminal system at some levels. Currently, it is undecided whether, in addition to the olfactory system, the SARS-CoV-2 virus impairs the trigeminal system. However, it is possible that the function of the trigeminal system is affected by the reduced olfactory ability per se (291).

The underlying mechanism of COVID-19 anosmia is not yet fully understood. However, it is very likely that SARS-CoV-2, similar to other strains of coronavirus, infiltrates the brain with resulting damages to the OB as well as other brain areas (292). The exact effect of COVID-19 on the function of OB is unknown and future research is needed to answer this aspect.

6.7 LIMITATIONS

To definitely validate the EBG method, intracranial recording from OB with simultaneous EBG recording on the surface during odor presentation is needed. However, accessing such data is extremely difficult, given that intracranial recording is restricted only to patients with intractable epilepsy. Moreover, the electrode placement is also strictly limited to the clinical need in those patients; placing an electrode on the OB without a clinical need would be a violation of the current ethical code. Another confounding factor is that some of the assumptions in the study are based animal research. Particularly the insensitivity of OB to repeated exposure of odors is based on recordings done in anesthetized animals.

The association between valence rating and OB function was assessed in **Study II**. However, odor valence perception is to a large degree dependent on the individual experience. When the individuals' odor valence RDMs were compared to that of group RDM, a mean similarity of 62% was found. Therefore, within the sample used in **Study II**, 38.2% of the total variance is explained by individual differences with the remaining variance linked to various aspects where the physicochemical properties of the odor can be hypothesized to be the most important one. Although the choice of method to some extent removed the potential impact of the physicochemical properties, it did not completely eliminate it. Furthermore, the demonstrated connection between the OB and motor response in this study was indirect. The results from the valence processing in OB and the whole-body approach avoidance were from independent experiments and therefore, connecting their results should be done with caution. To directly link OB functional and whole-body approach avoidance responses, one needs to assess the EEG source signal in individuals that are freely moving around. This would result in large motion artifacts and currently, there is no method available that is capable of assessing OB while participants are allowed to move in response to the odor.

In the **Study III**, the machine learning analysis found a significant cluster that could predict the odors in the gamma band during early time points. It is worth mentioning that the mean accuracy for this cluster is significantly above chance level (0.33); yet this is not a strong result. It is likely that the accuracy within this analysis is restricted by the low number of odors and their proximity in perceptual space. Moreover, Given the low number of odors and high dimensionality of the underlying data, it is difficult to indicate which specific odor dimension contributes to the machine learning odor classification.

The EBG method showed a promising ability to dissociate PDs from Controls in **Study IV**. However, the dataset is relatively small; therefore, before concluding that EBG can be implemented as a PD diagnostic tool, this finding must be replicated in a larger sample as well as in an at-risk population. Moreover, given the current montage of electrodes and the volume conduction, the method is currently unable to separate left and right OB and therefore unable to benefit from the clear laterality of early disease stages. Another confounding factor in this study is that the patients with late stages of PD might have a reduced sniff function (293). However, to alleviate this confounding parameter, several steps were taken. First, sniff-triggered design allowed odors to be delivered at the same speed for all participants to a point high up in the

nasal cavity and consequently the magnitude of sniff was similar for all participants. Second, the sniff-triggered event related response was removed from the EBG response. Finally, no early differences were found in the theta band, the frequency and time interval related to sniff.

The limiting factor of **Study V** was the low number of the individuals with confirmed COVID-19 diagnosis. Hence, the individuals in the symptom group were not confirmed to be infected with SARS-CoV-2. Nevertheless, the number of the symptoms negatively correlated with the odor intensity rating. Moreover, individuals who progressed from "No symptoms" to "Symptom" had a significant drop in the odor intensity perception on average. All that being said, it is worth mentioning that self-assessment of odors and subsequent potential decrease in the odor intensity perception per se should neither be interpreted as COVID-19 diagnosis nor clinical olfactory dysfunction measure on the individual level. Yet, the odor intensity ratings can track COVID-19 prevalence and potential other strains of coronavirus on the population level and therefore can be used as an alternative method in the countries without the sufficient infrastructure for screening in the similar outbreaks in future.

6.8 METHODOLOGICAL CONSIDERATION

Acquiring OB signals via the EBG method requires some methodological considerations. First, participants in all studies of this project were tested in a nutrition deprived state. They were asked to not eat or drink anything other than water at least for 6 hours prior to testing. Accordingly, past non-human studies have demonstrated that the OB is more sensitive to odors when the individual is in the hungry rather than satiated state (294,295). Relatedly, more MCs/TCs have been demonstrated to respond to odors when the individual is hungry, whereas during satiation, a large portion of MCs/TCs are inhibited. Second, in all studies of this thesis, except Experiment 3 within **Study I** and the full **Study V**, trials onset were time-locked to inhalation onset without a detectable onset cue given that past studies indicated that 50% of all MCs/TCs cells in the OB are locked to respiration cycle (56,296). However, it should be note that respiratory-locked oscillations occur in theta band; hence, respiration has minimal effect on the results found in the gamma and beta bands in this thesis. Moreover, the sniff signal was removed from OB responses to control for the nuisance effect of respiration wherever it was possible. Third, all odors used in this study were selected and diluted insofar that they did not produce a noticeable trigeminal percept. Frowning as an automatic motor and part of pain response is evoked by the trigeminal nerve. Therefore, if odors with larger trigeminal components are used, EBG response could be masked (297). Finally, all studies, except **Study V**, are dependent on a temporally accurate olfactometer (164). A small jitter in the trial onset can significantly reduce the signal and consequently reduce the EBG response to the point that is not detectable from the background noise.

6.9 CONCLUSION

The overarching aim of this thesis was to extend our understanding of human OB's function. The results presented in this thesis indicated two main points. First, using multiple experiments, it was demonstrated that the human OB function can reliably be measured using active

electrodes on the forehead and with the help of temporally precise olfactometer. Second, the function of human OB has been outlined in more detail. Specially, the similarities and differences of the human OB function compared to that of animals were further illuminated. The results in the thesis provided a new evidence for the two-stage model of olfaction (57) in humans, that has been originally introduced based on animal data. However, contrary to these similarities some other findings reported in this thesis indicated that some aspects of the human olfaction are unique. Notably, these similarities and differences emphasize the importance of shifting to translational research that involves cross-species experiments. Animal research is certainly a giant stride for understanding human olfaction, but it is not adequate. The non-invasive EBG method developed and described in this thesis can pave the way for such translational work.

Moreover, another critical finding of this thesis was the potential relevance of the EBG method for early PD diagnosis. Although assessment in the at-risk group is required before the EBG can be introduced as a reliable clinical test, but the results presented here are sufficient for proof of concept that EBG can serve as an early diagnostic tool for PD. Finally, in the last study, it was demonstrated that olfactory dysfunction is a salient symptom of COVID-19 insofar that odor intensity rating closely tracked COVID-19 prevalence prediction. The results in this study, increased the confidence in self olfactory test and demonstrated that even outside the strictly controlled lab environment, olfactory test can serve as an inexpensive and fairly accurate measure, albite on the population level. Therefore, such a simple olfactory test can be designed and used in future with greater trust on the group level.

6.10 POINTS OF PERSPECTIVES

The studies presented here used EBG to answer some critical questions about the role of the human OB in odor perception as well as potential diagnostic benefits that EBG can offer by measuring OB functions in disease. With EBG, odors were demonstrated to induce gamma activity, similar to what has been previously shown in non-human studies. However, when clean air was assessed, similar gamma-like activity was observed, albite in lower gamma band and at the onset of each trial. This observation brings up an indication that respiration alone entrails gamma activity. Future studies should assess what the function of respiration-induced gamma synchronization plays for perception or other aspects of human life.

All participants in this PhD project were nutrition deprived. Therefore, another possible future study is to assess effects of nutritional state within a feeding-controlled environment. Moreover, it has been demonstrated that negative odors are prioritized in the OB. This finding can be further assessed in future work where odors are either tailored for each individual based on their reward properties or, alternatively, odors are conditioned with positive outcomes to conclusively determine whether the human OB favors processing negative odor valence.

EBG has also been demonstrated to be capable of dissociating PDs from age-matched healthy controls. However, given that all the PD patients in **Study IV** had already been diagnosed with PD and most of them already developed olfactory dysfunction, future work should assess the

EBG response in at-risk groups employing a longitudinal study design; a method that is beyond the reach for a PhD that is limited to 4 years of full-time work. Moreover, the EBG data needs some preprocessing and artifact rejection before the main analysis. Converting these preprocessing and artifact rejection steps to an automatic pipeline should be implemented and assessed in future works. Consequently, the automation of the preprocessing and artifact rejection steps will render an implication of the EBG as a potential PD diagnostic tool more straightforward. Moreover, the automatic artifact detection may be implemented in an online manner to allow for the triggering of the olfactometer whenever there is no muscle activity detected. This way, the number of trials needed to obtain enough clean data would be minimized and consequently recording time would also be shortened and allow for better accuracy.

Olfactory dysfunction has been related to several diseases, including neurodegenerative diseases, psychiatric disorders (e.g., MDD) and recently COVID-19. Viral infection was among the most common causes of olfactory dysfunction (146), even before the COVID-19. Given the prevalence of the current pandemic, it is foreseen that anosmia will become a more serious challenge for the healthcare system in the near future. Therefore, the urgency for assessing human olfaction in an objective manner and at mechanistic level is developing to the greater level. This highlights the effectiveness of a non-invasive and easily accessible method for measuring the function of OB, a critical node of olfactory system. In future works, the EBG might be tested to better understand the pathophysiology appeared in post-viral anosmia including COVID-19.

7 ACKNOWLEDGEMENTS

At the end, I would like to thank all of those who have supported me during the years of my PhD study. Specially, I would like to thank my main supervisor **Johan N. Lundström** for the encouragement and generous support. Thank you for providing a pleasant and enthusiastic working environment. Working with you has been an educational and scholarly experience for me! Thank you!

Thank you **Artin Arshamian**, my co-supervisor, for being open and listening to my random thoughts whenever I dropped in. You have always inspired me with your curiosity and passion for science. I enjoyed discussing new and sometimes crazy ideas with you. Thanks for all the thoughtful comments you made, they were indeed very helpful.

I would also like to thank **Per Svenningsson** and **Mats J. Olsson**, my other co-supervisors. Thanks for your generous support. You always cleared your busy schedule to make time for me whenever I need to discuss different issues or hear your feedbacks.

My office mates and colleagues at Perception lab, thank you for being so considerate. Thank you, **Amy**, **Anna**, **Arnaud**, **Danja**, **Evelina**, **Fahimeh**, **Janina**, **Martin**, **Moa** and **Robin**. Moreover, I would like to acknowledge the financial supports by National Graduate School on Ageing and Health (**SWEAH**).

My dear parents, **Hossein** and **Parvin**, missed you so much! Thank you for all the things you have done for me, for all the self-devotion, adoration and affection. I am deeply sorry that I could not spend more time with you during the past years. I would not be able to accomplish any of this without your love and support. Thank you!

Finally, **Neda**, my wife, my true and dearest friend! You are always kind and generous to me. During the worst and best moments of past years you have been always next to me and gave me your love. Your intellect and ambition have always inspired me. Neda, your audacity and dedication have encouraged me through life. I love you and thank you for standing beside me!

8 REFERENCES

1. Golgi C. Sulla fina struttura dei bulbi olfattorii. Tipografia di Stefano Calderini; 1875.

2. McGann JP. Poor human olfaction is a 19th-century myth. Science. 2017 May 12;356(6338).

3. Broca P. Localisations Cerebrales: Recherches sur les centres olfactifs. Masson; 1879.

4. Kay LM, Sherman SM. An argument for an olfactory thalamus. Trends Neurosci. 2007 Feb;30(2):47–53.

5. Shepherd GM, editor. The synaptic organization of the brain. Oxford University Press; 2004.

6. Adrian ED. Olfactory reactions in the brain of the hedgehog. J Physiol (Lond). 1942 Mar 31;100(4):459–473.

7. Cobb M. Smell: A Very Short Introduction. Tantor Media Inc; 2020.

8. Gottfried JA. Smell: central nervous processing. Adv Otorhinolaryngol. 2006;63:44–69.

9. Buettner A, editor. Springer handbook of odor. Cham: Springer International Publishing; 2017.

10. Laska M, Seibt A. Olfactory sensitivity for aliphatic esters in squirrel monkeys and pigtail macaques. Behav Brain Res. 2002 Aug 21;134(1-2):165–174.

11. Bushdid C, Magnasco MO, Vosshall LB, Keller A. Humans can discriminate more than 1 trillion olfactory stimuli. Science. 2014 Mar 21;343(6177):1370–1372.

12. Meister M. On the dimensionality of odor space. Elife. 2015 Jul 7;4:e07865.

13. Wilson DA, Stevenson RJ, Stevenson PRJ. Learning to Smell: Olfactory Perception from Neurobiology to Behavior. illustrated. JHU Press; 2006.

14. Keller A, Gerkin RC, Guan Y, Dhurandhar A, Turu G, Szalai B, et al. Predicting human olfactory perception from chemical features of odor molecules. Science. 2017 Feb 24;355(6327):820–826.

15. Ravia A, Snitz K, Honigstein D, Finkel M, Zirler R, Perl O, et al. A measure of smell enables the creation of olfactory metamers. Nature. 2020 Nov 11;588(7836):118–123.

16. Cleland TA, Chen S-YT, Hozer KW, Ukatu HN, Wong KJ, Zheng F. Sequential mechanisms underlying concentration invariance in biological olfaction. Front Neuroengineering. 2011 Nov 16;4:21.

17. Uchida N, Mainen ZF. Odor concentration invariance by chemical ratio coding. Front Syst Neurosci. 2007;1:3.

18. Firestein S. How the olfactory system makes sense of scents. Nature. 2001 Sep 13;413(6852):211–218.

19. Lledo P-M, Gheusi G, Vincent J-D. Information processing in the mammalian olfactory system. Physiol Rev. 2005 Jan;85(1):281–317.

20. Shepherd GM. Smell images and the flavour system in the human brain. Nature. 2006 Nov 16;444(7117):316–321.

21. Del Bulbo M, Humano T, Cabra P. Comparative Morphometry of the Olfactory Bulb, Tract and Stria in the Human, Dog and Goat. Int J Morphol. 2011;29(3).

22. Zozulya S, Echeverri F, Nguyen T. The human olfactory receptor repertoire. Genome Biol. 2001;

23. Felten DL, O'Banion MK, Maida ME. Netter's Atlas of Neuroscience. 3rd ed. Elsevier Health Sciences; 2015.

24. Persaud K, Dodd G. Analysis of discrimination mechanisms in the mammalian olfactory system using a model nose. Nature. 1982 Sep 23;299(5881):352–355.

25. Li Q, Liberles SD. Aversion and attraction through olfaction. Curr Biol. 2015 Feb 2;25(3):R120–R129.

26. Yeshurun Y, Sobel N. An odor is not worth a thousand words: from multidimensional odors to unidimensional odor objects. Annu Rev Psychol. 2010;61:219–41, C1.

27. Callahan CD, Hinkebein J. Neuropsychological significance of anosmia following traumatic brain injury. J Head Trauma Rehabil. 1999 Dec;14(6):581–587.

28. Mann NM. Management of smell and taste problems. Cleve Clin J Med. 2002 Apr;69(4):329–336.

29. Deems DA, Doty RL, Settle RG, Moore-Gillon V, Shaman P, Mester AF, et al. Smell and taste disorders, a study of 750 patients from the University of Pennsylvania Smell and Taste Center. Arch Otolaryngol Head Neck Surg. 1991 May;117(5):519–528.

30. Seubert J, Freiherr J, Djordjevic J, Lundström JN. Statistical localization of human olfactory cortex. Neuroimage. 2013 Feb 1;66:333–342.

31. Price JL. Olfactory higher centers anatomy. Encyclopedia of Neuroscience. Elsevier; 2009. p. 129–136.

32. Schaefer AT, Margrie TW. Spatiotemporal representations in the olfactory system. Trends Neurosci. 2007 Mar;30(3):92–100.

33. Baron G, Frahm HD, Stephan H. Comparison of brain structure volumes in insectivora and primates. VIII. Vestibular complex. J Hirnforsch. 1988;29(5):509–523.

34. Mori K. Olfactory Bulb Mapping. Encyclopedia of Neuroscience. Elsevier; 2009. p. 71–75.

35. Mori K, Sakano H. How is the olfactory map formed and interpreted in the mammalian brain? Annu Rev Neurosci. 2011;34:467–499.

36. Nagayama S, Homma R, Imamura F. Neuronal organization of olfactory bulb circuits. Front Neural Circuits. 2014 Sep 3;8:98.

37. Secundo L, Snitz K, Sobel N. The perceptual logic of smell. Curr Opin Neurobiol. 2014 Apr;25:107–115.

38. Junek S, Kludt E, Wolf F, Schild D. Olfactory coding with patterns of response latencies. Neuron. 2010 Sep 9;67(5):872–884.

39. Buonviso N, Amat C, Litaudon P. Respiratory modulation of olfactory neurons in the rodent brain. Chem Senses. 2006 Feb;31(2):145–154.

40. Gschwend O, Abraham NM, Lagier S, Begnaud F, Rodriguez I, Carleton A. Neuronal pattern separation in the olfactory bulb improves odor discrimination learning. Nat Neurosci. 2015 Oct;18(10):1474–1482.

41. Martin C, Gervais R, Hugues E, Messaoudi B, Ravel N. Learning modulation of odor-induced oscillatory responses in the rat olfactory bulb: a correlate of odor recognition? J Neurosci. 2004 Jan 14;24(2):389–397.

42. Wilson DA, Sullivan RM. Cortical processing of odor objects. Neuron. 2011 Nov 17;72(4):506–519.

43. Doty RL, editor. Handbook of olfaction and gustation. Hoboken, NJ, USA: John Wiley & Sons, Inc; 2015.

44. Zou D-J, Chesler A, Firestein S. How the olfactory bulb got its glomeruli: a just so story? Nat Rev Neurosci. 2009 Aug;10(8):611–618.

45. Mombaerts P. Odorant receptor gene choice in olfactory sensory neurons: the one receptor-one neuron hypothesis revisited. Curr Opin Neurobiol. 2004 Feb;14(1):31–36.

46. Lane G, Zhou G, Noto T, Zelano C. Assessment of direct knowledge of the human olfactory system. Exp Neurol. 2020 Apr 9;329:113304.

47. Linster C, Cleland TA. Glomerular microcircuits in the olfactory bulb. Neural Netw. 2009 Oct;22(8):1169–1173.

48. Cleland TA, Sethupathy P. Non-topographical contrast enhancement in the olfactory bulb. BMC Neurosci. 2006 Jan 24;7:7.

49. Watts DJ, Strogatz SH. Collective dynamics of “small-world” networks. Nature. 1998 Jun;393(6684):440–442.

50. Grosmaitre X, Santarelli LC, Tan J, Luo M, Ma M. Dual functions of mammalian olfactory sensory neurons as odor detectors and mechanical sensors. Nat Neurosci. 2007 Mar;10(3):348–354.

51. Kay LM, Beshel J, Brea J, Martin C, Rojas-Líbano D, Kopell N. Olfactory oscillations: the what, how and what for. Trends Neurosci. 2009 Apr;32(4):207–214.

52. Kay LM. Olfactory system oscillations across phyla. Curr Opin Neurobiol. 2015 Apr;31:141–147.

53. Ito J, Roy S, Liu Y, Cao Y, Fletcher M, Lu L, et al. Whisker barrel cortex delta oscillations and gamma power in the awake mouse are linked to respiration. Nat Commun. 2014 Apr 1;5:3572.

54. Arshamian A, Iravani B, Majid A, Lundström JN. Respiration modulates olfactory memory consolidation in humans. J Neurosci. 2018 Nov 28;38(48):10286–10294.

55. Zelano C, Jiang H, Zhou G, Arora N, Schuele S, Rosenow J, et al. Nasal respiration entrains human limbic oscillations and modulates cognitive function. J Neurosci. 2016 Dec 7;36(49):12448–12467.

56. Kay LM. Circuit oscillations in odor perception and memory. Prog Brain Res. 2014;208:223–251.

57. Frederick DE, Brown A, Brim E, Mehta N, Vujovic M, Kay LM. Gamma and beta oscillations define a sequence of neurocognitive modes present in odor processing. J Neurosci. 2016 Jul 20;36(29):7750–7767.

58. Martin C, Ravel N. Beta and gamma oscillatory activities associated with olfactory memory tasks: different rhythms for different functional networks? Front Behav Neurosci. 2014 Jun 23;8:218.

59. Neville KR, Haberly LB. Beta and gamma oscillations in the olfactory system of the urethane-anesthetized rat. J Neurophysiol. 2003 Dec;90(6):3921–3930.

60. Kay LM, Beshel J. A beta oscillation network in the rat olfactory system during a 2-alternative choice odor discrimination task. J Neurophysiol. 2010 Aug;104(2):829–839.

61. Kay LM, Stopfer M. Information processing in the olfactory systems of insects and vertebrates. Semin Cell Dev Biol. 2006 Aug;17(4):433–442.

62. Jiang H, Schuele S, Rosenow J, Zelano C, Parvizi J, Tao JX, et al. Theta Oscillations Rapidly Convey Odor-Specific Content in Human Piriform Cortex. Neuron. 2017 Apr 5;94(1):207–219.e4.

63. Adrian ED. The electrical activity of the mammalian olfactory bulb. Electroencephalogr Clin Neurophysiol. 1950 Nov;2(4):377–388.

64. Sem-jacobsen, C. Human olfactory response recorded by depth electrography. Staff meetings of the mayo clinic. 1953;

65. Hummel T, Smitka M, Puschmann S, Gerber JC, Schaal B, Buschhüter D. Correlation between olfactory bulb volume and olfactory function in children and adolescents. Exp Brain Res. 2011 Oct;214(2):285–291.

66. Pollatos O, Kopietz R, Linn J, Albrecht J, Sakar V, Anzinger A, et al. Emotional stimulation alters olfactory sensitivity and odor judgment. Chem Senses. 2007 Jul;32(6):583–589.

67. Pause BM, Miranda A, Göder R, Aldenhoff JB, Ferstl R. Reduced olfactory performance in patients with major depression. J Psychiatr Res. 2001 Oct;35(5):271–277.

68. Negoias S, Croy I, Gerber J, Puschmann S, Petrowski K, Joraschky P, et al. Reduced olfactory bulb volume and olfactory sensitivity in patients with acute major depression. Neuroscience. 2010 Aug 11;169(1):415–421.

69. Gottfried JA. Central mechanisms of odour object perception. Nat Rev Neurosci. 2010 Sep 1;11(9):628–641.

70. Lundström JN, Boesveldt S, Albrecht J. Central processing of the chemical senses: an overview. ACS Chem Neurosci. 2011 Jan;2(1):5–16.

71. Poellinger A, Thomas R, Lio P, Lee A, Makris N, Rosen BR, et al. Activation and habituation in olfaction--an fMRI study. Neuroimage. 2001 Apr;13(4):547–560.

72. Zelano C, Bensafi M, Porter J, Mainland J, Johnson B, Bremner E, et al. Attentional modulation in human primary olfactory cortex. Nat Neurosci. 2005 Jan;8(1):114–120.

73. Zelano C, Mohanty A, Gottfried JA. Olfactory predictive codes and stimulus templates in piriform cortex. Neuron. 2011 Oct 6;72(1):178–187.

74. Gottfried JA, Deichmann R, Winston JS, Dolan RJ. Functional heterogeneity in human olfactory cortex: an event-related functional magnetic resonance imaging study. J Neurosci. 2002 Dec 15;22(24):10819–10828.

75. Manabe H, Kusumoto-Yoshida I, Ota M, Mori K. Olfactory cortex generates synchronized top-down inputs to the olfactory bulb during slow-wave sleep. J Neurosci. 2011 Jun 1;31(22):8123–8133.

76. Ghosh S, Larson SD, Hefzi H, Marnoy Z, Cutforth T, Dokka K, et al. Sensory maps in the olfactory cortex defined by long-range viral tracing of single neurons. Nature. 2011 Apr 14;472(7342):217–220.

77. Gottfried JA, Winston JS, Dolan RJ. Dissociable codes of odor quality and odorant structure in human piriform cortex. Neuron. 2006 Feb 2;49(3):467–479.

78. Zhou G, Lane G, Cooper SL, Kahnt T, Zelano C. Characterizing functional pathways of the human olfactory system. Elife. 2019 Jul 24;8.

79. Wilson JL, Jenkinson M, Jezzard P. Optimization of static field homogeneity in human brain using diamagnetic passive shims. Magn Reson Med. 2002 Nov;48(5):906–914.

80. Sobel N, Prabhakaran V, Zhao Z, Desmond JE, Glover GH, Sullivan EV, et al. Time course of odorant-induced activation in the human primary olfactory cortex. J Neurophysiol. 2000 Jan;83(1):537–551.

81. Arabkheradmand G, Zhou G, Noto T, Yang Q, Schuele SU, Parvizi J, et al. Anticipation-induced delta phase reset improves human olfactory perception. PLoS Biol. 2020 May 26;18(5):e3000724.

82. Jones N. The nose and paranasal sinuses physiology and anatomy. Adv Drug Deliv Rev. 2001 Sep;51(1-3):5–19.

83. Weiskopf N, Hutton C, Josephs O, Deichmann R. Optimal EPI parameters for reduction of susceptibility-induced BOLD sensitivity losses: a whole-brain analysis at 3 T and 1.5 T. Neuroimage. 2006 Nov 1;33(2):493–504.

84. Qureshy A, Kawashima R, Imran MB, Sugiura M, Goto R, Okada K, et al. Functional mapping of human brain in olfactory processing: a PET study. J Neurophysiol. 2000 Sep;84(3):1656–1666.

85. Francati V, Vermetten E, Bremner JD. Functional neuroimaging studies in posttraumatic stress disorder: review of current methods and findings. Depress Anxiety. 2007;24(3):202–218.

86. Boly M, Gosseries O, Massimini M, Rosanova M. Functional Neuroimaging Techniques. The neurology of conciousness. Elsevier; 2016. p. 31–47.

87. Crosson B, Ford A, McGregor KM, Meinzer M, Cheshkov S, Li X, et al. Functional imaging and related techniques: an introduction for rehabilitation researchers. J Rehabil Res Dev. 2010;47(2):vii–xxxiv.

88. Berger H. Über das elektrenkephalogramm des menschen. Archiv f Psychiatrie. 1931 Dec;94(1):16–60.

89. Cohen D. Magnetoencephalography: evidence of magnetic fields produced by alpha-rhythm currents. Science. 1968 Aug 23;161(3843):784–786.

90. Lopes da Silva F. EEG and MEG: relevance to neuroscience. Neuron. 2013 Dec 4;80(5):1112–1128.

91. Lopes da Silva F. Functional localization of brain sources using EEG and/or MEG data: volume conductor and source models. Magn Reson Imaging. 2004 Dec;22(10):1533–1538.

92. David O, Kilner JM, Friston KJ. Mechanisms of evoked and induced responses in MEG/EEG. Neuroimage. 2006 Jul 15;31(4):1580–1591.

93. Verhagen JV, Wesson DW, Netoff TI, White JA, Wachowiak M. Sniffing controls an adaptive filter of sensory input to the olfactory bulb. Nat Neurosci. 2007 May;10(5):631–639.

94. Ahlfors SP, Han J, Belliveau JW, Hämäläinen MS. Sensitivity of MEG and EEG to source orientation. Brain Topogr. 2010 Sep;23(3):227–232.

95. Marinkovic K, Cox B, Reid K, Halgren E. Head position in the MEG helmet affects the sensitivity to anterior sources. Neurol Clin Neurophysiol. 2004 Nov 30;2004:30.

96. Boto E, Meyer SS, Shah V, Alem O, Knappe S, Kruger P, et al. A new generation of magnetoencephalography: Room temperature measurements using optically-pumped magnetometers. Neuroimage. 2017 Apr 1;149:404–414.

97. Schiffman SS. Physicochemical correlates of olfactory quality. Science. 1974 Jul 12;185(4146):112–117.

98. Schiffman S, Robinson DE, Erickson RP. Multidimensional scaling of odorants: examination of psychological and physicochemical dimensions. Chem Senses. 1977;2(3):375–390.

99. Kobayakawa K, Kobayakawa R, Matsumoto H, Oka Y, Imai T, Ikawa M, et al. Innate versus learned odour processing in the mouse olfactory bulb. Nature. 2007 Nov 22;450(7169):503–508.

100. Soussignan R, Schaal B, Marlier L, Jiang T. Facial and autonomic responses to biological and artificial olfactory stimuli in human neonates. Physiol Behav. 1997 Oct;62(4):745–758.

101. Cain WS, Johnson F. Lability of odor pleasantness: influence of mere exposure. Perception. 1978;7(4):459–465.

102. Privitera GJ, Mulcahey CP, Orlowski CM. Human sensory preconditioning in a flavor preference paradigm. Appetite. 2012 Oct;59(2):414–418.

103. Prescott J, Murphy S. Inhibition of evaluative and perceptual odour-taste learning by attention to the stimulus elements. Q J Exp Psychol (Colchester). 2009 Nov;62(11):2133–2140.

104. Fondberg R, Lundström JN, Seubert J. Odor-taste interactions in food perception: Exposure protocol shows no effects of associative learning. 2020 Oct 20;

105. Russell JA. A circumplex model of affect. J Pers Soc Psychol. 1980;39(6):1161–1178.

106. Lang PJ, Greenwald MK, Bradley MM, Hamm AO. Looking at pictures: affective, facial, visceral, and behavioral reactions. Psychophysiology. 1993 May;30(3):261–273.

107. Anderson AK, Christoff K, Stappen I, Panitz D, Ghahremani DG, Glover G, et al. Dissociated neural representations of intensity and valence in human olfaction. Nat Neurosci. 2003 Feb;6(2):196–202.

108. Cecchetto C, Rumiati RI, Parma V. Relative contribution of odour intensity and valence to moral decisions. Perception. 2017 Apr;46(3-4):447–474.

109. Alaoui-Ismaïli O, Vernet-Maury E, Dittmar A, Delhomme G, Chanel J. Odor hedonics: connection with emotional response estimated by autonomic parameters. Chem Senses. 1997 Jun;22(3):237–248.

110. Bensafi M, Rouby C, Farget V, Bertrand B, Vigouroux M, Holley A. Autonomic nervous system responses to odours: the role of pleasantness and arousal. Chem Senses. 2002 Oct;27(8):703–709.

111. Toet A, Eijsman S, Liu Y, Donker S, Kaneko D, Brouwer A-M, et al. The relation between valence and arousal in subjective odor experience. Chemosens Percept. 2020 Oct;13(2):141–151.

112. Bensafi M, Rouby C, Farget V, Vigouroux M, Holley A. Asymmetry of pleasant vs. unpleasant odor processing during affective judgment in humans. Neurosci Lett. 2002 Aug 16;328(3):309–313.

113. Ehrlichman H, Brown S, Zhu J, Warrenburg S. Startle reflex modulation during exposure to pleasant and unpleasant odors. Psychophysiology. 1995 Mar;32(2):150–154.

114. Grabenhorst F, Rolls ET, Margot C, da Silva MAAP, Velazco MI. How pleasant and unpleasant stimuli combine in different brain regions: odor mixtures. J Neurosci. 2007 Dec 5;27(49):13532–13540.

115. Zou L-Q, van Hartevelt TJ, Kringelbach ML, Cheung EFC, Chan RCK. The neural mechanism of hedonic processing and judgment of pleasant odors: An activation likelihood estimation meta-analysis. Neuropsychology. 2016 May 19;30(8):970–979.

116. Masago R, Shimomura Y, Iwanaga K, Katsuura T. The effects of hedonic properties of odors and attentional modulation on the olfactory event-related potentials. J Physiol Anthropol Appl Human Sci. 2001 Jan;20(1):7–13.

117. Kroupi E, Yazdani A, Vesin J-M, Ebrahimi T. EEG correlates of pleasant and unpleasant odor perception. ACM Trans Multimedia Comput Commun Appl. 2014 Oct 1;11(1s):1–17.

118. Pause BM, Krauel K. Chemosensory event-related potentials (CSERP) as a key to the psychology of odors. Int J Psychophysiol. 2000 May;36(2):105–122.

119. Kay LM, Laurent G. Odor- and context-dependent modulation of mitral cell activity in behaving rats. Nat Neurosci. 1999 Nov;2(11):1003–1009.

120. Hummel T, Landis BN, Hüttenbrink K-B. Smell and taste disorders. GMS Curr Top Otorhinolaryngol Head Neck Surg. 2011;10:Doc04.

121. Murphy C, Schubert CR, Cruickshanks KJ, Klein BEK, Klein R, Nondahl DM. Prevalence of olfactory impairment in older adults. JAMA. 2002 Nov 13;288(18):2307–2312.

122. Haehner A, Hummel T, Reichmann H. Olfactory dysfunction as a diagnostic marker for Parkinson's disease. Expert Rev Neurother. 2009 Dec;9(12):1773–1779.

123. Doty RL. Olfactory dysfunction in Parkinson disease. Nat Rev Neurol. 2012 May 15;8(6):329–339.

124. Doty RL, Deems DA, Stellar S. Olfactory dysfunction in parkinsonism: a general deficit unrelated to neurologic signs, disease stage, or disease duration. Neurology. 1988 Aug;38(8):1237–1244.

125. Doty RL, Stern MB, Pfeiffer C, Gollomp SM, Hurtig HI. Bilateral olfactory dysfunction in early stage treated and untreated idiopathic Parkinson's disease. J Neurol Neurosurg Psychiatry. 1992 Feb;55(2):138–142.

126. Murphy C. Olfactory and other sensory impairments in Alzheimer disease. Nat Rev Neurol. 2019;15(1):11–24.

127. Hawkes CH, Shephard BC, Daniel SE. Is Parkinson's disease a primary olfactory disorder? QJM. 1999 Aug;92(8):473–480.

128. Doty RL. Olfaction in Parkinson's disease and related disorders. Neurobiol Dis. 2012 Jun;46(3):527–552.

129. Bohnen NI, Studenski SA, Constantine GM, Moore RY. Diagnostic performance of clinical motor and non-motor tests of Parkinson disease: a matched case-control study. Eur J Neurol. 2008 Jul;15(7):685–691.

130. Haehner A, Hummel T, Hummel C, Sommer U, Junghanns S, Reichmann H. Olfactory loss may be a first sign of idiopathic Parkinson's disease. Mov Disord. 2007 Apr 30;22(6):839–842.

131. Hummel T. Olfactory evoked potentials as a tool to measure progressionof Parkinson's disease. In: Chase T, Bedard P, editors. Focus onmedicine New developments in the drug therapy of Parkinson's disease. 1999. p. 47–53.

132. Zapiec B, Dieriks BV, Tan S, Faull RLM, Mombaerts P, Curtis MA. A ventral glomerular deficit in Parkinson's disease revealed by whole olfactory bulb reconstruction. Brain. 2017 Oct 1;140(10):2722–2736.

133. Gardner B, Dieriks BV, Cameron S, Mendis LHS, Turner C, Faull RLM, et al. Metal concentrations and distributions in the human olfactory bulb in Parkinson's disease. Sci Rep. 2017 Sep 5;7(1):10454.

134. Westermann B, Wattendorf E, Schwerdtfeger U, Husner A, Fuhr P, Gratzl O, et al. Functional imaging of the cerebral olfactory system in patients with Parkinson's disease. J Neurol Neurosurg Psychiatry. 2008 Jan;79(1):19–24.

135. Huisman E, Uylings HBM, Hoogland PV. A 100% increase of dopaminergic cells in the olfactory bulb may explain hyposmia in Parkinson's disease. Mov Disord. 2004 Jun;19(6):687–692.

136. Pearce RK, Hawkes CH, Daniel SE. The anterior olfactory nucleus in Parkinson's disease. Mov Disord. 1995 May;10(3):283–287.

137. Beach TG, White CL, Hladik CL, Sabbagh MN, Connor DJ, Shill HA, et al. Olfactory bulb alpha-synucleinopathy has high specificity and sensitivity for Lewy body disorders. Acta Neuropathol. 2009 Feb;117(2):169–174.

138. Ishizawa T, Mattila P, Davies P, Wang D, Dickson DW. Colocalization of tau and alpha-synuclein epitopes in Lewy bodies. J Neuropathol Exp Neurol. 2003 Apr;62(4):389–397.

139. Macknin JB, Higuchi M, Lee VM-Y, Trojanowski JQ, Doty RL. Olfactory dysfunction occurs in transgenic mice overexpressing human tau protein. Brain Res. 2004 Mar 12;1000(1-2):174–178.

140. Miao X, Yang L, Gu H, Ren Y, Chen G, Liu J, et al. Evaluation of post-traumatic anosmia with MRI and chemosensory ERPs. Eur Arch Otorhinolaryngol. 2015 Aug;272(8):1945–1953.

141. Hawkes CH, Shephard BC, Daniel SE. Olfactory dysfunction in Parkinson's disease. J Neurol Neurosurg Psychiatry. 1997 May;62(5):436–446.

142. Hawkes CH, Shephard BC, Kobal G. Assessment of olfaction in multiple sclerosis: evidence of dysfunction by olfactory evoked response and identification tests. J Neurol Neurosurg Psychiatry. 1997 Aug;63(2):145–151.

143. Rombaux P, Weitz H, Mouraux A, Nicolas G, Bertrand B, Duprez T, et al. Olfactory function assessed with orthonasal and retronasal testing, olfactory bulb volume, and chemosensory event-related potentials. Arch Otolaryngol Head Neck Surg. 2006 Dec;132(12):1346–1351.

144. Ishimaru T, Shimada T, Miwa T, Furukawa M. Electrically stimulated olfactory evoked potential in olfactory disturbance. Ann Otol Rhinol Laryngol. 2002 Jun;111(6):518–522.

145. Boesveldt S, Stam CJ, Knol DL, Verbunt JPA, Berendse HW. Advanced time-series analysis of MEG data as a method to explore olfactory function in healthy controls and Parkinson's disease patients. Hum Brain Mapp. 2009 Sep;30(9):3020–3030.

146. Blomqvist EH, Brämerson A, Stjärne P, Nordin S. Consequences of olfactory loss and adopted coping strategies. Rhinology. 2004 Dec;42(4):189–194.

147. Mueller A, Rodewald A, Reden J, Gerber J, von Kummer R, Hummel T. Reduced olfactory bulb volume in post-traumatic and post-infectious olfactory dysfunction. Neuroreport. 2005 Apr 4;16(5):475–478.

148. Zhu N, Zhang D, Wang W, Li X, Yang B, Song J, et al. A Novel Coronavirus from Patients with Pneumonia in China, 2019. N Engl J Med. 2020 Feb 20;382(8):727–733.

149. Lechien JR, Chiesa-Estomba CM, Beckers E, Mustin V, Ducarme M, Journe F, et al. Prevalence and 6-month recovery of olfactory dysfunction: a multicentre study of 1363 COVID-19 patients. J Intern Med. 2021 Jan 5;

150. Lu Y, Li X, Geng D, Mei N, Wu P-Y, Huang C-C, et al. Cerebral Micro-Structural Changes in COVID-19 Patients - An MRI-based 3-month Follow-up Study. EClinicalMedicine. 2020 Aug 3;25:100484.

151. Han AY, Mukdad L, Long JL, Lopez IA. Anosmia in COVID-19: Mechanisms and Significance. Chem Senses. 2020 Jun 17;

152. Meinhardt J, Radke J, Dittmayer C, Franz J, Thomas C, Mothes R, et al. Olfactory transmucosal SARS-CoV-2 invasion as a port of central nervous system entry in individuals with COVID-19. Nat Neurosci. 24(2):168–175.

153. Netland J, Meyerholz DK, Moore S, Cassell M, Perlman S. Severe acute respiratory syndrome coronavirus infection causes neuronal death in the absence of encephalitis in mice transgenic for human ACE2. J Virol. 2008 Aug;82(15):7264–7275.

154. Politi LS, Salsano E, Grimaldi M. Magnetic Resonance Imaging Alteration of the Brain in a Patient With Coronavirus Disease 2019 (COVID-19) and Anosmia. JAMA Neurol. 2020 Aug 1;77(8):1028–1029.

155. Aragão MFVV, Leal MC, Cartaxo Filho OQ, Fonseca TM, Valença MM. Anosmia in COVID-19 Associated with Injury to the Olfactory Bulbs Evident on MRI. AJNR Am J Neuroradiol. 2020 Jun 25;

156. Laurendon T, Radulesco T, Mugnier J, Gérault M, Chagnaud C, El Ahmadi A-A, et al. Bilateral transient olfactory bulbs edema during COVID-19-related anosmia. Neurology. 2020 May 22;

157. Chiu A, Fischbein N, Wintermark M, Zaharchuk G, Yun PT, Zeineh M. COVID-19-induced anosmia associated with olfactory bulb atrophy. Neuroradiology. 2021 Jan;63(1):147–148.

158. Galougahi MK, Ghorbani J, Bakhshayeshkaram M, Naeini AS, Haseli S. Olfactory Bulb Magnetic Resonance Imaging in SARS-CoV-2-Induced Anosmia: The First Report. Acad Radiol. 2020 Apr 11;27(6):892–893.

159. Hughes JR, Hendrix DE, Wetzel N, Johnston JW. Correlations between electrophysiological activity from the human olfactory bulb and subjective responses to odoriferous stimuli. Olfaction and taste. 1969;3:172–191.

160. Ross GW, Petrovitch H, Abbott RD, Tanner CM, Popper J, Masaki K, et al. Association of olfactory dysfunction with risk for future Parkinson's disease. Ann Neurol. 2008 Feb;63(2):167–173.

161. Menni C, Valdes AM, Freidin MB, Sudre CH, Nguyen LH, Drew DA, et al. Real-time tracking of self-reported symptoms to predict potential COVID-19. Nat Med. 2020 May 11;26(7):1037–1040.

162. Gane SB, Kelly C, Hopkins C. Isolated sudden onset anosmia in COVID-19 infection. A novel syndrome? Rhinology. 2020 Jun 1;58(3):299–301.

163. Hummel T, Sekinger B, Wolf SR, Pauli E, Kobal G. Sniffin" sticks": olfactory performance assessed by the combined testing of odor identification, odor discrimination and olfactory threshold. Chem Senses. 1997 Feb;22(1):39–52.

164. Lundström JN, Gordon AR, Alden EC, Boesveldt S, Albrecht J. Methods for building an inexpensive computer-controlled olfactometer for temporally-precise experiments. Int J Psychophysiol. 2010 Nov;78(2):179–189.

165. Biasiucci A, Franceschiello B, Murray MM. Electroencephalography. Curr Biol. 2019 Feb 4;29(3):R80–R85.

166. Riitta Hari, Anna Puce. MEG-EEG Primer. Oxford University Press; 2017.

167. Xu J, Mitra S, Van Hoof C, Yazicioglu RF, Makinwa KAA. Active electrodes for wearable EEG acquisition: review and electronics design methodology. IEEE Rev Biomed Eng. 2017 Jan 20;10:187–198.

168. Flexer A, Gruber G, Dorffner G. A reliable probabilistic sleep stager based on a single EEG signal. Artif Intell Med. 2005 Mar;33(3):199–207.

169. Na SH, Jin S-H, Kim SY, Ham B-J. EEG in schizophrenic patients: mutual information analysis. Clin Neurophysiol. 2002 Dec;113(12):1954–1960.

170. Do Valle BG, Cash SS, Sodini CG. Low-Power, 8-Channel EEG Recorder and Seizure Detector ASIC for a Subdermal Implantable System. IEEE Trans Biomed Circuits Syst. 2016 Apr 20;10(6):1058–1067.

171. Aurlien H, Gjerde IO, Aarseth JH, Eldøen G, Karlsen B, Skeidsvoll H, et al. EEG background activity described by a large computerized database. Clin Neurophysiol. 2004 Mar;115(3):665–673.

172. Xu J, Busze B, Van Hoof C, Makinwa KAA, Yazicioglu RF. A 15-Channel Digital Active Electrode System for Multi-Parameter Biopotential Measurement. IEEE J Solid-State Circuits. 2015 Sep;50(9):2090–2100.

173. Marwan Abed T. Preamplifier Design for Active Electrodes in Single-Channel EEG Applications. 2018.

174. Thompson T, Steffert T, Ros T, Leach J, Gruzelier J. EEG applications for sport and performance. Methods. 2008 Aug 3;45(4):279–288.

175. Klem GH, Lüders HO, Jasper HH, Elger C. The ten-twenty electrode system of the International Federation. The International Federation of Clinical Neurophysiology. Electroencephalogr Clin Neurophysiol Suppl. 1999;52:3–6.

176. Commission IE. Medical Electrical Equipment: Particular Requirements for the Basic Safety and Essential Performance of Medical Beds. IEC60601-2-26 2015.

177. Buzsáki G, Draguhn A. Neuronal oscillations in cortical networks. Science. 2004 Jun 25;304(5679):1926–1929.

178. Cannon J, McCarthy MM, Lee S, Lee J, Börgers C, Whittington MA, et al. Neurosystems: brain rhythms and cognitive processing. Eur J Neurosci. 2014 Mar;39(5):705–719.

179. Ainsworth M, Lee S, Cunningham MO, Roopun AK, Traub RD, Kopell NJ, et al. Dual γ rhythm generators control interlaminar synchrony in auditory cortex. J Neurosci. 2011 Nov 23;31(47):17040–17051.

180. Roopun AK, Kramer MA, Carracedo LM, Kaiser M, Davies CH, Traub RD, et al. Period concatenation underlies interactions between gamma and beta rhythms in neocortex. Front Cell Neurosci. 2008 Apr 8;2:1.

181. Roopun AK, Kramer MA, Carracedo LM, Kaiser M, Davies CH, Traub RD, et al. Temporal Interactions between Cortical Rhythms. Front Neurosci. 2008 Dec 15;2(2):145–154.

182. Adrian ED, Matthews BH. The interpretation of potential waves in the cortex. J Physiol (Lond). 1934 Jul 31;81(4):440–471.

183. Kropotov JD. Quantitative EEG, Event-Related Potentials and Neurotherapy. Elsevier; 2009.

184. Gastaut, H. Etude electrocorticographique de la reactivite des rythmes rolandiques. Rev Neurol (Paris). 1952;

185. Tiihonen J, Kajola M, Hari R. Magnetic mu rhythm in man. Neuroscience. 1989;32(3):793–800.

186. Salmelin R, Hari R. Spatiotemporal characteristics of sensorimotor neuromagnetic rhythms related to thumb movement. Neuroscience. 1994 May;60(2):537–550.

187. Salmelin R, Hämäläinen M, Kajola M, Hari R. Functional segregation of movement-related rhythmic activity in the human brain. Neuroimage. 1995 Dec;2(4):237–243.

188. Srinivasan R, Nunez PL, Tucker DM, Silberstein RB, Cadusch PJ. Spatial sampling and filtering of EEG with spline laplacians to estimate cortical potentials. Brain Topogr. 1996;8(4):355–366.

189. Kay LM. Two species of gamma oscillations in the olfactory bulb: dependence on behavioral state and synaptic interactions. J Integr Neurosci. 2003 Jun;2(1):31–44.

190. Eisthen HL. Why are olfactory systems of different animals so similar? Brain Behav Evol. 2002;59(5-6):273–293.

191. Lagier S, Carleton A, Lledo P-M. Interplay between local GABAergic interneurons and relay neurons generates gamma oscillations in the rat olfactory bulb. J Neurosci. 2004 May 5;24(18):4382–4392.

192. Rall W, Shepherd GM. Theoretical reconstruction of field potentials and dendrodendritic synaptic interactions in olfactory bulb. J Neurophysiol. 1968 Nov;31(6):884–915.

193. Freeman WJ. Mass action in the nervous system. Elsevier; 1975.

194. Stopfer M, Bhagavan S, Smith BH, Laurent G. Impaired odour discrimination on desynchronization of odour-encoding neural assemblies. Nature. 1997 Nov 6;390(6655):70–74.

195. Walter WG. The location of cerebral tumours by electro-encephalography. Lancet. 1936 Aug;228(5893):305–308.

196. Hasselmo ME, Stern CE. Theta rhythm and the encoding and retrieval of space and time. Neuroimage. 2014 Jan 15;85 Pt 2:656–666.

197. Hsieh L-T, Ranganath C. Frontal midline theta oscillations during working memory maintenance and episodic encoding and retrieval. Neuroimage. 2014 Jan 15;85 Pt 2:721–729.

198. Colgin LL. Mechanisms and functions of theta rhythms. Annu Rev Neurosci. 2013 Jul 8;36:295–312.

199. Ottoson D. Studies on the relationship between olfactory stimulating effectiveness and physico-chemical properties of odorous compounds. Acta Physiol Scand. 1958 Aug 25;43(2):167–181.

200. Ravel N, Caille D, Pager J. A centrifugal respiratory modulation of olfactory bulb unit activity: a study on acute rat preparation. Exp Brain Res. 1987;65(3):623–628.

201. Macrides F, Eichenbaum HB, Forbes WB. Temporal relationship between sniffing and the limbic theta rhythm during odor discrimination reversal learning. J Neurosci. 1982 Dec;2(12):1705–1717.

202. Kay LM. Theta oscillations and sensorimotor performance. Proc Natl Acad Sci USA. 2005 Mar 8;102(10):3863–3868.

203. Revonsuo A, Newman J. Binding and consciousness. Conscious Cogn. 1999 Jun;8(2):123–127.

204. Bressler SL, Menon V. Large-scale brain networks in cognition: emerging methods and principles. Trends Cogn Sci (Regul Ed). 2010 Jun;14(6):277–290.

205. Singer W. Neuronal synchrony: a versatile code for the definition of relations? Neuron. 1999 Sep;24(1):, 111.

206. Gross J, Kujala J, Hamalainen M, Timmermann L, Schnitzler A, Salmelin R. Dynamic imaging of coherent sources: Studying neural interactions in the human brain. Proc Natl Acad Sci USA. 2001 Jan 16;98(2):694–699.

207. Michel CM, Murray MM, Lantz G, Gonzalez S, Spinelli L, Grave de Peralta R. EEG source imaging. Clin Neurophysiol. 2004 Oct;115(10):2195–2222.

208. Van Veen BD, van Drongelen W, Yuchtman M, Suzuki A. Localization of brain electrical activity via linearly constrained minimum variance spatial filtering. IEEE Trans Biomed Eng. 1997 Sep;44(9):867–880.

209. Vrba J, Robinson SE. Signal processing in magnetoencephalography. Methods. 2001 Oct;25(2):249–271.

210. Leske S, Dalal SS. Reducing power line noise in EEG and MEG data via spectrum interpolation. Neuroimage. 2019 Apr 1;189:763–776.

211. Quinn AJ, Lopes-dos-Santos V, Huang N, Liang W-K, Juan C-H, Yeh J-R, et al. Within-cycle instantaneous frequency profiles report oscillatory waveform dynamics. BioRxiv. 2021 Apr 14;

212. Samar VJ, Bopardikar A, Rao R, Swartz K. Wavelet analysis of neuroelectric waveforms: a conceptual tutorial. Brain Lang. 1999 Jan;66(1):7–60.

213. Structural Health Monitoring with Piezoelectric Wafer Active Sensors. Elsevier; 2014.

214. Percival DB, Walden AT. Spectral Analysis for Physical Applications. Cambridge: Cambridge University Press; 1993.

215. Hillebrand A, Barnes GR. A quantitative assessment of the sensitivity of whole-head MEG to activity in the adult human cortex. Neuroimage. 2002 Jul;16(3 Pt 1):638–650.

216. Welch P. The use of fast Fourier transform for the estimation of power spectra: A method based on time averaging over short, modified periodograms. IEEE Trans Audio Electroacoust. 1967 Jun;15(2):70–73.

217. Gloor P. Hans berger on electroencephalography. American Journal of EEG Technology. 1969 Mar;9(1):1–8.

218. Bendat JS, Piersol AG. Random data: analysis and measurement procedures. Hoboken, NJ, USA: John Wiley & Sons, Inc.; 2010.

219. Vatta F, Meneghini F, Esposito F, Mininel S, Di Salle F. Realistic and spherical head modeling for EEG forward problem solution: a comparative cortex-based analysis. Comput Intell Neurosci. 2010 Feb 14;972060.

220. Halder T, Talwar S, Jaiswal AK, Banerjee A. Quantitative evaluation in estimating sources underlying brain oscillations using current source density methods and beamformer approaches. Eneuro. 2019 Aug 6;6(4).

221. Kriegeskorte N, Mur M, Bandettini P. Representational similarity analysis - connecting the branches of systems neuroscience. Front Syst Neurosci. 2008 Nov 24;2:4.

222. Hyafil A, Giraud A-L, Fontolan L, Gutkin B. Neural Cross-Frequency Coupling: Connecting Architectures, Mechanisms, and Functions. Trends Neurosci. 2015 Nov;38(11):725–740.

223. Buzsáki G, Buhl DL, Harris KD, Csicsvari J, Czéh B, Morozov A. Hippocampal network patterns of activity in the mouse. Neuroscience. 2003;116(1):201–211.

224. Bragin A, Jandó G, Nádasdy Z, Hetke J, Wise K, Buzsáki G. Gamma (40-100 Hz) oscillation in the hippocampus of the behaving rat. J Neurosci. 1995 Jan;15(1 Pt 1):47–60.

225. Kendrick K, Zhan Y, Fischer H, Nicol A, Zhang X, Feng J. Learning alters theta-nested gamma oscillations in inferotemporal cortex. Nature Precedings. 2009 Apr 28;

226. Lakatos P, Shah AS, Knuth KH, Ulbert I, Karmos G, Schroeder CE. An oscillatory hierarchy controlling neuronal excitability and stimulus processing in the auditory cortex. J Neurophysiol. 2005 Sep;94(3):1904–1911.

227. Axmacher N, Henseler MM, Jensen O, Weinreich I, Elger CE, Fell J. Cross-frequency coupling supports multi-item working memory in the human hippocampus. Proc Natl Acad Sci USA. 2010 Feb 16;107(7):3228–3233.

228. Cohen MX, Axmacher N, Lenartz D, Elger CE, Sturm V, Schlaepfer TE. Good vibrations: cross-frequency coupling in the human nucleus accumbens during reward processing. J Cogn Neurosci. 2009 May;21(5):875–889.

229. Canolty RT, Knight RT. The functional role of cross-frequency coupling. Trends Cogn Sci (Regul Ed). 2010 Nov;14(11):506–515.

230. Lisman J, Buzsáki G. A neural coding scheme formed by the combined function of gamma and theta oscillations. Schizophr Bull. 2008 Sep;34(5):974–980.

231. Lisman JE, Jensen O. The θ-γ neural code. Neuron. 2013 Mar 20;77(6):1002–1016.

232. Schroeder CE, Lakatos P. Low-frequency neuronal oscillations as instruments of sensory selection. Trends Neurosci. 2009 Jan;32(1):9–18.

233. Händel B, Haarmeier T. Cross-frequency coupling of brain oscillations indicates the success in visual motion discrimination. Neuroimage. 2009 Apr 15;45(3):1040–1046.

234. Tort ABL, Komorowski RW, Manns JR, Kopell NJ, Eichenbaum H. Theta-gamma coupling increases during the learning of item-context associations. Proc Natl Acad Sci USA. 2009 Dec 8;106(49):20942–20947.

235. Losacco J, Ramirez-Gordillo D, Gilmer J, Restrepo D. Learning improves decoding of odor identity with phase-referenced oscillations in the olfactory bulb. Elife. 2020 Jan 28;9.

236. Samiee S, Baillet S. Time-resolved phase-amplitude coupling in neural oscillations. Neuroimage. 2017 Oct 1;159:270–279.

237. Kaboodvand N. Modelling and quantifying brain connectivity and dynamics with applications in aging and ADHD [Doctoral dissertation]. 2019.

238. Shaw JC. Correlation and coherence analysis of the EEG: A selective tutorial review. Int J Psychophysiol. 1984 Mar;1(3):255–266.

239. Kaboodvand N, van den Heuvel MP, Fransson P. Adaptive frequency-based modeling of whole-brain oscillations: Predicting regional vulnerability and hazardousness rates. Network Neuroscience. 2019 Jul 30;3(4).

240. Kaboodvand N, Iravani B, Fransson P. Dynamic synergetic configurations of resting-state networks in ADHD. Neuroimage. 2020;207:116347.

241. Kaboodvand N, Bäckman L, Nyberg L, Salami A. The retrosplenial cortex: A memory gateway between the cortical default mode network and the medial temporal lobe. Hum Brain Mapp. 2018 Jan 23;39(5):2020–2034.

242. Granger CWJ. Investigating Causal Relations by Econometric Models and Cross-spectral Methods. Econometrica. 1969 Aug;37(3):424.

243. Dhamala M, Rangarajan G, Ding M. Analyzing information flow in brain networks with nonparametric Granger causality. Neuroimage. 2008 Jun;41(2):354–362.

244. Wilmott P. Machine Learning: An Applied Mathematics Introduction. illustrated. Panda Ohana Publishing; 2019.

245. Maris E, Oostenveld R. Nonparametric statistical testing of EEG- and MEG-data. J Neurosci Methods. 2007 Aug 15;164(1):177–190.

246. Blair RC, Karniski W. An alternative method for significance testing of waveform difference potentials. Psychophysiology. 1993 Sep;30(5):518–524.

247. Maris E. Randomization tests for ERP topographies and whole spatiotemporal data matrices. Psychophysiology. 2004 Jan;41(1):142–151.

248. Kaiser J, Hertrich I, Ackermann H, Lutzenberger W. Gamma-band activity over early sensory areas predicts detection of changes in audiovisual speech stimuli. Neuroimage. 2006 May 1;30(4):1376–1382.

249. Kaiser J, Lutzenberger W. Human gamma-band activity: a window to cognitive processing. Neuroreport. 2005 Feb 28;16(3):207–211.

250. Zhao F, Wang X, Zariwala HA, Uslaner JM, Houghton AK, Evelhoch JL, et al. fMRI study of olfaction in the olfactory bulb and high olfactory structures of rats: Insight into their roles in habituation. Neuroimage. 2016 Feb 15;127:445–455.

251. Wilson DA. Habituation of odor responses in the rat anterior piriform cortex. J Neurophysiol. 1998 Mar;79(3):1425–1440.

252. Huart C, Meusel T, Gerber J, Duprez T, Rombaux P, Hummel T. The depth of the olfactory sulcus is an indicator of congenital anosmia. AJNR Am J Neuroradiol. 2011 Dec;32(10):1911–1914.

253. Abdi H, O'Toole AJ, Valentin D, Edelman B. DISTATIS: the analysis of multiple distance matrices. 2005 IEEE Computer Society Conference on Computer Vision and Pattern Recognition (CVPR'05) - Workshops. IEEE; 2005. p. 42–42.

254. Newman MEJ, Girvan M. Finding and evaluating community structure in networks. Phys Rev E, Stat Nonlin Soft Matter Phys. 2004 Feb 26;69(2 Pt 2):026113.

255. Maslov S, Sneppen K. Specificity and stability in topology of protein networks. Science. 2002 May 3;296(5569):910–913.

256. Frank RA, Dulay MF, Gesteland RC. Assessment of the Sniff Magnitude Test as a clinical test of olfactory function. Physiol Behav. 2003 Feb;78(2):195–204.

257. Seth AK, Barrett AB, Barnett L. Granger causality analysis in neuroscience and neuroimaging. J Neurosci. 2015 Feb 25;35(8):3293–3297.

258. Oleszkiewicz A, Schriever VA, Croy I, Hähner A, Hummel T. Updated Sniffin' Sticks normative data based on an extended sample of 9139 subjects. Eur Arch Otorhinolaryngol. 2019 Mar;276(3):719–728.

259. Kohli P, Soler ZM, Nguyen SA, Muus JS, Schlosser RJ. The association between olfaction and depression: A systematic review. Chem Senses. 2016 May 11;41(6):479–486.

260. Whitcroft KL, Hummel T. Olfactory Dysfunction in COVID-19: Diagnosis and Management. JAMA. 2020 Jun 23;323(24):2512–2514.

261. Martin C, Gervais R, Messaoudi B, Ravel N. Learning-induced oscillatory activities correlated to odour recognition: a network activity. Eur J Neurosci. 2006 Apr;23(7):1801–1810.

262. Kobal G, Klimek L, Wolfensberger M, Gudziol H, Temmel A, Owen CM, et al. Multicenter investigation of 1,036 subjects using a standardized method for the assessment of olfactory function combining tests of odor identification, odor discrimination, and olfactory thresholds. Eur Arch Otorhinolaryngol. 2000;257(4):205–211.

263. Thesen T, Murphy C. Reliability analysis of event-related brain potentials to olfactory stimuli. Psychophysiology. 2002 Nov;39(6):733–738.

264. Nordin S, Andersson L, Olofsson JK, McCormack M, Polich J. Evaluation of auditory, visual and olfactory event-related potentials for comparing interspersed- and single-stimulus paradigms. Int J Psychophysiol. 2011 Sep;81(3):252–262.

265. Voytek B, Kramer MA, Case J, Lepage KQ, Tempesta ZR, Knight RT, et al. Age-Related Changes in 1/f Neural Electrophysiological Noise. J Neurosci. 2015 Sep 23;35(38):13257–13265.

266. Rinberg D, Koulakov A, Gelperin A. Sparse odor coding in awake behaving mice. J Neurosci. 2006 Aug 23;26(34):8857–8865.

267. Gray CM, Skinner JE. Centrifugal regulation of neuronal activity in the olfactory bulb of the waking rabbit as revealed by reversible cryogenic blockade. Exp Brain Res. 1988;69(2):378–386.

268. Mainland J, Sobel N. The sniff is part of the olfactory percept. Chem Senses. 2006 Feb;31(2):181–196.

269. Richter CG, Thompson WH, Bosman CA, Fries P. Top-Down Beta Enhances Bottom-Up Gamma. J Neurosci. 2017 Jul 12;37(28):6698–6711.

270. Gnaedinger A, Gurden H, Gourévitch B, Martin C. Multisensory learning between odor and sound enhances beta oscillations. Sci Rep. 2019 Aug 2;9(1):11236.

271. Gourévitch B, Kay LM, Martin C. Directional coupling from the olfactory bulb to the hippocampus during a go/no-go odor discrimination task. J Neurophysiol. 2010 May;103(5):2633–2641.

272. Li W, Howard JD, Parrish TB, Gottfried JA. Aversive learning enhances perceptual and cortical discrimination of indiscriminable odor cues. Science. 2008 Mar 28;319(5871):1842–1845.

273. Djordjevic J, Lundstrom JN, Clément F, Boyle JA, Pouliot S, Jones-Gotman M. A rose by any other name: would it smell as sweet? J Neurophysiol. 2008 Jan;99(1):386–393.

274. Kumar S, Riddoch MJ, Humphreys G. Mu rhythm desynchronization reveals motoric influences of hand action on object recognition. Front Hum Neurosci. 2013 Mar 7;7:66.

275. Matsumoto J, Fujiwara T, Takahashi O, Liu M, Kimura A, Ushiba J. Modulation of mu rhythm desynchronization during motor imagery by transcranial direct current stimulation. J Neuroeng Rehabil. 2010 Jun 11;7:27.

276. Hermer-Vazquez R, Hermer-Vazquez L, Srinivasan S, Chapin JK. Beta- and gamma-frequency coupling between olfactory and motor brain regions prior to skilled, olfactory-driven reaching. Exp Brain Res. 2007 Jun;180(2):217–235.

277. Bensafi M, Rinck F, Schaal B, Rouby C. Verbal cues modulate hedonic perception of odors in 5-year-old children as well as in adults. Chem Senses. 2007 Nov;32(9):855–862.

278. Joussain P, Chakirian A, Kermen F, Rouby C, Bensafi M. Physicochemical influence on odor hedonics: Where does it occur first? Commun Integr Biol. 2011 Sep 1;4(5):563–565.

279. Poncelet J, Rinck F, Ziessel A, Joussain P, Thévenet M, Rouby C, et al. Semantic knowledge influences prewired hedonic responses to odors. PLoS One. 2010 Nov 8;5(11):e13878.

280. Piastra MC, Nüßing A, Vorwerk J, Clerc M, Engwer C, Wolters CH. A comprehensive study on electroencephalography and magnetoencephalography sensitivity to cortical and subcortical sources. Hum Brain Mapp. 2021 Mar;42(4):978–992.

281. Fourcaud-Trocmé N, Lefèvre L, Garcia S, Messaoudi B, Buonviso N. High beta rhythm amplitude in olfactory learning signs a well-consolidated and non-flexible behavioral state. Sci Rep. 2019 Dec 30;9(1):20259.

282. Bastos AM, Vezoli J, Bosman CA, Schoffelen J-M, Oostenveld R, Dowdall JR, et al. Visual areas exert feedforward and feedback influences through distinct frequency channels. Neuron. 2015 Jan 21;85(2):390–401.

283. Roland B, Deneux T, Franks KM, Bathellier B, Fleischmann A. Odor identity coding by distributed ensembles of neurons in the mouse olfactory cortex. Elife. 2017 May 10;6.

284. Lu XC, Slotnick BM. Olfaction in rats with extensive lesions of the olfactory bulbs: implications for odor coding. Neuroscience. 1998 Jun;84(3):849–866.

285. Mrochen A, Marxreiter F, Kohl Z, Schlachetzki J, Renner B, Schenk T, et al. From sweet to sweat: Hedonic olfactory range is impaired in Parkinson's disease. Parkinsonism Relat Disord. 2016 Jan;22:9–14.

286. Iannilli E, Stephan L, Hummel T, Reichmann H, Haehner A. Olfactory impairment in Parkinson's disease is a consequence of central nervous system decline. J Neurol. 2017 Jun;264(6):1236–1246.

287. Hedner M, Larsson M, Arnold N, Zucco GM, Hummel T. Cognitive factors in odor detection, odor discrimination, and odor identification tasks. J Clin Exp Neuropsychol. 2010 Dec;32(10):1062–1067.

288. Barz S, Hummel T, Pauli E, Majer M, Lang CJ, Kobal G. Chemosensory event-related potentials in response to trigeminal and olfactory stimulation in idiopathic Parkinson's disease. Neurology. 1997 Nov;49(5):1424–1431.

289. Devanand DP. Olfactory identification deficits, cognitive decline, and dementia in older adults. Am J Geriatr Psychiatry. 2016 Aug 17;24(12):1151–1157.

290. Svenningsson P, Westman E, Ballard C, Aarsland D. Cognitive impairment in patients with Parkinson's disease: diagnosis, biomarkers, and treatment. Lancet Neurol. 2012 Aug;11(8):697–707.

291. Frasnelli J, Schuster B, Hummel T. Interactions between olfaction and the trigeminal system: what can be learned from olfactory loss. Cereb Cortex. 2007 Oct;17(10):2268–2275.

292. Ahmad I, Rathore FA. Neurological manifestations and complications of COVID-19: A literature review. J Clin Neurosci. 2020 Jul;77:8–12.

293. Sobel N, Thomason ME, Stappen I, Tanner CM, Tetrud JW, Bower JM, et al. An impairment in sniffing contributes to the olfactory impairment in Parkinson's disease. Proc Natl Acad Sci USA. 2001 Mar 27;98(7):4154–4159.

294. Pager J, Giachetti I, Holley A, Le Magnen J. A selective control of olfactory bulb electrical activity in relation to food deprivation and satiety in rats. Physiol Behav. 1972 Oct;9(4):573–579.

295. Royet JP, Pager J. Olfactory bulb responsiveness to an aversive or novel food odor in ;the unrestrained rat. Brain Res Bull. 1981 Oct;7(4):375–378.

296. Bhalla US, Bower JM. Multiday recordings from olfactory bulb neurons in awake freely moving rats: spatially and temporally organized variability in odorant response properties. J Comput Neurosci. 1997 Jul;4(3):221–256.

297. Albrecht J, Kopietz R, Frasnelli J, Wiesmann M, Hummel T, Lundström JN. The neuronal correlates of intranasal trigeminal function-an ALE meta-analysis of human functional brain imaging data. Brain Res Rev. 2010 Mar;62(2):183–196.